PHYSICOCHEMICAL STUDY OF SOLID CYCLODEXTRIN INCLUSION COMPLEXES OF THE ANTITHROMBOTIC AJOENE

BY: Vincent Joseph Smith

B.Sc. University of Cape Town

THESIS PRESENTED TO THE UNIVERSITY OF CAPE TOWN FOR THE DEGREE OF MASTER OF SCIENCE

August 2004

ACKNOWLEDGEMENTS

I would like to thank:

Supervisors

Professor Mino R Caira, for his excellent supervision, patience, kindness, understanding and for providing the rudder during the storm.

Professor Susan A Bourne, Susan, who gives impeccable advice and help as well as knowing how to find absolutely everything.

Professor Roger Hunter, for his supervision and guidance throughout the course of this project.

Supramolecular group

Professor Luigi R Nassimbeni, for his kindness, encouragement, advice, concern and not least of all, the fantastic **watch**.

Professor Peter W Linder, friend and colleague.

Dejana Vujovic, Hong Su and Sibulelo Vilakazi, for lunch and the daily 4:50 pm chat.

Clive Oliver and Thabani Mhlongo, for their enduring friendship and sense of humour.

All the members of the Supramolecular group, past and present, for offering their various interpretations of life.

My Friends and Family for their support and encouragement.

The National Research Foundation and the University of Cape Town for financial support.

PUBLICATIONS AND CONFERENCES

Parts of this thesis have been published:

Preparation, thermal behaviour and structural characterization of inclusion complexes of permethylated β-cyclodextrin with the garlic-derived antithrombotics (*E*)- and (*Z*)-Ajoene.

Caira, M.R., Hunter, R., Bourne S.A. and Smith V.J. *Supramol. Chem.*, (in press **2004**).

Parts of this thesis have been Presented at the following Conferences

(presenting author underlined)

2nd International Conference on Pharmaceutical and Pharmacological Sciences, 3-6 October 1999, Cape Town, South Africa.

Poster P50: More definitive characterization of cyclodextrin-drug inclusion complexes using powder X-ray diffraction.

M R Caira and V J Smith.

International Immunopharmacology Congress 2001, Sun City, Pilanesberg, South Africa, September 16-20, 2001.

Poster: Cyclodextrin inclusion of synthetic (Z)-Ajoene, a compound from garlic.

M R Caira, R Hunter, S A Bourne and V J Smith.

Annual Meeting of the South African Crystallographic Society, University of Stellenbosch, RSA, 4-5 April, 2002.

Oral presentation: Cyclodextrin inclusion of synthetic (Z-)-Ajoene, a compound from garlic.

M R Caira, V J Smith, R Hunter and S A Bourne.

21st European Crystallographic Meeting, ECM-21, Durban, South Africa, 24-29 August 2003.

Poster f4.m6.p4: Stabilisation of the volatile, biologically-active compound Ajoene via Cyclodextrin Inclusion. V J Smith, R Hunter, S A Bourne and M R Caira.

22nd European Crystallographic Meeting, ECM-22, Budapest, Hungary, 26-31 August 2004.

Poster: Characterization of (*E*)- and (*Z*)-ajoene inclusion complexes with α-, β-, γ- and permethylated-β-cyclodextrin using PXRD, single crystal X-ray diffraction and thermal analysis. V J Smith, R Hunter, S A Bourne and M R Caira

ABSTRACT

This study describes the preparation and physicochemical characterization of inclusion complexes formed between selected cyclodextrins (CDs) and ajoene, an antithrombotic found in garlic. The *E* and *Z* isomers of ajoene (4,5,9,-trithiadodeca-1,6,11-triene-9-oxide) were reacted with α-, β-, γ-CD, heptakis(2,6-di-O-methyl)-β-CD (DIMEB) and heptakis(2,3,6-tri-O-methyl)-β-CD (TRIMEB) to yield inclusion compounds α-CD•(*E*)-ajoene (**1**), α-CD•(*Z*)-ajoene (**2**), β-CD•(*E*)-ajoene (**3**), β-CD•(*Z*)-ajoene (**4**), γ-CD•(*E*)-ajoene (**5**), γ-CD•(*Z*)-ajoene (**6**), DIMEB•(*E*)-ajoene (**7**), DIMEB•(*Z*)-ajoene (**8**), TRIMEB•(*E*)-ajoene•0.5H_2O (**9**) and TRIMEB•(*Z*)-ajoene (**10**). These species were investigated by thermal techniques (HSM, DSC, TGA), FTIR, NMR, UV spectrophotometry, powder X-ray diffraction (PXRD) and, in the case of **9** and **10**, single crystal X-ray diffraction. The complexes yielded similar PXRD traces within their CD type except for TRIMEB where the complexes have distinctly different traces. Single crystal X-ray diffraction methods revealed the space groups $P2_1$ (**9**) and $P2_12_12_1$ (**10**) and the simultaneous presence of the guest stereoisomers in both complexes. Refinement of guest site-occupancies showed that each complex crystal consists of a mixture of diastereomers in a 1:1 molar ratio. The different crystal packing arrangements for **9** and **10** are induced by the distinctly different modes of inclusion of the *E* and *Z* isomers. Complexes for which microcrystalline precipitates were obtained, **1** through **8**, were classified into isostructural series by matching their PXRD traces with those in an existing set of reference patterns. In this way the space group for each of the complexes **1**

through **8** was established together with an estimate of the unit cell parameters which would otherwise only be known from single crystal X-ray diffraction data. The results of this study are significant in the context of possible further development of CD – ajoene inclusion complexes as medicinal agents.

TABLE OF CONTENTS

CHAPTER 1

In this chapter we discuss the origins of cyclodextrins, their physico-chemical and geometrical properties, their ability to form inclusion complexes and the characterization of such complexes. We also discuss powder X-ray diffraction, isostructurality and how these are related to the characterization of the cyclodextrin inclusion complexes.

NATURAL ORIGIN OF CYCLODEXTRINS

Natural origin

Normal enzymatic degradation of starch generally produces glucose, maltose and maltotriose as well as a series of long linear or branched chain malto-oligomers, known as dextrins.[1] This is a hydrolytic process, as the primary product from the splitting of the glycosidic linkage reacts with one molecule of water.[1] If, however, the degradation of starch occurs by means of glucosyltransferase enzyme (CGTase), the primary product of the chain splitting undergoes an intramolecular reaction without the participation of a water molecule yielding α(1,4)-linked cyclic end products,[1] known as cyclodextrins (henceforth CDs). The enzyme CGTase which produces the cyclodextrins is isolated from the microbe *Bacillus macerans* but can also be obtained for this purpose from other less well known micro-organisms, such as *Klebsiella oxytoca*, *Bacillus circulans* and *Alkalophylic bacillus* No.38-2.[2] CDs are also referred to as Schardinger dextrins, cellulosines, cycloamyloses, cycloglucans and cycloglucoamyloses. They are characterised by a ring (or truncated cone) built up of glucose units which vary in number. The most abundant of the cyclodextrins produced in this way are α-, β- and γ-CD containing 6, 7, and 8 glycosidic units respectively. Larger

CDs that have in excess of 100 glycosidic units have been prepared by the action of disproportionating enzyme on amylose.[3] However, molecules with fewer than 6 units are sterically strained and therefore are not produced enzymatically.[4] A pentameric α(1,4)-linked CD has been produced synthetically from a linear glucopentaose derivative.[5]

Historical origins

The earliest reference to cyclodextrins (then called cellulosines) appeared in 1891 by Villiers[6] who discovered them while degrading starch in the presence of *Bacillus amylobacter*. The next reference to "cellulosines" was made by Schardinger[7] in 1903. He was the first to use *Bacillus macerans* specifically to produce small amounts of (mostly α- and β-) cellulosines.[8,9] In the period 1904-1911 Schardinger proceeded to establish the fundamentals of cyclodextrin chemistry.[10] However, the most important aspect of CDs, namely their complexing ability, is attributed to Pringsheim[11,12] who discovered this phenomenon in the period 1911-1935.

Characterization history

Freudenberg *et al.*[13,14] with the aid of data obtained from Karrer[15] and Miekeley[16] concluded that CDs were made up of maltose units and contained only α(1,4)-glycosidic linkages. In 1936 Freudenberg *et al.*[13] postulated the cyclic structure of these dextrins. Single crystal X-ray diffraction was first applied to α-CD and β-CD in 1942 by French and Rundle in order to determine their molecular weights.[17] The structure of γ-cyclodextrin was elucidated in 1948-1950.[18] In the early 1950s French[19] and Cramer[20] started

to characterize the physicochemical properties of cyclodextrins. In 1953 Freudenberg, Cramer and Plieninger[21] obtained a patent listing the application of CDs in drug formulations. The first full X-ray structure was published in 1965 by Hybl *et al.* when they reported the structure of an α-CD complex with potassium acetate.[22] By the end of the 1960s laboratory-scale preparation of CDs had been successfully achieved.[2]

MACROCYCLIC STRUCTURE OF CYCLODEXTRINS

Building block

The cyclodextrins α-, β- and γ-CD (shown in Figure 1), as previously mentioned, are made up of 6, 7 or 8 α-D-glucopyranose units which are α(1,4)-linked in the $^4C_1$-chair conformation.[23-25] α-D-glucopyranose is a rigid building block and when linked to other identical units achieves some flexibility, while retaining its overall rigidity. The macrocycle has the appearance of a truncated cone or torus and is often referred to as such. The structural rigidity of the α-D-glucopyranose does not always hold true. In the case of a fully methylated β-CD inclusion complex severe distortions of the $^4C_1$-chair form are observed.[26] Moreover, in one crystalline modification of permethylated β-CD, one glucose residue adopts the inverted $^1C_4$ form.[27]

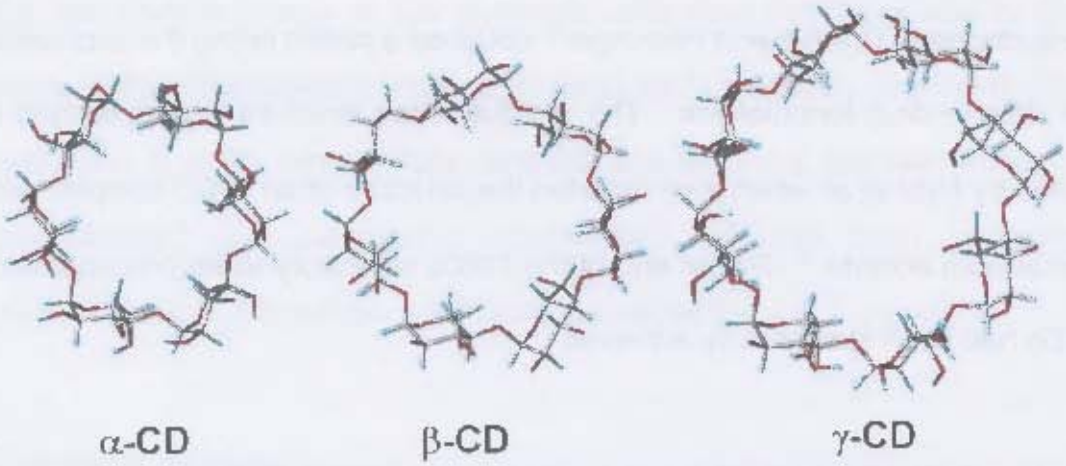

Figure 1. Parent cyclodextrins α-, β-, and γ-CD.

Truncated cone

Cyclodextrin molecules are amphiphilic truncated cones (Figure 2), which consist of a slightly apolar cavity (hydrophobic) and a polar, water soluble (hydrophilic) exterior. Each end of the cavity is guarded by a rim/edge of hydroxyl groups which promote solubilisation of the CD.[4]

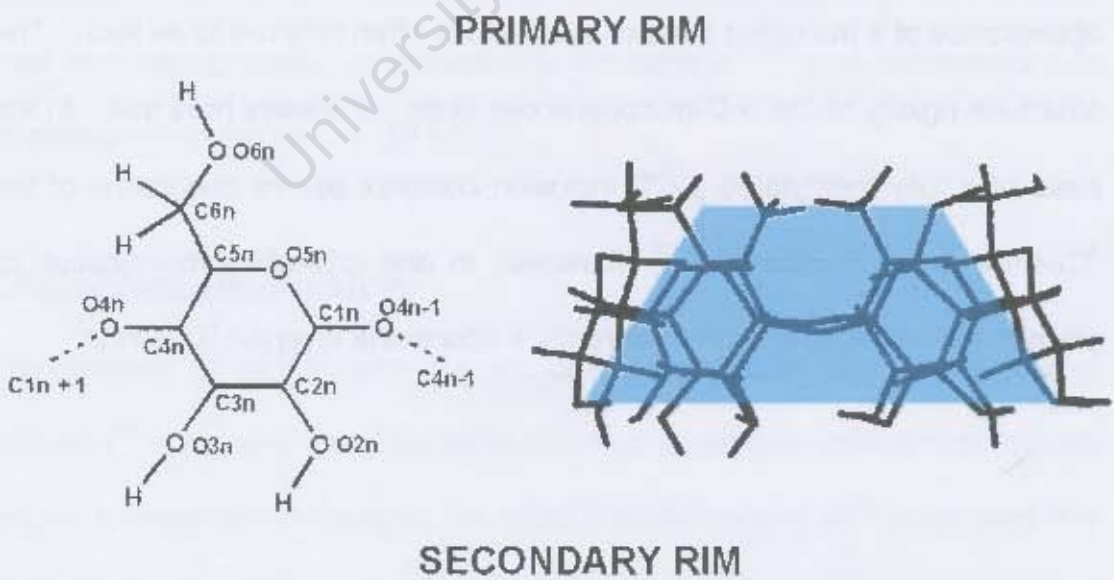

Figure 2. A labelled glucopyranose residue (left) and the truncated cone-like shape of cyclodextrins (right).

These rims are named according to the type and number of attached hydroxyl groups. The upper or primary rim contains one hydroxyl group (O(6)-H) per

glycosidic unit, while the lower or secondary rim contains two hydroxyl groups (O(2)-H and O(3)-H) per glycosidic unit. The glycosidic units are aligned in such a way that they are all in register (syn) with one another (Figure 3).[4] The O(6)-H hydroxyl group of the glycosidic unit has rotational freedom around the C(5)-C(6) bond.

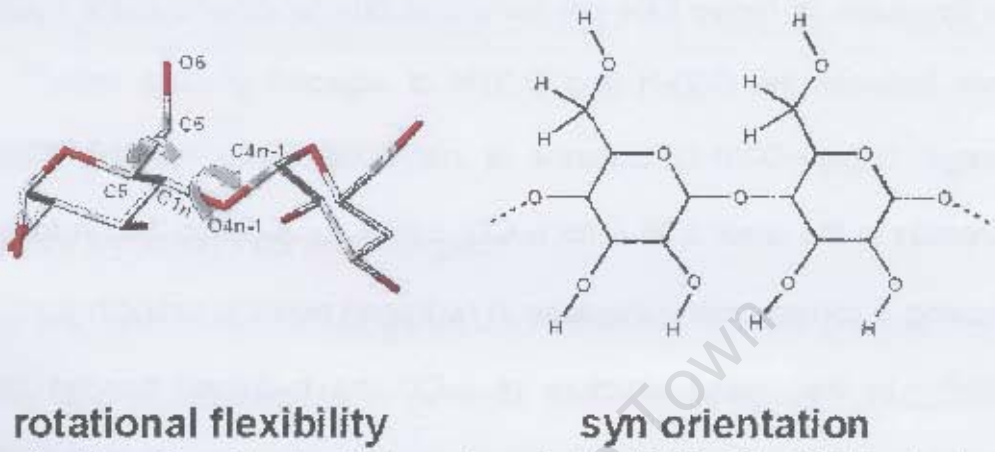

Figure 3. Glycosidic units orientated syn to each other (right). The O6-H hydroxyl group possesses rotational freedom with respect to C5-C6 (left) while the glycosidic units have rotational flexibility about the glycosidic oxygen bonds C(1n)-O4(n-1)-C(4n-1).

This rotational freedom is retained after the individual units have been linked. The macrocycle possesses limited rotational flexibility of the C(1n)-O(4n-1)-C(4n-1) glycosidic linkage[4] (Figure 3) forcing the macrocycle to remain relatively rigid.

Hydrophobic cavity

CD cavities provide a hydrophobic matrix in an aqueous solution or, as it is also termed, a "microheterogeneous environment".[20] The $^4C_1$ conformation of the glucopyranose units, in conjunction with the limited rotational flexibility of the glycosidic linkage allows the C(3)-H, C(5)-H methine and C(6)-H_2 methylene hydrogen atoms as well as the lone pairs of the glycosidic oxygen

bridges to line the cavity of the cyclodextrin, increasing its hydrophobic nature and at the same time giving the cavity an electrically positive character. [20, 28]

Hydrogen bonded ring

The structures of native CDs are fairly rigid due to intramolecular hydrogen bonds between the O(2)-H and O(3)-H of adjacent glucose units.[28] The average O2(n)•••O3(n-1) distance is not constant for all the CDs but decreases in the order 2.98 Å for α-CD, 2.88 Å for β-CD to 2.82 Å for γ-CD, indicating a corresponding increase in hydrogen bonding strength from α- to γ-CD.[29] In the crystal structure of α-CD the hydrogen bonded ring is incomplete since one glucopyranose unit is severely tilted such that the O(2)-H and O(3)-H groups are outside hydrogen bonding distance; consequently, only four hydrogen bonds form, rendering α-CD less rigid than β-CD.[30,31] β-CD is more rigid since it has a complete ring of hydrogen bonds.[32] γ-CD on the other hand has the strongest hydrogen bonds of the three native CDs but its structure is more flexible than either α-CD or β-CD.[32] An explanation of the phenomenon of γ-CD having strong hydrogen bonds while remaining more flexible than either α- or β-CD is still absent from the literature. As a direct consequence of the complete ring of hydrogen bonds, β-CD is far less soluble than α- or γ-CD, with γ-CD being the most soluble (Table 1).[32]

Table 1[32] Characteristic parameters describing parent cyclodextrins

Parameter	α-CD	β-CD	γ-CD
Number of glucose units	6	7	8
Molecular weight g/mol	972	1135	1297
Solubility in water (g per 100 cm^3 @ 25°C)	14.5	1.85	23.2
Cavity diameter (Å)	4.70 – 5.30	6.00 – 6.50	7.50 – 8.30
Height of torus (Å)	7.90 ± 0.10	7.90 ± 0.10	7.90 ± 0.10
Diameter of outer periphery (Å)	14.60 ± 0.40	15.40 ± 0.40	17.50 ± 0.40
Cavity volume ($Å^3$)	174	262	427
Cavity volume per 1g of CD (cm^3)	0.10	0.14	0.20
$[\alpha]_D$ @ 25°C (°)	150 ± 0.5	162.5 ± 0.5	177.4 ± 0.5

MACROCYCLIC GEOMETRY

Primary hydroxyl torsion angles

There are three principal staggered conformations, namely *(+)-gauche, (-)-gauche* and *trans*, that can in principle be adopted by the O5-C5-C6-O6 torsion angle (ω).[33] Only two of the three have thus far been observed, namely (+)-*gauche* with ω = +60° and (-)-*gauche* with ω = -60°.[34] Possible reasons for the non-observance of the *trans* orientation may be due to adverse steric interactions between O(6)-H and adjacent glucose units as well as the *gauche* effect that comes into play in O-C-C-O systems which destabilizes the *trans* arrangement.[33,35] The (-)-*gauche* conformer with O(6)-H pointing away from the center of the cavity is preferred over that of the (+)-*gauche* conformer which has the O(6)-H turned towards the cavity.[4] The (+)-*gauche* conformer may be involved in hydrogen bonding with a guest or may be adopted due to packing requirements.[4]

Geometric descriptors

Polygons, composed of the glycosidic O(4) atoms, offer a good approximation to the macrocyclic ring (as presented in Figure 4 below).[36] These O(4) atoms

are usually coplanar within *ca.* 0.3 Å deviation.[36] The side length (l) of the polygon is the O(4)•••O(4') distance between two consecutive glycosidic linking oxygen atoms. The radius (r) is measured from the centre of gravity (C, or centroid) of the O(4) atoms to each individual O(4) atom.

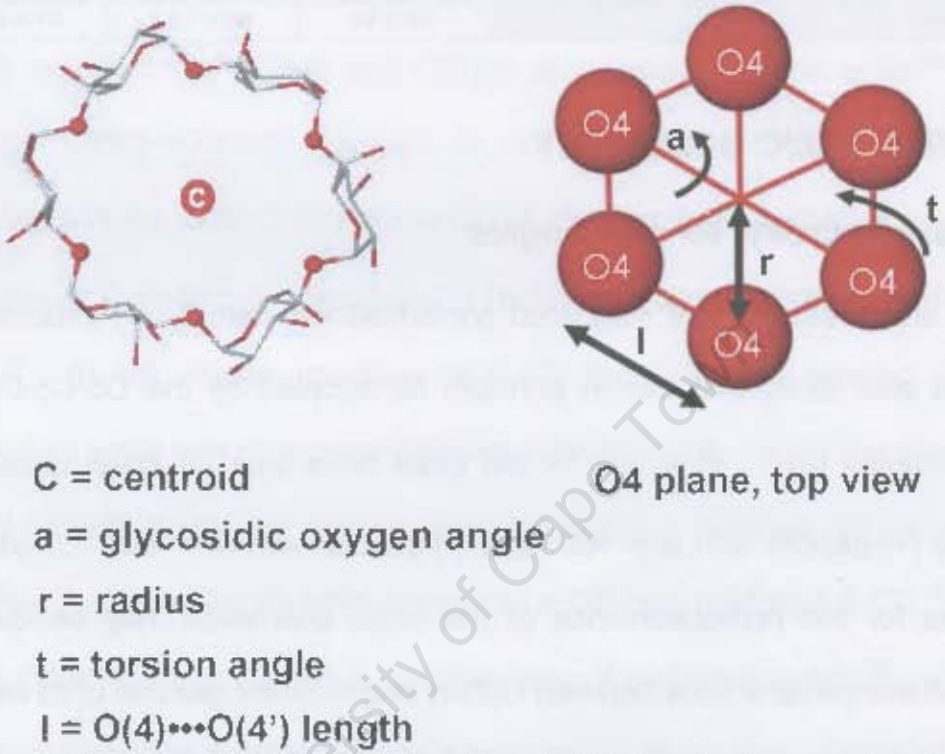

Figure 4. The parameters listed are normally quoted to describe the geometry of the host cyclodextrin.

The O(4)•••O(4')•••O(4'') angle (a) provides a measure of the deviation from the respective symmetries C_6, C_7 and C_8 for α-, β- and γ-CD. Ideally they should be 120, 128 and 132° respectively. The O(4)•••O(4')•••O(4'')•••O(4''') torsion angle (t) is sensitive to any deviations from planarity since for a planar macrocycle all torsion angles are 0°. The glycosidic O(4) bond angle is an excellent indicator of conformational strain and is defined by C(1n)•••O(4n-1)•••C(4n-1). The average glycosidic oxygen angle is in good agreement among the three native CDs.[36] Glucose units are not perpendicular to the O(4) plane but incline mostly with the O(6) side towards the inside of the

macrocycle.[36] This angle of inclination is formally referred to as the tilt angle. It has two designators, namely τ_1 and τ_2, where τ_1 is the angle between the O(4) plane and the mean plane passing through C(1), C(2), C(3), C(4), C(5) and O(5) of each glycosidic unit, and τ_2 is the angle between the O(4) plane and the mean plane passing through C(1), C(4), O(4) and O(4') of each glycosidic unit.[36] A positive value of the tilt angle implies that the glycosidic unit is inclined with the O(6)-H towards the inside of the macrocycle, while a negative value has the O(6)-H inclined towards the outside of the macrocycle.[36]

INCLUSION COMPLEXATION

Complexation

Considering that no covalent bond is established between the host and guest, and moreover that the dissociation-association equilibrium in solution is one of the most characteristic features of the host-guest unit, the name 'inclusion complex' (or CD complex) seems apt.[1] Inclusion complexes are entities comprising two or more molecules, in which one of the molecules, the 'host', includes a 'guest' molecule, totally or partially, only by physical forces, i.e. without covalent bonding.[1] In an aqueous solution (see Figure 5), the slightly apolar cyclodextrin cavity is occupied by water molecules which are energetically less favoured (polar-apolar interaction), and therefore can be readily substituted by appropriate 'guest molecules' which are less polar than water.[2]

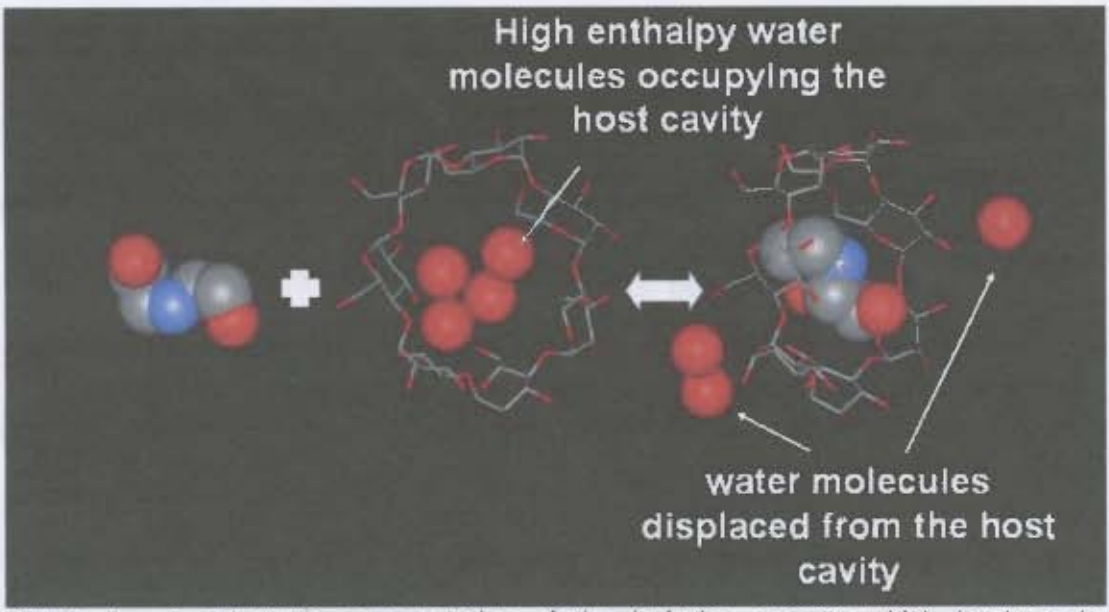

Figure 5. A schematic representation of the inclusion process which involves the displacement of 'high enthalpy' water molecules from the hydrophobic cavity and its occupation by the hydrophobic guest molecule.

The dissolved cyclodextrin is the host, and the driving force of the complex formation is the substitution of the high enthalpy water molecules by an appropriate guest molecule.[2] Both enthalpy and entropy changes play a role in this process.[1] However, according to a recent paper by L. Liu *et al.*,[37] due to the enthalpy-entropy compensation, release of conformational strain and the exclusion of cavity bound water are not energetically contributive to complex formation, and thus these effects evidently do not play a significant role in the thermodynamics of complexation.

The most probable mode of binding involves the insertion of the less polar part of the guest molecule into the cavity, while the more polar and often charged group of the guest molecule is exposed to the bulk solvent outside the secondary side of the cavity.[38] This process involves substantial rearrangement and removal of water molecules that solvate both the CD and guest molecule.[38] The principal factors involved in binding are believed to be

primarily van der Waals and hydrophobic interactions[23,39-47] although hydrogen bonding and steric effects may also partake in the process.[42,48] Electrostatic forces also make a contribution to binding in the form of ion-ion, ion-dipole, dipole-dipole, dipole-induced dipole attractions and those of higher order.[49]

METHYLATED CYCLODEXTRINS

Modifications of CDs have been intensively pursued with the intention of possibly enhancing their properties. Methylation is the simplest modification, and the inclusion properties of methylated cyclodextrins have been extensively studied.[28] Since hydroxyl groups are amenable to modification and since α-, β- and γ-CD have 18, 21 and 24 hydroxyl groups respectively, the outcomes of these methylations are numerous, interesting and important. The reactivities of hydroxyl groups are as follows: C(6)-OH > C(2)-OH > C(3)-OH, but are totally dependent on the reaction conditions.[50] The effect of attaching methyl groups at both ends of the cavity of a CD is an increase in depth of the cavity of *ca.* 2 Å, as well as making both ends hydrophobic and this directly influences the manner in which guest molecules are included with respect to native CDs.[29] The two methylated derivatives of β-CD that are of interest here are heptakis(2,6-di-O-methyl)-β-cyclodextrin and heptakis(2,3,6-tri-O-methyl)-β-cyclodextrin or more commonly DIMEB and TRIMEB respectively. DIMEB is thus methylated at the C(2)-OH and C(6)-OH hydroxyl positions while TRIMEB is methylated at the C(2)-OH, C(3)-OH and C(6)-OH hydroxyl positions. The conformations of DIMEB and β-CD are very similar except for the extension of the cavity in the former case. The round shape of

the macrocyclic ring is maintained by the intramolecular O(2)•••H-O(3') hydrogen bonds. The O(2)•••O(3') distances are in the range 2.8 - 3.1 Å, nearly the same as for β-CD.[51] Due to the increased number of methyl groups of DIMEB relative to β-CD the intermolecular space has become more hydrophobic than the cavity. The hydrophobic guest is thus more readily accommodated in the intermolecular space if its size and shape are more suited to the intermolecular space than the DIMEB cavity.[51]

The TRIMEB molecule in its inclusion complexes is much more distorted than β-CD and the seven O(4) atoms are no longer coplanar.[36] This is evident from the fact that the root mean-square deviation of the seven O(4) atoms from their mean plane is 0.44 Å.[51] Generally, five of the seven methylglucose units are inclined with the O(6) side towards the centre of the macrocycle, while the remaining two residues are tilted in the opposite direction.[36] Methylation influences overall macrocycle shape but more importantly it also affects pyranose conformation. In the case of TRIMEB monohydrate[27] the $^1C_4$ conformation is adopted by one methylglucose residue and there is partial self-inclusion of one of the methyl groups of a neighbouring molecule. The inverted conformation is adopted to help stabilise the structure of the CD by the partial occupancy of the CD cavity. The structure of TRIMEB is further stabilized by the formation of C(6)-H•••O(5) hydrogen bonds which form between adjacent methylglucose units. Recently two new TRIMEB structures were found which have all seven residues in the $^4C_1$ conformation.[52] In both structures there is complete self-inclusion of two methoxyl groups from a

screw-related molecule so as to occupy the available space and better stabilise the structure of TRIMEB.

PACKING ARRANGEMENTS

When CDs crystallise, whether as complexes or hydrates, they generally arrange in one of two packing modes described as cage or channel structures.[53]

This description is based on the appearance of the formed cavities. For complexes, the cage type structure is characteristic of small guests which are completely enveloped by the cavity. The channel type is observed when the guests are large enough to protrude from the cavity. In channel-type structures CD molecules stack on top of each other such that their cavities form infinite channels. These stacks are stabilized by hydrogen bonds between O(2)-H/O(3)-H and O(6)-H in the case of a head-to-tail alignment, or O(2)-H/O(3)-H with O(2)-H/O(3)-H for head-to-head assembly. 'Head-to-tail' therefore refers to the situation in which the primary rim of one CD faces the secondary rim of another CD within hydrogen bonding distance. Similarly, a 'head-to-head' arrangement occurs when the secondary rims of two CDs are within hydrogen bonding distance. Frequently observed for β-CD is the tendency to dimerise in a head-to-head manner (as in Figure 6 below), thus doubling the cavity volume in which larger guests, or even more than one guest can be accommodated. These dimers stack in such a way that their O(6)-H groups interact through hydrogen bonding to complete the channel structure.

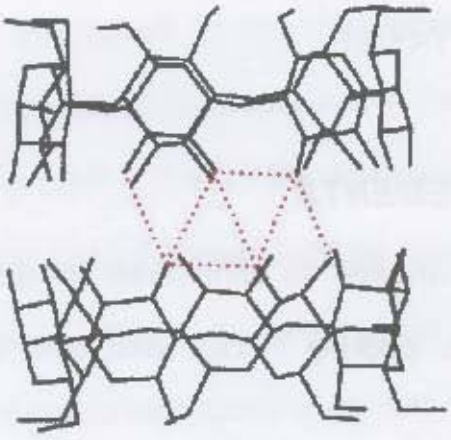

Hydrogen bonded dimer

Figure 6. The β-CD dimer is held together by an intricate hydrogen bond motif. Often included water molecules are involved in the extension of this hydrogen bond network. Representative hydrogen bonds are shown as dotted lines.

The cavities in cage type crystal structures are blocked off on both sides by adjacent CD molecules such that they are isolated and there is no contact between guests. Cage type structures are subdivided into two categories. The first of these is the herringbone motif, a common motif with hydrates and small molecule guests such as iodine, methanol and propanol. In this motif the CD molecules arrange themselves much the same as a fishbone. The second of the two categories is the brick motif. Here the CD molecules are arranged in layers, adjacent layers being laterally displaced. This isolates the CD cavity on both sides by molecules in adjacent layers. The brick type motif is limited to α- and β-CD. β-CD can form a different brick type arrangement in which the dimer is stabilised intermolecularly by hydrogen bonding between the secondary (O(2)-H/O(3)-H) sides while the layers are displaced laterally, again isolating the double volume cavities.

Monomeric structures of β-CD complexes

Broadly speaking, monomeric structures of β-CD complexes are subdivided into five packing arrangements. These are: herringbone with space group $P2_1$, layer type in $P2_1$, zigzag in $P2_12_12_1$, helical channel with space group $P6_1$ and finally brick type belonging to space group $P2_1$ (Figure 7).[54]

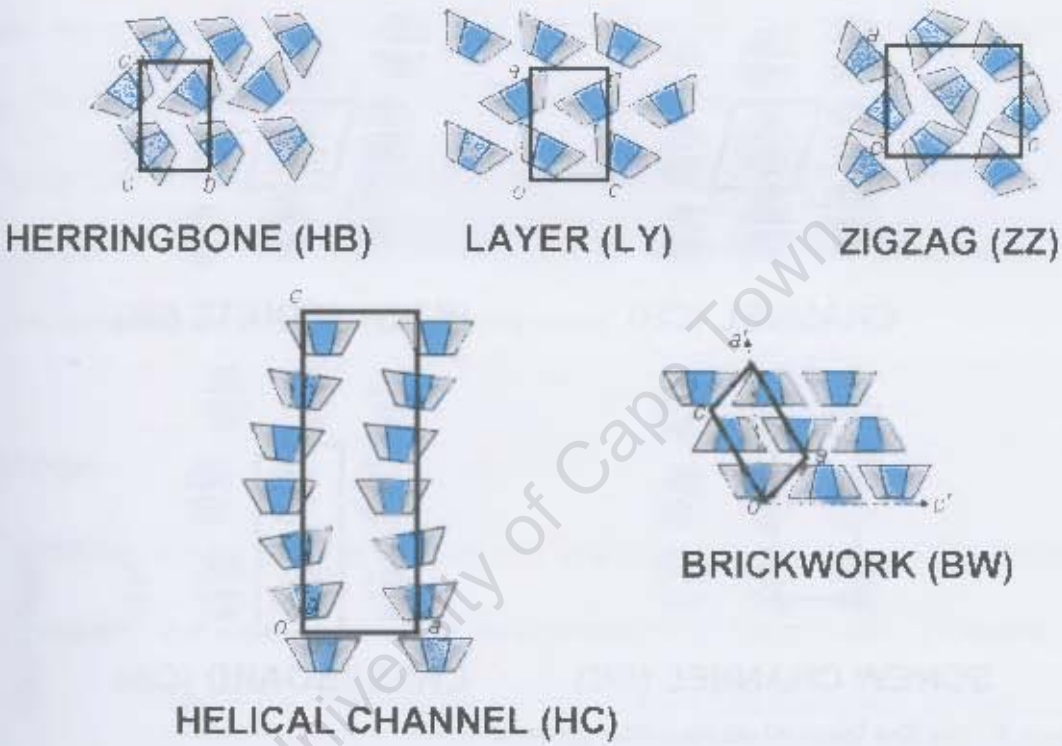

Figure 7. Diagrammatic representation of five monomeric packing arrangements.

As it turns out, the herringbone packing arrangement is the most efficient packing system as well as the preferred arrangement for monomeric structures of β-CD inclusion complexes.

Dimeric structures of β-CD complexes

Similarly, dimeric structures of β-CD complexes are split into four different packing arrangements and may be further classified as layer arrangements (shown in Figure 8). The four groups are as follows:[55] channel in the space

groups P1 and C2, screw channel in $P2_1$, intermediate in P1 and chessboard with space group $C222_1$. It must be pointed out that recently more categories have been identified through the classification of X-ray powder diffraction (PXRD) patterns of hydrates and complexes into isostructural series of PXRD patterns.[56]

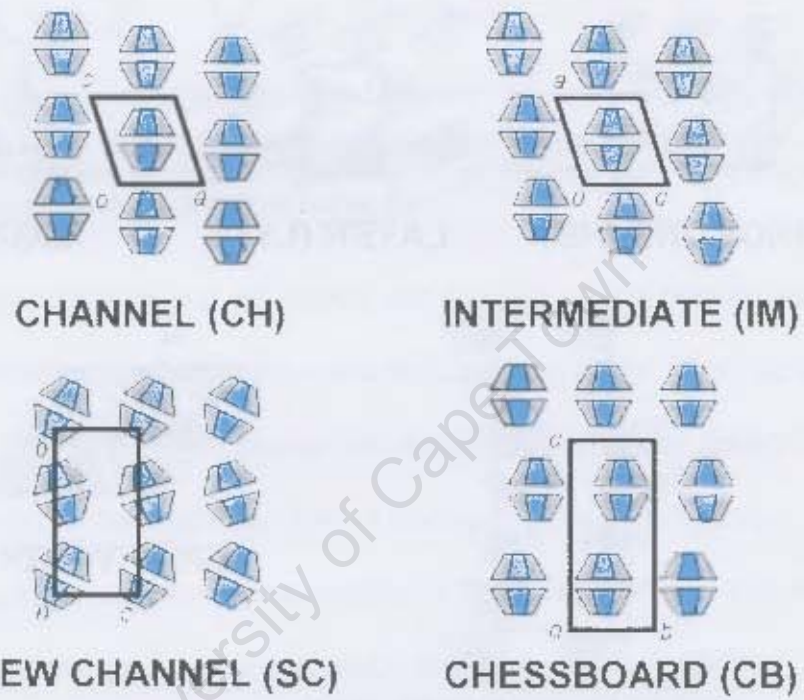

Figure 8. The four favoured packing arrangements of dimeric β-CD complexes.

DIMEB packing

By and large, DIMEB and its complexes crystallize in the space groups $P2_1$ and $P2_12_12_1$.[57] The packing arrangements are various and range from channel type head-to-tail stacking of the host to modified brick type and modified herringbone arrangements. These include structures where the guest is located in the intermolecular spaces.

TRIMEB packing

TRIMEB and its inclusion complexes seem to prefer to crystallize in the space group $P2_12_12_1$ with the molecules in a screw channel type structure,[28] though recently, structures with space group $P2_1$ have been identified.[58] Similarly to DIMEB complexes, the molecules are also arranged in a head-to-tail manner.

As complexes of both native and permethylated CDs have relatively few preferred three-dimensional packing arrangements which generate, in most instances, very distinct powder X-ray diffraction (PXRD) patterns, it is not difficult to see how important the PXRD technique has become in the characterization of CD inclusion complexes.

PXRD

Powder x-ray diffraction has been, and still is, an important tool in the evaluation and characterisation of complexes. However, its use in the identification of new phases has been very rudimentary.

The traditional way in which PXRD is applied follows a procedure whereby a minimum of four PXRD traces are recorded to characterize the product of a reaction between any two compounds A and B (where A and B are solids). These include the traces for the starting materials, a physical mixture, A + B, and the suspected new phase AB. The process of determining the formation of a new phase involves making a detailed comparison of each trace A, B and A + B, with that of AB. The peak angular positions of AB are matched against those of the other traces. Any peaks present in AB but absent from traces A,

B and A + B are indicative of a new phase. However, the presence of unmatched peaks in the trace of AB does not exclude the possibility of either compound A or B having undergone polymorphic or other transformations during or after their reaction. Therefore, it is generally the practice to employ PXRD in conjunction with complementary techniques, such as UV spectrophotometry, IR and Raman spectroscopy, thermogravimetry and differential scanning calorimetry to support conclusions drawn regarding inclusion complex formation. The recognition and application of the principles of isostructurality (*definition follows*) adds a new level of sophistication to the interpretation of data obtained from PXRD while simultaneously speeding up the objective of determining the identity and characteristics (i.e. unit cell dimensions, space group) of the new phase.

ISOSTRUCTURALITY

Since Mitscherlich's discovery (1819), the isomorphism of crystals has been interpreted in various, sometimes controversial ways.[59] This can be attributed to the fact that the word 'isomorphous' strictly refers only to the external morphological similarities between crystalline substances. As a consequence, Kálmán and co-workers[59] recently recommended the exclusive use of the term 'isostructural' for organic crystals (isotypic for organometallic and organo-inorganic crystals). The fundamental difference between the terms 'isomorphous' and 'isostructural' is the fact that the former describes crystal morphology while the latter is used in the case where two or more crystals share the same three-dimensional packing arrays.[59] Thus, as a definition, isostructural compounds crystallize with similar

unit cell dimensions, the same space group, and nearly identical atomic coordinates for common atoms. Implicitly, one is able to superimpose isostructural crystal phases (i.e. any two compounds which conform to this definition).[60] In addition, isostructurality is inversely related to the phenomenon of polymorphism, where instead a single compound crystallizes in different packing arrays. A better understanding of the isostructurality phenomenon may conversely lead to a better understanding of polymorphism. Figure 9 shows this relationship more clearly.

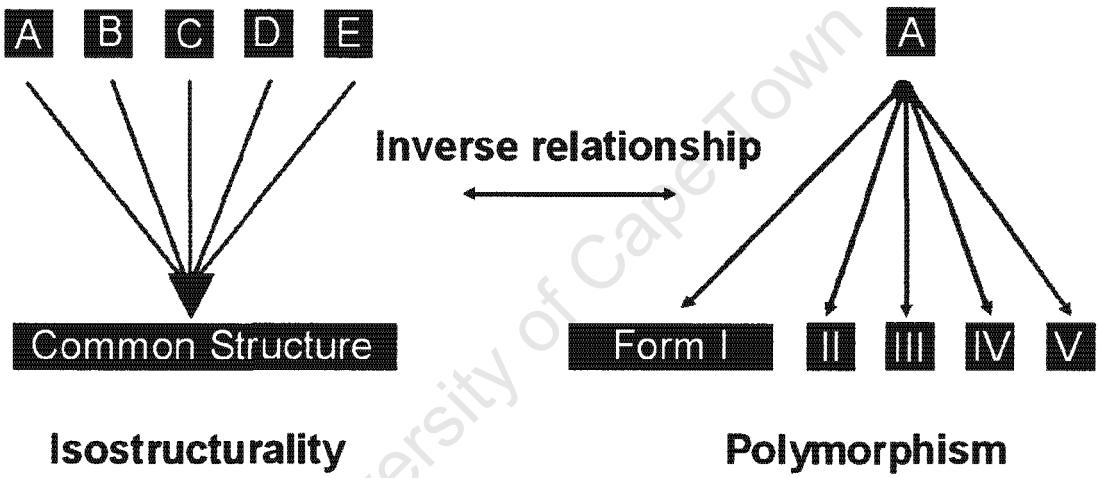

Figure 9. A diagrammatic depiction of the relationship between isostructurality and polymorphism.

Two important methods used to check for the occurrences of isostructurality are single crystal X-ray diffraction and powder X-ray diffraction. Single crystal X-ray diffraction allows an explicit determination of the parameters for isostructurality i.e. unit cell dimensions, space group and atomic coordinates. These parameters allow the direct comparison between two structures and the determination of the level/degree of isostructurality between two or more structures. This is achieved through the calculation of indices/numerical descriptors, namely the unit cell similarity index[59] Π, isostructurality

index[63] $I_i(n)$ and the volumetric isostructurality index[61] I_v which provide a percentage quantification for the level of agreement between structures.

Unit cell similarity (Π)

A basic prerequisite of isostructurality is the similarity of unit cells. According to Kálmán *et al.* they can be compared using

$$\Pi = \frac{a+b+c}{a'+b'+c'} - 1 \quad (a+b+c > a'+b'+c'),$$

where a, b, c and a', b', c' are the orthogonalized unit cell parameters of the related crystals.[61] For identical unit cells $\Pi = 0$. Calculated values of Π are only comparable when they have been orthogonalized by the same method.[61]

Isostructurality index ($I_i(n)$)

As isostructurality involves similar unit cells and similar internal arrangements of molecules it is important that in related structures common atoms should have virtually identical coordinates. This is a key factor in calculating the Isostructurality index

$$I_i(n) = \left[1 - \left(\frac{\sum \Delta R_i^2}{n}\right)^{1/2}\right] \times 100\%,$$

Where the ΔR_i^2 values are the squares of the differences between the orthogonalized coordinates of *n* identical heavy atoms in the related structures. Here again, the molecules are transformed to the same asymmetric unit and origin choice.[61] As examples become more complex, the limits of this index are encountered. For instance, the general ΔR_i distance

between equivalent points in two unit cells increases with their distance from the common origin, fixed at (0,0,0) or even at $(\frac{1}{2},\frac{1}{2},\frac{1}{2})$.

Volumetric isostructurality index I_v

The volumes occupied in a unit cell should be more closely related in isostructural pairs. However, it still remains possible to compare certain parts of a structure as in the case where host molecules display a higher level of isostructurality in a given inclusion compound than the guest molecules. This viewpoint is expressed as,

$$I_v = \frac{2V_{\cap}}{V_1 + V_2} \times 100,$$

where V_1 and V_2 are the volumes of the compared fragments and $V_{\cap}$ is the intersection of these volumes. As $(V_1 + V_2)/2$ is the average volume, I_v may also be expressed as the ratio of volume overlap to the average volume. The calculation is performed on a whole unit cell to avoid the problem raised by unit cell dissimilarity.[63] An implicit averaging is performed over the asymmetric units and the results are dependent on the degree of similarity of unit cells.

In contrast, powder X-ray diffraction provides a direct way in which to determine whether two or more compounds are isostructural with respect to one another. When isostructurality applies there is a near one to one agreement in peak angular position of the respective PXRD traces with the greatest differences appearing in the relative intensities. Of course, the closer

the match between the relative intensities, the greater the level of isostructurality.

In the case where two compounds, A and B, crystallize and A forms large monocrystals while B forms only microcrystalline precipitates, and if there is agreement between their PXRD traces, it can safely be assumed that A and B are isostructural. If, however, the structure of A has been determined (by means of single crystal X-ray diffraction) with known unit cell dimensions and space group, then since A and B are isostructural, one is able to implicitly obtain the unit cell dimensions of B as well as its space group. The importance and application of this technique becomes clearer in the case of cyclodextrins and cyclodextrin inclusion complexes. Large single crystals of CD inclusion complexes cannot routinely be isolated. They are often relatively poorly diffracting and this prevents structure determination.[56] Since most CD complexes tend to form microcrystalline precipitates, PXRD is needed for the characterisation of these phases. In their crystal structures CDs pack in a small number of well-defined packing modes (as previously described). For this reason they are well suited to this kind of isostructural analysis.

This technique, however, relies on the existence of a set of index patterns or more accurately "reference patterns" for CDs and their inclusion complexes (see Table 2 for average unit cell parameters for the corresponding isostructural series). The reader is referred to the paper by Caira[56] for details on the construction of the reference patterns.

Table 2[56] Unit cell data for isostructural reference patterns

CD	Space group	No	a(Å)	b(Å)	c(Å)	α(°)	β(°)	γ(°)
Parent CDs								
α-CD, I	$P2_12_12_1$	1	14.858	34.038	9.529	90.0	90.0	90.0
α-CD, II	$P2_12_12_1$	2	13.700	29.350	11.920	90.0	90.0	90.0
α-CD, III	$P2_12_12_1$	3	14.356	37.538	9.400	90.0	90.0	90.0
β-CD	$P2_1$	4	21.233	10.294	15.103	90.0	112.22	90.0
γ-CD	$P2_1$	5	16.847	11.098	20.271	90.0	104.97	90.0
DIMEB	$P2_12_12_1$	6	13.821	17.424	29.610	90.0	90.0	90.0
TRIMEB	$P2_12_12_1$	7	14.823	19.382	26.534	90.0	90.0	90.0
COMPLEXES								
α-CD	$P2_12_12_1$	8	9.4	14.3	37.3	90.0	90.0	90.0
α-CD	$P2_12_12$	9	21.6	16.5	8.2	90.0	90.0	90.0
α-CD	$P2_1$	10	7.2	13.3	24.6	90.0	92.6	90.0
α-CD	$P2_12_12_1$	11	13.5	15.3	24.5	90.0	90.0	90.0
*α-CD	P1	12	13.9	13.9	16.7	93.0	91.8	119.4
MONOMERIC								
β-CD	$P2_1$	13	21.6	10.5	15.2	90.0	111.8	90.0
β-CD	$P2_1$	14	20.1	10.3	15.4	90.0	102.2	90.0
β-CD	$P2_1$	15	16.2	16.5	15.4	90.0	117.2	90.0
DIMERIC								
β-CD	P1	16	15.6	15.9	15.9	101.5	101.5	103.5
β-CD	C2	17	19.2	24.4	15.8	90.0	109.6	90.0
β-CD	P1	18	17.1	15.3	15.3	102.7	113.6	99.8
β-CD	$C222_1$	19	19.2	24.6	32.6	90.0	90.0	90.0
β-CD	$P2_1$	20	15.2	32.4	15.2	90.0	101.5	90.0
γ-CD	$P42_12$	21	23.8	23.8	23.1	90.0	90.0	90.0
DIMEB	$P2_12_12_1$	22	14.7	18.8	28.8	90.0	90.0	90.0
*DIMEB	$P2_1$	23	15.1	10.6	28.1	90.0	102.0	90.8
TRIMEB	$P2_12_12_1$	24	15.6	21.5	28.5	90.0	90.0	90.0

* The blue highlighted rows indicate newly added isostructural classes identified by the author of this dissertation, from examination of structures in the CSD.

The reference patterns were computed from crystal structure data retrieved from the CSD.[57] Thus, all the important parameters, such as unit cell dimensions, space group and atomic coordinates, are known for each of the representative patterns, of which there are 24.[56] To determine the identity of

a putative CD complex one has to match its experimental trace with the respective reference pattern (taking into account the CD type). Once the match has been made, one is able to confirm with reasonable confidence that complexation has occurred while also determining the unit cell dimensions and space group of the new species. More important still is the fact that the host (CD) arrangement as well as the void topology are immediately defined.[56]

Properties, applications and implications

Isostructurality occurs more frequently and more widely than was previously thought.[64] Therefore it remains important to illustrate this with suitably chosen examples. One of the earliest references to the application of isomorphism results from Berzelius (the teacher of Mitscherlich) who determined the atomic weight of selenium in 1928, following the discovery of the isomorphism (isostructurality) of Na_2SO_4, Ag_2SO_4, Na_2SeO_4 and Ag_2SeO_4.[64] A basic condition of isomorphism (isostructurality) of compounds was developed from Berzelius's work. Crystals of isomorphous pairs are similar in shape and will continue growing in the mother liquor of any of the other isomorphous pairs.[64] The manifestation of isostructurality in the form of solid solutions is a practical outcome of this property. It shows that isostructurality may influence physical and/or chemical behaviour. A homologous series of four alkylparabens (esters of 4-hydroxybenzoic acid) in which the alkyl substituent increases in order methyl, ethyl, propyl and *n*-butyl displays isostructurality amongst two of its members, namely ethyl- and propylparaben, sharing very similar unit cell dimensions and the common space group $P2_1/c$.[65] The remaining methyl-

and *n*-butylparaben crystallize in the space groups Cc and C2/c respectively, with different crystal packing arrangements from each other and from the isostructural pair.[65] The isostructural pair of ethyl- and propylparaben forms substitutional solid solutions, resulting in the substantial lowering of the aqueous solubility of these two components, specifically when measured in the quaternary system of alkylparabens, in ternary systems containing this pair or any binary system.[65] The result is a direct link between a macroscopic property (solubility) and crystal isostructurality at the molecular level.[56]

The 'Holy Grail' of structural studies is the complete understanding of the structure-function relationship. Isostructurality is perhaps key in this regard as it allows one a unique entry into understanding the structure-function relationship. Isostructural host-guest systems, where the host and its conformation remain unchanged, provide one with the opportunity of studying the mechanism of guest exchange isolated from other effects such as the rearrangement of the crystal structure during desolvation and recrystallisation.[60] The number of parameters under investigation is reduced while allowing for a greater understanding of those same parameters. An example of this is the host-guest isostructural clathrate series of 1,4-bis(9-hydroxyfluoren-9-yl)benzene (host, **H**) with acetone and DMSO (guests, $\mathbf{G_1}$ and $\mathbf{G_2}$ respectively).[66] Previous selectivity experiments showed no selectivity between $\mathbf{G_1}$ and $\mathbf{G_2}$ with **H**, and crystal structures $\mathbf{HG_1}$ and $\mathbf{HG_2}$ are isostructural.[66] The thermal analysis results reflected the thermal stabilities as $\mathbf{HG_2}$>$\mathbf{HG_1}$. When the powdered complex of $\mathbf{HG_1}$ (obtained by exposing powder **H** to the vapours of $\mathbf{G_1}$) was exposed to the vapours of $\mathbf{G_2}$ with

intermittent sampling and DSC analysis after 3 h, 26 h, 47 h and 64 h, it was found that the complex had undergone progressive conversion to $\mathbf{HG_2}$ and that complete conversion was effected after 86 h. The DSC trace always showed only two thermal events, namely the endotherm for the desolvation of the included guest ($\mathbf{G_1}$ or $\mathbf{G_2}$, or $\mathbf{G_1}$ and $\mathbf{G_2}$) and the endotherm for the melt of the host which remained unchanged at T_{on} = 261°C (where T_{on} is the onset temperature of the melt/desolvation). The endotherm for desolvation underwent migration from its starting point T_{on} = 81°C (acetone complex) to T_{on} = 197°C (DMSO complex) in the final DSC trace.[66] A direct conclusion that could be drawn from this result (though other experiments would be required to prove this) is that the process of guest exchange proceeded without the structural rearrangement of the host and that in all probability the guests were able to penetrate and exit (diffuse into or out of the structure) via the channels that span the crystal.

The isostructurality of host-guest systems has had another very interesting spin-off, this being the rather novel idea of tunability of host-guest systems.[67] Isostructurality provides the constant host framework within which the guests locate themselves. Selectivity is the affinity of a host for a particular guest, in the presence of other competing guests, under very particular conditions of concentration and temperature. Tunability is thus the ability of the experimentalist to predict the outcome of the selectivity experiment. In other words, in a system of host **H** plus guests **A** and **B**, where **A** and **B** are both in the liquid phase and present in a set ratio (i. e. under competition conditions) and where the inclusion product with formula $\mathbf{H{\cdot}A_n{\cdot}B_m}$ is obtained, one can

with some certainty predict the value of the integers **n** and **m** thus affording a tunable system. A unique example of this is the host-guest system of the diol host *trans*-9,10-dihydroxy-9,10-bis(*p-tert*-bisphenyl)-9,10-dihydroanthracene with guests DMF and DMSO.[67] In this system, it was possible to isolate the distinct inclusion complexes H•4(DMF), H•4(DMSO), H•3(DMF)•(DMSO), H•2(DMF)•2(DMSO) and H•(DMF)•3(DMSO).

Occurrence of isostructurality

In a survey of the literature performed in 1996, Kálmán found 45 isostructural pairs formed by more than 60 structures where the type of isostructurality presented was of the isometric type.[64] Taking into account the rate at which the number of published crystal structures increases every year, it can with some certainty be said that this number has long since been exceeded.

MOTIVATION, AIMS AND OBJECTIVES

Motivation

Garlic or *Allium Sativa, L.* has for some time been of interest due to the fact that it contains pharmacologically active components. Only in the last twenty years have there been extensive investigations of the beneficial effects of these constituents on human health.[68,69] Block *et al.*[70,71] with the aid of spectroscopic and chemical methods revealed the presence in garlic of an organosulfur compound derived from the decomposition of allicin (allyl 2-propenethiosulfinate) in aqueous acetone. The result is an oily mixture of *E* and *Z* isomers of ajoene (Figure 10), a compound which has gained in interest due to its remarkable variety of biological effects.

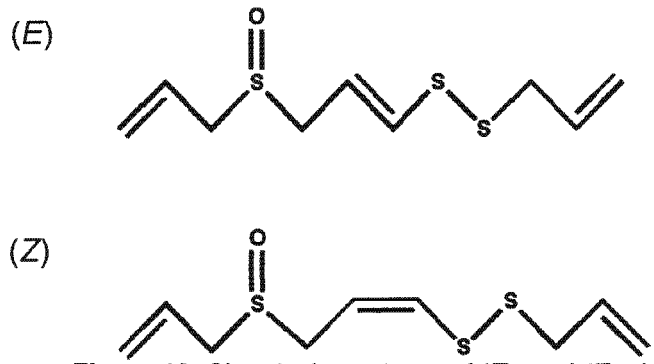

Figure 10. Chemical structures of (*E*)- and (*Z*)-ajoene.

Ajoene or 4,5,9-trithiadodeca-1,6,11-triene-9-oxide has a wide range of activities which includes antithrombotic,[72] antimicrobial,[73] antifungal,[74] antiviral,[75] cytostatic and cytotoxic,[76] hypocholesterolemic,[77] antidiabetic,[78] immunosuppressive and antineoplastic[79] and most interestingly anti-HIV[80] as well as other effects. Its isolation and *in vitro* inhibition of human platelet aggregation were reported in 1983.[72] While many studies of the pharmacological effects of ajoene continued to employ mixtures of the two isomers, more recent studies also gave attention to establishing their individual properties. Thus, both (*E*)- and (*Z*)-ajoene were recently shown to possess antidiabetic activity[78] and hypocholesterolemic activity,[77] and to lower the levels of uric acid in the blood,[81] while (*E*)-ajoene was specifically used to control the fungus Candida Albicans[82] at doses of 5 μg cm^{-3} and (*Z*)-ajoene as an experimental antileukemic, was recently shown to induce apoptosis in human promyeloleukemic HL-60 cells.[83] Our interest in ajoene focused on its possible complexation with cyclodextrins, which could result in the formation of inclusion complexes with potential medicinal applications. We considered an approach in which well-defined, pharmacologically active constituents are selected for inclusion to be more desirable than one employing mixtures or whole extracts.

Aims and objectives

In the present study, we underscore this approach by investigating the inclusion properties of the individual *E* and *Z* isomers of ajoene. A practical advantage to be gained by CD inclusion complex formation in this instance is the conversion of these liquid guests into solids, rendering them more manageable for formulation. Production of stoichiometric inclusion complexes should further contribute to reproducible dosage formulations. Many other advantages may be gained from CD inclusion: the masking of offensive tastes and odours, better control of the release rate of drugs using suitably selected CDs, protecting oxidizable drugs from air oxidation through inclusion, stabilising volatiles and the solubility enhancement of water-insoluble drugs.[84] Finally, the bioavailability of ajoene should be improved, as usually results when drugs are administered in the form of their CD inclusion complexes.[2] The bioavailability of an orally administered drug depends on several factors such as the dissolution rate, solubility and the rate of intestinal absorption.[84] CD inclusion of drugs usually enhances oral bioavailability through an increased dissolution rate affording a fine dispersion in the gastrointestinal fluids.[84] The protection from heat-induced decomposition, sublimation and loss through volatility by CD complexation has been well demonstrated for many drugs such as salicylic acid,[85] vitamin D_3,[86] essential oils,[87] and nitroglycerin.[84,88] In the case of nitroglycerin, on complexation with CDs, it was found that after being stored for 108 h at 40°C a minimum of 50% of the nitroglycerin was detectable. When, instead, nitroglycerin was mixed with an inert excipient (pullulan), after 16 h no nitroglycerin was detectable.

Previous use of CDs in relation to ajoene involved dissolution of its precursor allicin in water and/or a water miscible solvent and complexation of the allicin with α-, β-, or γ-CD or a mixture of these. Further processing evidently led to the subsequent formation of ajoene and its recovery by decomplexation and extraction of the dried complex.[89]

In this dissertation we report the preparation of inclusion complexes formed between (*E*)- and (*Z*)-ajoene and the hosts α-, β-, γ-CD, DIMEB and TRIMEB, as well as their characterisation by thermal analysis, hot stage microscopy, powder X-ray diffraction, FTIR, ^{1}H-NMR, UV spectrophotometry and single crystal X-ray diffraction. Here, PXRD is used in the identification of new cyclodextrin inclusion complexes while the output (PXRD trace) is used in conjunction with a set of reference traces for CD inclusion complexes to determine their isostructural class or series. Single crystal X-ray diffraction was used to determine the modes of guest inclusion in two cases. Thermal analysis and hot stage microscopy were used during the thermal characterisation of the complexes while UV spectrophotometry was used to determine host-guest ratios of the inclusion complexes. Infrared spectroscopy and ^{1}H-NMR were utilised to determine the effect of CD inclusion on the characteristic stretching frequencies and resonances of the guest.

REFERENCES

1. Frömming, K.H., Szejtli, J. *Topics in inclusion science - Cyclodextrins in pharmacy*, Kluwer Academic Publishers, Dordrecht, The Netherlands, **1993**, Vol. 5, Chapter 1.
2. Szejtli, J. *Chem. Rev.*, **1998**, 98, 1743.
3. Takaha, T., Yanase, M., Takata, S., Okada, S., Smith, S.M. *J. Biol. Chem.*, **1996**, 271, 2902.
4. Saenger, W., Jacob, J., Gessler, K., Hoffman, D., Sanbe, H., Koizumi, K., Smith, S.M. and Takaha, T. *Chem. Rev.*, **1998**, 98, 1787.
5. Nakagawa, T., Ueno, K., Koshiwa, M., Watanabe, J. *Tetrahedron Lett.*, **1994**, 35, 1921.
6. Villiers, A. *Compt. Rend.*, **1891**, 112, 536.
7. Schardinger, F.Z. *Unters. Nahr. u. Genussm.*, **1903**, 6, 865.
8. Schardinger, F.Z. *Wien. Klin. Wochenschr.*, **1904**, 17, 207.
9. Schardinger, F.Z. *Zentralbl. Bakteriol. Parasintek. Abt. 2*, **1905**, 14, 772.
10. Schardinger, F.Z. *Zentralbl. Bakteriol. Parasintek. Abt. 2*, **1911**, 29, 188.
11. Pringsheim, H. *Chemistry Of Saccharides*, McGraw-Hill: *New York*, **1932**, 280.
12. Pringsheim, H. *A Comprehensive Survey of Starch Chemistry*; Walton, R.P., Ed., Chemical Catalogue Co., Inc.: New York, NY, **1928**, 35.
13. Freudenberg, K., Rapp. W. *Ber. Dtsch. Chem. Ges.*, **1936**, 69, 2041.
14. Freudenberg, K., Boppel, H. Meyes-Delius, M., *Naturwissen-Schaften*, **1938**, 26, 123.
15. Karrer, P., Nägeli, C. *Helv. Chim. Acta.*, **1921**, 4, 169.
16. Miekeley, A. *Ber. Dtsch-Chem. Ges.*, **1932**, 65, 69.
17. French, D., Rundle, R.E. *J. Am. Chem. Soc.*, **1942**, 64, 1651.
18. Freudenberg, K., Cramer, F.Z. *Naturforsch.*, **1948**, 3b, 346.
19. French, D. *Adv. Carbohydr. Chem.*, **1957**, 12, 189.
20. Cramer, F. *Einschlusverbindungen (Inclusion Compounds)*, Springer-Verlag: Berlin, **1954**.

21. Freudenberg, K., Cramer, F., Plieninger, H. ***Ger. Patent*** 895-769, **1953**.

22. Hybl, A., Rundle, R.E., Williams, D.E. *J. Am. Chem. Soc.,* **1965**, 87, 2779.

23. Saenger, W. *Angew. Chem. Int. Ed. Engl.*, **1980**, 19, 344.

24. Saenger, W. In *Inclusion Compounds*, Atwood, J.L., Davies, J.E.D., MacNicol, D.D., (eds.), Oxford University Press, London, **1984**, Vol. 2, Chapter 8.

25. Harata, K. In *Inclusion Compounds*, Atwood, J.L., Davies, J.E.D., MacNicol, D.D., (eds.), Oxford University Press, London, **1991**, Vol. 5, Chapter 9.

26. Harata, K., Hirayama, F., Arima, H., Mekama, K., Miyaji, T. *J. Chem. Soc. Perkin Trans. 2*, **1992**, 7, 1159.

27. Caira, M.R., Griffith, V.J., Nassimbeni, L.R., van Oudtshoorn, B. *J. Chem. Soc., Perkin Trans. 2*, **1994**, 10, 2071.

28. Harata, K. *Chem. Rev.,* **1998**, 98, 1803.

29. Saenger, W., Jacob, J., Gessler, K., Steiner, T., Hoffmann, D., Sanbe, H., Koizumi, K., Smith, S.M. and Takaha, T. *Chem. Rev.*, **1998**, 98, 1787.

30. Rees, D.A. *J. Chem. Soc.,* (B), **1970**, 877.

31. Schonberger, B.P., Jansen, A.C.A. and Janssen, L.H.M. in *Proceedings of the 4th International Symposium on Cyclodextrins*, Munich, (eds.), Huber, O. and Szejtli J., Kluwer, Dordrecht, **1988**, 61.

32. Szejtli, J. In *Comprehensive Supramolecular Chemistry, Cyclodextrins*, Atwood, J.L., Davies, J.E.D., MacNicol, D.D., Vogtle, F., (eds.), Pergamon: Oxford, **1996**, Vol. 3, Chapter 2.

33. Bruck, T.K., Weinhold, F. *J. Am. Chem. Soc.*, **1979**, 101, 1700.

34. Szejtli, J. *Cyclodextrin Technology*, Kluwer, Dordrecht, **1988.**

35. Perez, S., St-Pierre, J., Marchesault, R.H. *Can. J. Chem.*, **1978**, 56, 2866.

36. Harata, K. In *Comprehensive Supramolecular Chemistry, Cyclodextrins*, Atwood, J.L., Davies, J.E.D., MacNicol, D.D., Vogtle, F., (eds.), Pergamon: Oxford, **1996**, Vol. 3, Chapter 9.

37. Liu, L., Guo, Q-X. *J. Incl. Phenom. Macrocycl. Chem.*, **2002**, 42, 1.

38. Rekharsky, M.V., Inoue, Y. *Chem. Rev.*, **1998**, 98, 1875.

39. Bender, M.L., Komiyama, M. *Cyclodextrin Chemistry*, Springer-Verlag, Berlin, **1978**.

40. Hallen, D., Schoen, A., Shehatta, I., Wadsoe, I. *J. Chem. Soc. Faraday Trans.*, **1992**, 88, 2859.

41. Rekharsky, M.V., Mayhew, M.P., Goldberg, R.N., Ross, P.D., Yamashoji, Y., Inoue, Y. *A. J. Phys. Chem.*, **1997**, 101, 87.

42. Matsui, Y., Mochida, K. *Bull. Chem. Soc. Jpn.*, **1979**, 52, 2808.

43. Barone, G., Castranuovo, G., Del Vecchio, P., Elia, V., Muscetta, M. *J. Chem. Soc. Faraday Trans. 1*, **1986**, 82, 2089.

44. Fujiwara, H., Arakawa, H., Murata, S., Sasaki, Y. *Bull. Chem. Soc. Jpn.*, **1987**, 60, 3891.

45. Sanemasa, I., Osajima, T., Deguchi, T. *Bull. Chem. Soc. Jpn.*, **1990**, 63, 2814.

46. Harrison, J.C., Eftink, M.R. *Biopolymers,* **1982**, 21, 1153.

47. Tabushi, I., Kiyosuke, Y., Sugimoto, T., Yamamura, K. *J. Am. Chem. Soc.*, **1978**, 100, 916.

48. Ross, P.D., Rekharsky, M.V. *Biophys. J.*, **1996**, 71, 2144.

49. Sakurai, M., Kitagawa, M., Hoshi, H., Inoue, Y. *Chem. Lett.*, **1988**, 895.

50. Frömming, K.H., Szejtli, J. *Topics in inclusion science - Cyclodextrins in pharmacy.* Kluwer Academic Publishers, Dordrecht, The Netherlands, **1993**, Vol. 5, Chapter 2.

51. Harata, K. *Seimei Kogaku Kogyo Gijutsu Kenkyusho Kenkyu Hokoku*, **1993**, 1, 1.

52. Caira, M.R., Bourne, S.A., Mhlongo, W.T. and Dean, P.M. *Chem. Commun.*, (in press **2004**).

53. Frömming, K.H., Szejtli, J. *Topics in inclusion science - Cyclodextrins in pharmacy.* Kluwer Academic Publishers, Dordrecht, The Netherlands, **1993**, Vol. 5, Chapter 4.

54. Caira, M.R., Griffith, V.J., Nassimbeni, L.R., van Oudtshoorn, B. *J. Chem. Soc., Chem. Commun.*, **1994**, 9, 1061.

55. Mentzafos, D., Mavridis, I.M., Le Bas, G. and Tsoucaris, G. *Acta Crystallogr., Sect. B*, **1991**, B47, 746.

56. Caira, M.R. *Rev. Roum. Chim.,* **2001**, 46, 371.

57. Cambridge Structural Database and Cambridge Structural Database System, Version 5.25, November **2003**, Cambridge Crystallographic Data Center, University Chemical Laboratory, Cambridge, England.

58. Caira, M.R., Bourne, S.A., Vilakazi, S.L. and Reddy, L. *Supramol. Chem.*, **2004**, 16, 279.

59. Kálmán, A., Párkányi, L., Argay, G. *Acta Crystallogr. Sect. B: Struct. Sci.,* **1993**, B49, 1039.

60. Caira, M.R. *Isostructurality of Inclusion Compounds, In Encyclopedia of Supramolecular Chemistry*, Atwood, J.L., Steed, J.W., (eds.), (in press **2004**).

61. Fábián, L., Kálmán, A. *Acta Crystallogr. Sect. B: Struct. Sci.,* **1999**, B55, 1099.

62. Dunitz, J.D. *X-ray Analysis and the Structure of Organic Molecules.* London: Cornell University Press, **1979**.

63. Kálmán, A. Párkányi, L., *Advances in Molecular Structure Research,* Hargittai, M. and Hargittai, I., (eds.), Greenwich, CT: JAI Press., **1997**, Vol. 3, 189.

64. Kálmán, A. *Fundamental Principles of Molecular Modeling.* Gans, W., Ammon, A., Boeyens, J.C.A., (eds.), Plenum Press: New York, **1996**, 209.

65. Giordano, F., Bettini, R., Donini, C., Gazzaniga, A., Caira, M.R., Zhang, G.G.Z., and Grant, D.J.W. *J. Pharm. Sci.*, **1999**, 88, 1210.

66. Caira, M.R., Nassimbeni, L.R., Vujovic, D. and Weber, E. *J. Chem. Soc., Perkin Trans.* 2, **2001**, 861.

67. Caira, M.R., le Roex, T., Nassimbeni, L.R. *Chem. Commun.*, **2001**, 2128.

68. Qi, R., Wang, Z. *Trends Pharmacol. Sci.,* **2003**, 24, 62.

69. Agarwal, K.C. *Med. Res. Rev.*, **1996**, 16, 111.

70. Block, E., Ahmad, S., Jain, M.K., Crecely, R.W., Apitz-Castro, R., Cruz, M.R. *J. Am. Chem. Soc.,* **1984**, 106, 8295.

71. Block, E., Ahmad, S., Catalfamo, J.L., Jain, M.K., Apitz-Castro, R. *J. Am. Chem. Soc.*, **1986**, 108, 7045.

72. Apitz-Castro, R., Cabrera, S., Cruz, M.R., Ledezma, E. and Jain, M.K. *Thromb. Res.*, **1983**, 32, 155.

73. Whitmore, B.B., Naidu, A.S. USA. Editor(s): Naidu, A. S., *Natural Food Antimicrobial Systems,* Publisher: CRC Press LLC, Boca Raton, F., **2000**, 349.

74. Yoshida, S., Kasuga, S., Hayashi, N., Ushiroguchi, T., Matsuura, H., Nakagawa, S. *Appl. and Environ. Microb.*, **1987**, 53, 615.

75. Weber, N.D., Andersen, D.O., North, J.A., Murray, B.K., Lawson, L.D., Hughes, B.G. *Planta Med.*, **1992**, 58, 417.

76. Baydoun, H., Wagner, K.G., Wagner, R., Plank-Schumacher, K., Scharfenberg, K., Jain, M.K., Apitz-Castro, R. Ger. Offen. Patent Application: DE 88-3821964 19880629, **1990**.

77. Hibi, K. Application: JP 2000-18521 20000127, **2001**.

78. Hibi, K. Application: JP 2000-122588 20000424, **2001**.

79. Tatarintsev, A.V., Turgiev, A.S., Davidson, J.B. (USA), U.S., Application: US 96-584038 19960111, **1999**.

80. Walder, R., Kalvatchev, Z., Garzaro, D., Barrios, M.M., Apitz-Castro, R. *Biomed. & Pharmacother.*, **1997**, 51, 397.

81. Hibi, K. Patent application JP 2000-18522-20000127, **2001**.

82. Yoshida, S., Nakagawa, S., Gokuchi, T., Matsura, H. and Uesugi, T. Patent application JP 86-105429-19860508, **1987**.

83. Min, L., Min, J-M., Cui, J.R., Zhang, L-H., Wang, K., Valette, A., Davriche, C., Wright, M. and Leung-Tack, J. *Nutr. Cancer*, **2002**, 42, 241.

84. Nagai, T. and Ueda, H. In *Comprehensive Supramolecular Chemistry*, *Cyclodextrins*, Atwood, J.L., Davies, J.E.D., MacNicol, D.D., Vogtle, F., (eds.), Pergamon: Oxford, **1996**, Vol. 3, Chapter 14.

85. Frömming, K.H., Sandman, R. and Weyermann, I. *Dtsch. Apoth. Z.*, **1972**, 112, 707.

86. Szejtli, J., Bolla, E. *Starch*, **1980**, 32, 386.

87. Ikeda, Y., Matsumoto, K., Kunihiro, K., Fuwa, T., and Uekama, K. *Yakugaku Zasshi*, **1982**, 102, 83.

88. Tomono, K., Ueda, H., Saitoh, T. and Nagai, T. *Yakuzaigakui.*, **1987**, 47, 133.

89. Dressnandt, G., Rockinger, H., Prigge, H. and Treiber, A. Patent application Ep 96-100318 19960111, **1996**.

Long Room at UCT 1974

Luigi Nassimbeni with his first PhD students, Mino Caira and Allen Rodgers.

CHAPTER 2

EXPERIMENTAL MATERIALS AND METHODS

Host compounds

α-Cyclodextrin, β-cyclodextrin, γ-cyclodextrin, DIMEB and TRIMEB were obtained from Cyclolab [Budapest, Hungary] and were used as received.

Guest compounds

(*E*)- and (*Z*)-ajoene were synthesised and supplied by Professor Roger Hunter of the Department of Chemistry, University of Cape Town, South Africa. Synthesis was performed according to Block *et al.*[1] Further details are given in chapter 3.

Complex preparation and crystal growth

Complexes of ajoene with α-, β- and γ-CD were prepared by the co-precipitation method. For co-precipitation, a solution of cyclodextrin was prepared by dissolving a known quantity of cyclodextrin in de-ionised distilled water. An equimolar amount of (*E*)- or (*Z*)-ajoene was added to the solution of cyclodextrin with prolonged stirring. Generally, two methods of crystal growth were used to obtain crystals of sufficiently high quality for X-ray data-collection. These were slow evaporation and crystal growth at elevated temperature. The solutions were left in an open vial so that the solvent (water) could evaporate slowly at room temperature. To reduce the evaporation rate even further the vials were covered with parafilm which was punctured a few times. Complexes of DIMEB and TRIMEB were prepared by dissolving the cyclodextrin in cold

water. Once all the cyclodextrin had dissolved an equimolar amount of (*E*)- or (*Z*)-ajoene was slowly added with stirring. The solutions were placed in a water bath on a hot plate stirrer set to *ca.* 60°C. Crystal growth occurred at elevated (*ca.* 60°C) temperature overnight. The solubility of TRIMEB and DIMEB decreases with an increase in temperature.

THERMAL ANALYSIS

Thermal analysis is the measurement of changes in physical properties of a substance as a function of temperature, whilst the substance is subjected to a controlled temperature programme.[2] The main methods employed here are Hot Stage Microscopy (HSM), Thermogravimetric analysis (TGA) and Differential Scanning Calorimetry (DSC).

HSM

HSM can be used as a tool for the visual characterisation of those events which are not fully characterised by the standard techniques of TGA and DSC. Events such as colour or opacity changes in crystals which go undetected by the DSC and TGA methods are easily captured by HSM. In hot stage microscopy it is also possible to detect guest loss by immersing the complex crystal in high boiling inert oil such as silicone oil and observing the emergence of bubbles upon guest release. Most importantly it plays a complementary role alongside that of the more traditional TGA and DSC methods of analysis. For this study, all crystals were immersed in silicone oil between two glass coverslips and then positioned on a Linkam THMS600 hot stage apparatus fitted with a Linkam TP92 manual temperature controller. The

hot stage was mounted on a Nikon SMZ-10 stereoscopic microscope. The images were captured using a real time Sony Digital Hyper HAD colour video camera and analysed using the Soft Imaging System program, analySIS.[3]

TGA and DSC

TGA is the measurement of changes in the sample mass with temperature made using a thermobalance which is an electronic microbalance coupled to a furnace with an associated temperature programmer. In the DSC technique, the sample (s) and a reference (r) material are maintained at the same temperature throughout ($\Delta T = T_s - T_r = 0$). In other words, the energy difference in the independent supplies to the sample and reference are recorded against the temperature.[2] Some of the various uses of thermal analysis are determination of accurate melting points, measurement of onset temperature (T_{on}) for desolvation, characterisation of purity, degradation, desorption, phase transformations, polymorphic changes and thermal stability.[4]

All TGA and DSC runs were performed on a Perkin Elmer PC7-Series instrument, more specifically PE-TGA7 and PE-DSC7 for the TGA and DSC respectively. The experimental traces for both TGA and DSC were recorded at a scanning rate of 10 K min^{-1} and under an inert atmosphere of N_2 gas with a flow rate of 30 cm^3 min^{-1}. The sample masses ranged between 4-7 mg for both TGA and DSC. In the case of the DSC, 50 μL crimped, vented aluminium pans were used. The results obtained were plotted by a Hewlett Packard Colour plotter connected to the thermal station. The calibration of the

TGA instrument was performed against the Curie points of alumel (163°C) and nickel (354°C) and the balance calibrated using a standard (100 mg) mass. The DSC was calibrated by measuring the onset temperatures of indium (156.6°C) and zinc (419.5°C) while the heat flow was calibrated from the enthalpy of fusion of indium (28.62 J/g).

POWDER X-RAY DIFFRACTION

Powder X-ray diffraction (PXRD) patterns were recorded using a Huber Imaging Plate Guinier Camera 670 using nickel-filtered $CuK\alpha_1$ radiation (λ = 1.5405981 Å) produced at 40 kV and 20 mA by a Philips PW1120/00 generator fitted with a Huber long fine-focus tube PW2273/20 and a Huber Guinier Monochromator Series 611/15. For high temperature PXRD, the Huber High Temperature Controller HTC 9634 unit was used with the capillary rotation device 670.2. All samples were manually ground and packed into Lindemann capillaries with an internal diameter of 1 mm and a glass thickness of 0.01 mm. The capillaries were obtained from Hilgenberg, Germany. Samples for PXRD were generally not amenable to sieving. A 2θ range of 4 - 100.0° was used with a step size of 0.005° 2θ. The PXRD patterns of the materials suspected to be complexes were overlaid on reference patterns of hosts and known complexes to establish (a) whether they were inclusion complexes, and if so (b) to which isostructural series they belonged.[5]

For each crystal structure determined in this study by full three dimensional X-ray analysis, refined unit cell parameters, space group symmetry, atomic co-ordinates and thermal parameters were used as input to the program LAZY

PULVERIX[6] in order to generate an idealised PXRD pattern. LAZY PULVERIX uses the formula $I(hkl) = mLp|F(hkl)|^2$, where $I(hkl)$ is the intensity of the reflection with indices *hkl*, *m* is the reflection multiplicity, L the Lorentz factor, *p* the polarization factor, and *F(hkl)* the structure factor. Calculated powder patterns can also be used to conveniently assess the purity of a sample and, when compared with the corresponding experimental patterns, to prove that the crystallographic model is correct.

FOURIER TRANSFORM INFRARED SPECTROSCOPY

The formation of an inclusion compound is known to have an effect on the spectroscopic properties of the guest molecule.[7] Here, Fourier Transform Infrared spectroscopy (*FTIR*) was used in an attempt to determine the effect of cyclodextrin inclusion on the C-S=(O)-C and C=C stretching frequencies of the guest molecules. FTIR spectra were recorded on a Perkin Elmer Spectrum One FTIR spectrophotometer. Samples were prepared by grinding the material in nujol mull® and spectra recorded over the range 600-4000 cm^{-1}. Percentage transmittance was recorded against frequency.

UV SPECTROPHOTOMETRY

UV spectra were recorded on a Cintra 20 UV system at a fixed wavelength of 241 nm for TRIMEB•(*E*)-ajoene•0.5H_2O and 235 nm for TRIMEB•(*Z*)-ajoene. The samples were dissolved in water-ethanol (40/60 v/v). The solutions were placed in 10 mm quartz cuvettes and the concentrations were adjusted such that all absorbance readings were taken between zero and one absorbance unit. Calibration curves for TRIMEB•(*E*)-ajoene•0.5H_2O and TRIMEB•(*Z*)-

ajoene were constructed using the respective λ_{max} for the relevant guest molecule.

NMR SPECTROSCOPY

Crystals and oils (ajoene isomers) were dissolved in deuterated chloroform or in deuterated DMSO and their ^{1}H- and ^{13}C-NMR spectra collected at 400 MHz and 75.5 MHz respectively, on a Varian Unity 400 NMR spectrometer using tetramethylsilane as internal reference for ^{1}H-NMR and $CDCl_3$ (77.00 ppm) for ^{13}C-NMR.

CRYSTAL STRUCTURE DETERMINATION

In each case single crystals of good quality were selected for their ability to extinguish plane-polarised light uniformly. Crystals were mounted on a glass fibre and coated with paratone N oil (Exxon),[8] to prevent the loss of included solvent (water) and to provide a rigid mount in the instance of low temperature data-collection. The glass fibre was mounted on a goniometer head.

X-ray photography

The preliminary unit cell parameters and crystal systems were obtained by X-ray photography. Oscillation and Weissenberg photographs were recorded on a Stoë goniometer with a film radius of 28.65 mm. Photography was performed using nickel-filtered CuKα radiation (λ = 1.5418 Å). The generator settings were 20 mA and 40 kV.

Oscillation method

When the crystal was mounted on the goniometer head it was aligned in such a way that one of the crystallographic axes coincided with the axis of rotation, which in turn was orthogonal to the X-ray beam. The reflections were recorded on film placed in a cylindrical cassette which surrounded the crystal. From the oscillation photography it was possible to determine the unit cell dimension parallel to the oscillation axis – a prerequisite for Weissenberg photography.

Weissenberg method

Weissenberg photography allows the deconvolution of a one-dimensional layer line into two dimensions. This is achieved by simultaneously rotating a crystal and moving the X-ray film parallel to the oscillation axis. This allows the diffraction pattern of the chosen layer line to be spread over the entire film. A screen is used to ensure that only those X-ray reflections corresponding to the selected layer line reach the film. The resulting image is a distorted reciprocal lattice plane. The photographic image was interpreted using a Weissenberg co-ordinate chart to produce an undistorted reciprocal lattice. One is able to determine the remaining two unit cell dimensions plus the angle subtended by these in the unit cell. Also, from the Laue symmetry we were able to determine the crystal system. From the systematic absences the space group was indicated.

Oscillation method

When the crystal was mounted on the goniometer head it was aligned in such a way that one of the crystallographic axes coincided with the axis of rotation, which in turn was orthogonal to the X-ray beam. The reflections were recorded on film placed in a cylindrical cassette which surrounded the crystal. From the oscillation photography it was possible to determine the unit cell dimension parallel to the oscillation axis – a prerequisite for Weissenberg photography.

Weissenberg method

Weissenberg photography allows the deconvolution of a one-dimensional layer line into two dimensions. This is achieved by simultaneously rotating a crystal and moving the X-ray film parallel to the oscillation axis. This allows the diffraction pattern of the chosen layer line to be spread over the entire film. A screen is used to ensure that only those X-ray reflections corresponding to the selected layer line reach the film. The resulting image is a distorted reciprocal lattice plane. The photographic image was interpreted using a Weissenberg co-ordinate chart to produce an undistorted reciprocal lattice. One is able to determine the remaining two unit cell dimensions plus the angle subtended by these in the unit cell. Also, from the Laue symmetry we were able to determine the crystal system. From the systematic absences the space group was indicated.

Data-collection

Crystal intensity data were collected on a Nonius Kappa CCD (Charge Coupled Device) Single Crystal X-ray Diffractometer, using graphite monochromated MoKα radiation (λ = 0.71069 Å) generated by a Nonius FR590 generator operated at 50 kV and 30 mA. All data were measured at 173 K. The low temperatures were maintained by cooling with a constant stream of N_2 gas at a flow rate of 20 cm^3 min^{-1} with the aid of a Cryostream cooler (Oxford Cryosystems UK). Data were corrected for Lorentz-polarisation effects; unit cell refinement and data reduction were performed using the programs DENZO and SCALEPACK.[9] Absorption corrections were not required for either of the structures reported in this study as there was no significant variation in absorption correction factors A* for cylinders with successive values of θ and radius R.[10] The μR values for the crystals of the complexes TRIMEB•(*E*)-ajoene•0.5H_2O and TRIMEB•(*Z*)-ajoene were μR_{min} = 0.021, μR_{max} = 0.058 and μR_{min} = 0.025, μR_{max} = 0.048 respectively, for the reported crystal sizes. Space group determinations were carried out by examining the systematic absences and matching the observed conditions to a known space group.[11] These assignments were confirmed by running the data through the program Xprep.[12]

Structure solution and refinement

The structures were solved either by the Patterson search technique with the program PATSEE[13,14] or by the isomorphous replacement method, using the published coordinates for selected cyclodextrin atoms of an isomorphous structure. In the case where structures were solved by isomorphous

replacement, the published coordinates for the skeleton CD atoms of an isostructural complex were used as a trial model for refinement in the program SHELXL-97.[15] All structures were refined with SHELXL-97 operated through the interface X-seed.[16]

PATSEE

PATSEE attempts to combine the merits of both Patterson search and direct methods techniques in order to position a fragment of known geometry in a unit cell.[13,14] The reflection data are processed with SHELXS[17] using the PSEE command to calculate the sharpened Patterson map and a set of the largest E-values. A fragment search is then performed using PATSEE. The search consists of a rotational search for the best orientation of the fragment followed by a translational search.

The orientation of the search model is determined by a conventional but highly automated real-space Patterson rotation search. A comparison between the weights of a number of vectors (n) produced by the orientations of the search model (w_i) and the closest matching Patterson map vectors (P_i) is used to calculate rotational figures of merit (RFOMs), where

RFOM = $\left(\sum P_i / w_i\right)/n$.

The translational positions of a set of the fragments with the highest RFOM values is located by maximising the weighted sum of cosines of a small number of strong translational-sensitive triple-phase invariants (TPRSUM):

$$\text{TPRSUM} = \left(\sum E_h E_k E_{-h-k} \cos\left(\varphi_h + \varphi_k + \varphi_{-h-k}\right)\right) / \left(\sum E_h E_k E_{-h-k}\right)$$

For the solutions obtained, the correlation between the Patterson function and the intermolecular vector set is used to determine a translational figure of merit (TFOM), in an analogous manner to that for a combined figure of merit (CFOM), with $\text{TFOM} = \left(\sum P_i / w_i\right) / n$.

An *R-index* (R_E) based on *E* magnitudes is computed for sets of solutions with the best TFOM values; thus $R_E = \left(\sum \left\langle \left|E_{obs}\right| - \left|E_{calc}\right| / p \right\rangle\right) / \left(\sum \left|E_{obs}\right|\right)$.

The best solutions are sorted according to a combined figure of merit (CFOM) based upon agreement with the Patterson function (TFOM), triple phase consistency (TPRSUM) and the R-index involving E_{obs} and E_{calc} (R_E), with $\text{CFOM} = \left(0.2x\left(\left(RFOM + TFOM\right)/2\right) + xTPRSUM^{1/2}\right) / R_E$.

PATSEE produces a list of the best solutions found for the fragment. The various fractional coordinate sets can be chosen for partial structure expansion in SHELXS. If the partial structure is successful, atomic coordinates can be inserted for refinement.

SHELXL-97

Refinement in SHELXL-97 involves minimisation of the function $\sum w\left(F_o^2 - F_c^2\right)^2$ using the full-matrix least-squares technique. The agreement between the observed (F_o) and calculated (F_c) structure factors is expressed by the residual index (R_1), where (R_1) is low for a satisfactory model and where

$$R_1 = \left(\sum \| F_o | - | F_c \| \right) / \sum | F_o |.$$

Refinement against F^2 tends to magnify the deviations of the Goodness of Fit, S (defined later), from unity compared with refinement against F and therefore these values are not directly comparable to structures refined against F.

The weighting scheme (w) in $wR_2 = \left[\left(\sum w \left(F_o^2 - F_c^2 \right)^2 \right) / \left(\sum w \left(F_o^2 \right)^2 \right) \right]^{1/2}$ and the parameters a and b were refined for each structure using the following expressions: $w = 1/\left[\sigma^2 \left(F_o^2 \right) + (aP)^2 + bP \right]$ and $P = \left[\max \left(0, F_o^2 \right) + 2F_c^2 \right] / 3$. The terms a and b are chosen in the above weighting scheme to yield constant distributions of $\left[w \left(F_o^2 - F_c^2 \right)^2 \right]$ with $\sin\theta$ and $(F_o / F_{max})^{1/2}$. S (Goodness of Fit) is defined by the expression $S = \left[\sum \left(w \left(F_o^2 - F_c^2 \right)^2 \right) / (n - p) \right]^{1/2}$, where n is the number of reflections and p is the total number of parameters refined. Therefore, for a well-behaved structure S should be close to unity, and the over-determination ratio should be of the order $n/p \approx 10$.

ADDITIONAL RESOURCES

The Cambridge Structural Database (CSD)[18] was used to obtain coordinate data for the fragments used to solve the structures reported in this thesis. Molecular parameters and geometrical data with their associated e.s.d.s and non-bonding distances were calculated using the program PLATON.[19] WinGX[20] was used as an interface for PLATON. Molecular diagrams were created with POV-Ray for Windows.[21] Molecular packing, stereo and CPK

diagrams were produced using the program Weblab ViewerPro Version 3.5.[22] Diagrams showing anisotropic thermal ellipsoids were drawn with the aid of Ortep-3 for Windows.[23]

Table 1 lists the final crystallographic data files pertinent to compounds **9** and **10**.

Table 1. File types found in Appendix 2.

File extension/format	Contents
.HKL	Reflection data
.RES	SHELX co-ordinate data
.CIF	Crystallographic information file
.FCF	Structure factor tables
.LIS	Platon output
.XL	
.SUP	Tabulated supplementary data

References

1. Block, E., Ahmad, S., Catalfamo, J.L., Jain, M.K. and Apitz-Castro, R. *J. Am. Chem. Soc.*, **1986**, 108, 7045.

2. Brown, M.E. *Introduction to Thermal Analysis: Techniques and Applications*, Chapman and Hall, London, New York, **1988**, 1.

3. Soft Imaging System GmbH, *Digital Solutions for Imaging and Microscopy*, Version 3.1 for Windows © **1987-2000**.

4. Giron, D. *Thermochim. Acta*, **1965**, 248, 1.

5. Caira, M.R. *Roum. Chim. Rev.*, **2001**, 46, 371.

6. Yvon, K., Jeitschko, W., Parthé, E. *J. Appl. Crystallogr.*, **1977**, 10, 73.

7. Frömming, K.H., Szejtli, J. *Topics in inclusion science - Cyclodextrins in pharmacy*, Kluwer Academic Publishers, Dordrecht, The Netherlands, **1993**, Vol. 5, Chapter 1.

8. Paratone N oil (Exxon Chemical Co., Texas, USA).

9. Otwinowski, Z., Minor, W., *Processing of X-ray Diffraction Data in Oscillation Mode in* ***Methods in Enzymology***, Vol. 276, Carter, C.W., Sweet, R.M., (eds.), Academic Press, New York, **1997**, 307.

10. *International Tables for Crystallography*, Vol. II: Mathematical Tables, Kasper, J.S. and Lonsdale, K. (eds.), Kynoch Press, Birmingham, England, **1967**, 291.

11. *International Tables for Crystallography*, Vol. C: Mathematical, Physical and Chemical Tables, Wilson, A.J.C. (ed.), Kluwer Academic Publishers, Dordrecht, **1992**, 691.

12. *Data Preparation and Reciprocal Space Exploration*, Version 5.1, © Bruker Analytical X-ray Systems, **1997**.

13. Egert, E. *Acta Crystallogr.*, **1983**, A39, 936.

14. Egert, E., Sheldrick, G.M. *Acta Crystallogr.*, **1985**, A41, 262.

15. Sheldrick, G.M. SHELXL-97, *Program for the Refinement of Crystal Structures*, University of Göttingen, Germany, **1997**.

16. Barbour, L.J. *X-Seed, A software tool for Supramolecular Crystallography, Supramol. Chem.*, **2001**, 1, 189.

17. Sheldrick, G.M. *Crystallographic Computing*, Vol. 3, Sheldrick, G.M., Kruger, C., Goddard, R., (eds.), Oxford University Press, London, **1985**, 175.

18. Cambridge Structural Database and Cambridge Structural Database System, version 5.25, November **2003**, Cambridge Crystallographic Data Centre, University Chemical Laboratory, Cambridge, England.

19. Spek, A.L. PLATON, *A multipurpose crystallographic tool*, Version 10500 © **1980-2000**.

20. Farrugia, L.J. WinGX, An integrated system of windows programs for the solution, refinement and analysis of single crystal X-ray diffraction data, Version 1.63, *J. Appl. Cryst.*, **1999**, 32, 837.

21. Pov-Ray for Windows Version 3.1e.watcom.win32, The persistence of vision development team, © **1991-1999**.

22. Weblab ViewerPro Version 3.5 © **1999** by Molecular Simulations Inc., San Diego, CA.

23. Ortep-3 for Windows: Farrugia, L.J. *J. Appl. Cryst.*, **1997**, 30, 565.

CHAPTER 3

SYNTHESIS AND CHARACTERIZATION OF (E)- AND (Z)-AJOENE (4,5,9-TRITHIADODECA-1,6,11-TRIENE-9-OXIDE)

The synthesis of ajoene proceeded in two main stages, the first being the synthesis of allicin, and the second the rearrangement reaction of allicin to ajoene. Both were carried out as described by Block *et al.*[1] by Professor R. Hunter of the Department of Chemistry, University of Cape Town, South Africa.

Synthesis of allicin

To a solution of diallyl disulfide (10 g, 68 mmol) in glacial acetic acid (30 cm^3), was added hydrogen peroxide (11 cm^3, 8.8 M, 97 mmol) at 4°C, and the reaction mixture was stirred overnight (Scheme 1). Water was then added to the reaction mixture and the product extracted into dichloromethane (3 x 100 cm^3). The combined organic layers were washed with water (2 x 30 cm^3) followed by aqueous Na_2CO_3 (2 x 30 cm^3). The organic layers were dried over $MgSO_4$, the solution filtered and concentrated under reduced pressure to give crude allicin (14.5 g).

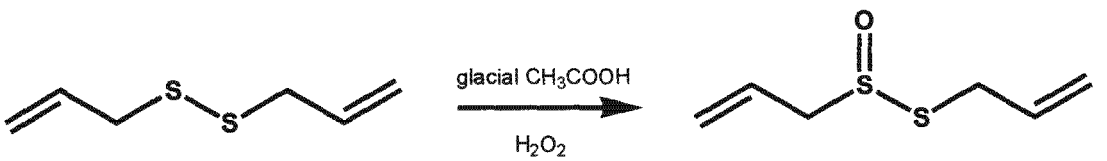

diallyl disulfide allicin

Scheme 1

Synthesis of ajoene

Crude allicin (14.5 g) was dissolved in an acetone/water mixture (2:1, 39 cm^3) (see Scheme 2). The reaction mixture was refluxed with constant stirring for approximately three hours before being concentrated under reduced pressure. The product was then extracted with ethyl acetate (3 x 100 cm^3) and the combined organic layers were dried and concentrated under reduced pressure to give crude ajoene (12 g), which was purified on silica gel (200 g) (eluent ethyl acetate/hexane) to afford a mixture of (*E*)- and (*Z*)-ajoene (1.2 g). This mixture was further subjected to slow silica-gel chromatography (200 g) using ethyl acetate/hexane as before to afford (*Z*)-ajoene (0.33 g, 2.1 %), (*E*)-ajoene (0.33 g, 2.1 %) and a mixture of the two (0.2 g). For clarity, the numbering system used in Scheme 2 follows that used in the crystallographic model (see chapter 5).

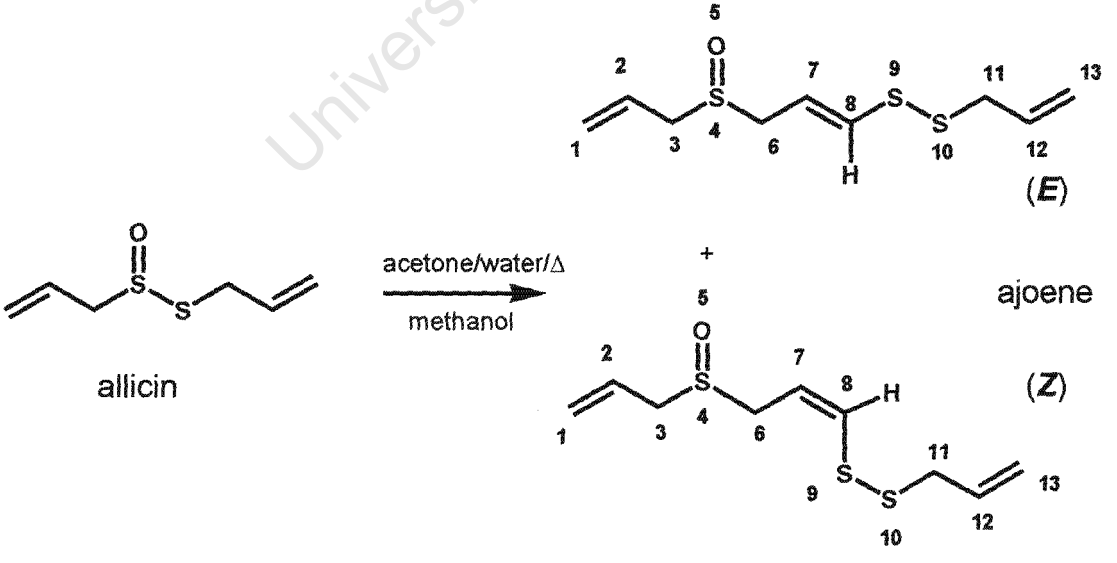

Scheme 2

CHARACTERIZATION OF (E)- AND (Z)-AJOENE

The identity of these isomers (designated (***E***) and (***Z***) hereinafter) was deduced from ^{1}H-NMR and ^{13}C-NMR spectra. For the assignment of *E*- and *Z*-isomers, we used the assignments of Block in his original paper,[1] in which the vinyl H-8 proton attached to carbon C8 (Scheme 1) was used as a marker (doublet in the ^{1}H NMR spectrum, Figures 1 and 2). This appeared at different chemical shifts (δ_H ppm) for (***E***) and (***Z***), at 6.35 and 6.58 ppm respectively, the signal for (***Z***)-H-8 being more downfield than that for (***E***)-H-8. The assignments were based on the coupling constant, which was greater for (***E***)-H-8 (J_{trans} = 14.6 Hz) than for (***Z***)-H-8 (J_{cis} = 9.6 Hz), as shown in Tables 1 and 2 below. The ^{13}C NMR spectra for both isomers gave the expected distribution of three aliphatic (allylic) and six vinylic resonances (Table 3 and Figure 3), and the data are compared in Table 3 with those from Block's original paper.

Table 1. ^{1}H-NMR data for compound (*E*)

(*E*) δ_H (ppm)	(*E*) *J* (Hz)	(*E*) Multiplicity	No. of Protons	Assignment
6.35	14.6	d	1	H-8
5.72-5.94	-	m	3	H-12, H-7, H-2
5.3-5.5	-	m	2	H-1
5.1-5.2	-	m	2	H-13
3.5	-	m	4	H-6, H-3
3.36	-	m	2	H-11

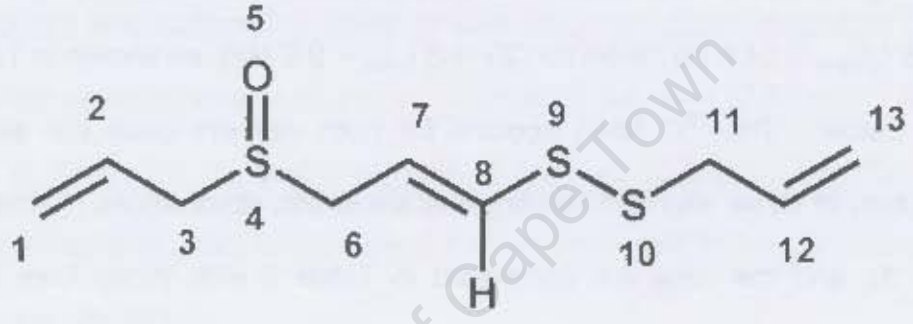

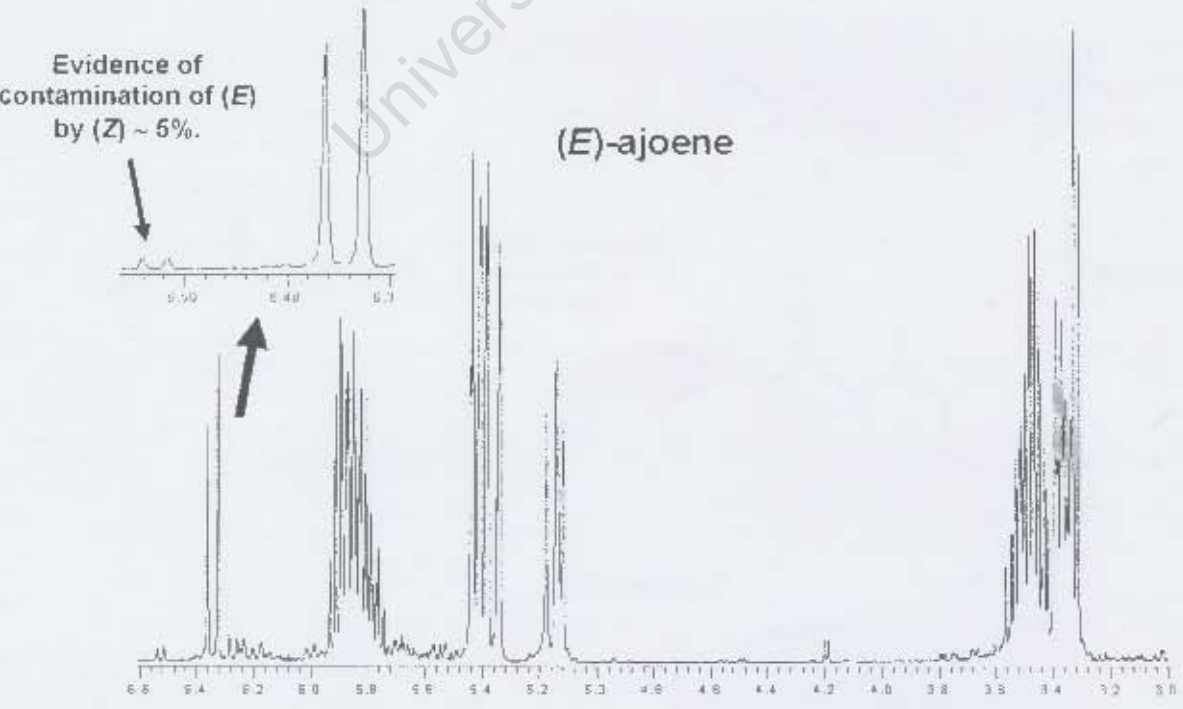

Figure 1. ^{1}H-NMR spectrum for (*E*) with the characteristic doublet at δ 6.35 ppm. J = 14.6 Hz. The insert shows evidence of contamination of (*E*) by (*Z*) δ 6.58 ppm.

Table 2. ^{1}H-NMR data for compound (**Z**).

(Z) δ_H (ppm)	(Z) J (Hz)	(Z) Multiplicity	No. of protons	Assignment
6.57	9.6	d	1	H-8
5.7-6.0	-	m	3	H-12, H-7, H-2
5.39-5.5	-	m	2	H-1
5.15-5.23	-	m	2	H-13
3.6	-	m	4	H-6, H-3
3.35	-	m	2	H-11

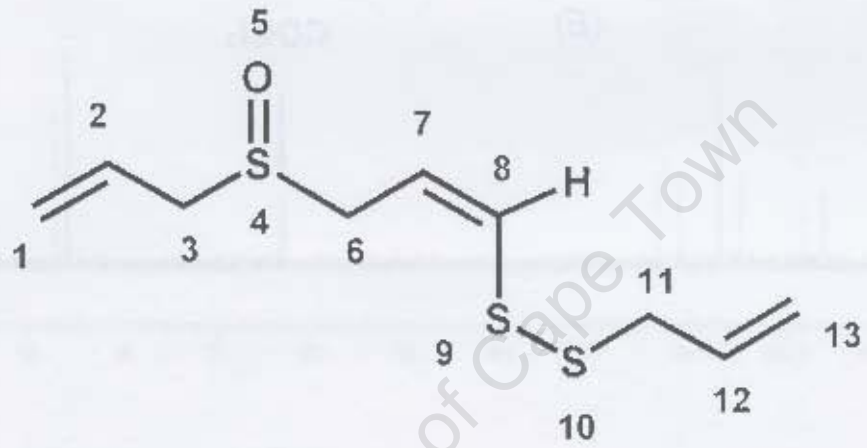

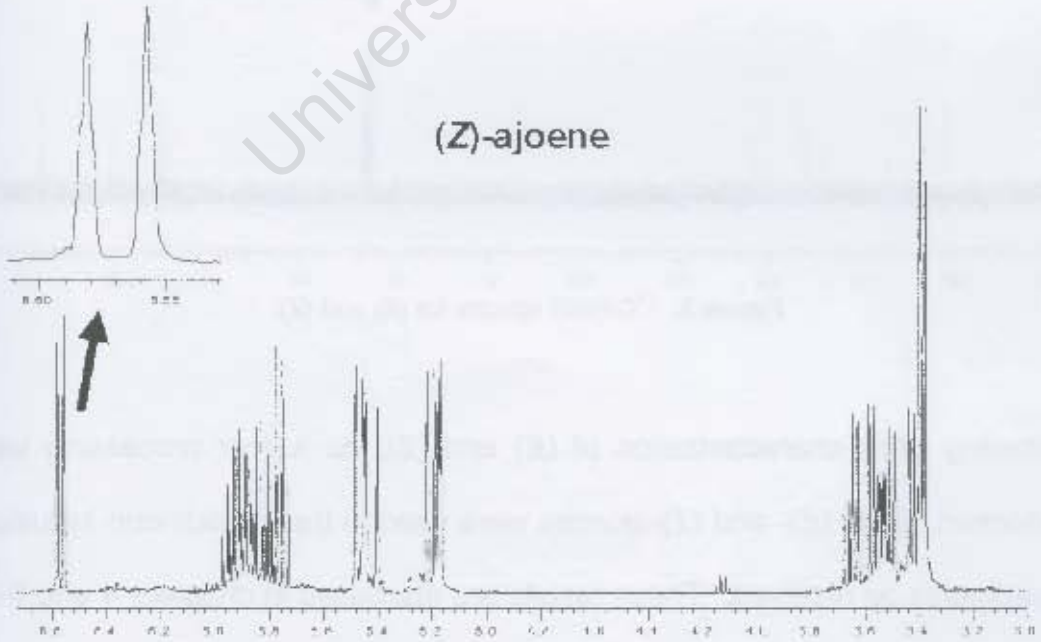

Figure 2. ^{1}H-NMR for (**Z**), identified through the characteristic doublet at δ 6.57 ppm, J = 9.6 Hz.

Table 3. ^{13}C-NMR data for compounds (*E*) and (*Z*).

Assignment	(*E*) δ_C	(*E*) δ_C/Block	(*Z*) δ_C	(*Z*) δ_C/Block
C-11	41.20	41.37	42.13	42.18
C-3	52.93	53.08	49.66	49.73
C-6	54.17	54.48	54.98	55.02
C-13	116.85	116.94	118.10	118.13
C-1	119.06	119.26	119.27	119.32
C-12	123.44	123.74	123.80	123.85
C-2	125.54	125.68	125.69	125.74
C-7	132.40	132.59	132.62	132.64
C-8	134.52	134.75	138.53	138.58

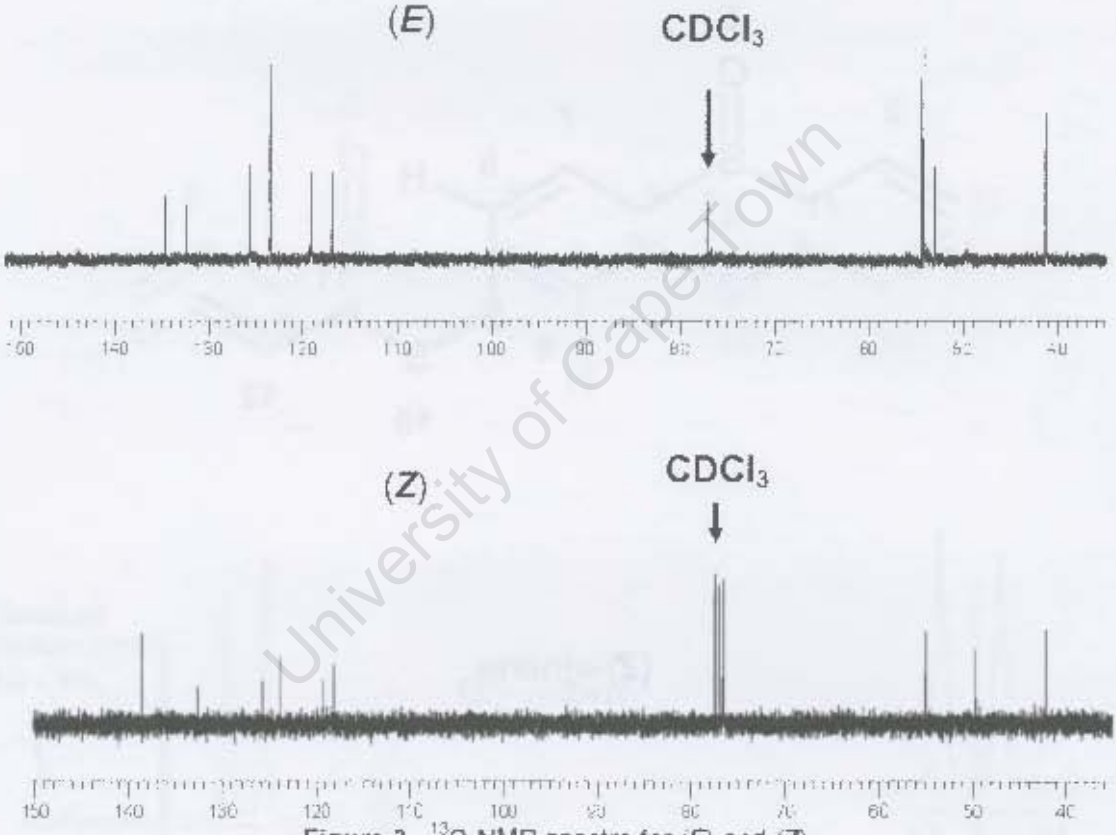

Figure 3. ^{13}C-NMR spectra for (*E*) and (*Z*).

Following NMR characterization of (*E*) and (*Z*), no further processing was performed. Both (*E*)- and (*Z*)-ajoenes were used in the cyclodextrin inclusion experiments as received. These results are discussed in chapters 4 and 5 of this dissertation.

References

1. Block, E., Ahmad, S., Catalfamo, J.L., Jain, M.K. and Apitz-Castro, R. *J. Am. Chem. Soc.* **1986**, 108, 7045.

PREPARATION OF α-, β-, γ-CD AND DIMEB INCLUSION COMPLEXES OF AJOENE AND THEIR CHARACTERISATION USING PXRD

CHAPTER 4

PREPARATION OF α-, β-, γ-CD AND DIMEB INCLUSION COMPLEXES OF AJOENE AND THEIR CHARACTERISATION USING PXRD

Complex preparation

For β-CD, a hot solution of the cyclodextrin was prepared by dissolving a known quantity (105 mg) in distilled de-ionised water (1 cm^3) at *ca.* 65°C. In the case of α- and γ-CD, saturated solutions (77 mg in 0.5 cm^3 and 115.6 mg in 0.5 cm^3, respectively) were prepared at room temperature (*ca.* 26°C). DIMEB solutions were prepared by dissolving the cyclodextrin (106 mg) in cold distilled de-ionised water (0.5 cm^3) at *ca.* 4°C. The DIMEB solutions were further cooled in ice to a temperature of *ca.* 0°C. Once all the cyclodextrin had dissolved, equimolar (0.08 mmol, 20 mg) amounts of (*E*)- or (*Z*)-ajoene were added to the solutions of cyclodextrin followed by prolonged stirring. The DIMEB solutions were placed in a hot water bath and stirred at *ca.* 60°C. The reaction of (*E*)- and (*Z*)-ajoene with the various cyclodextrins resulted in the immediate precipitation of inclusion complexes: α-cyclodextrin•(*E*)-ajoene (**1**), α-cyclodextrin•(*Z*)-ajoene (**2**), β-cyclodextrin•(*E*)-ajoene (**3**), β-cyclodextrin•(*Z*)-ajoene (**4**), γ-cyclodextrin•(*E*)-ajoene (**5**), γ-cyclodextrin•(*Z*)-ajoene (**6**), DIMEB•(*E*)-ajoene (**7**) and DIMEB•(*Z*)-ajoene (**8**). Filtration was required to isolate the solid phase from the suspension.

The nature of ajoene (an oil-like substance), coupled with the microcrystalline nature of the product complex, results in an increased possibility of obtaining a mixture of phases. For this reason it was decided not to attempt the determination of complex stoichiometry but rather to use PXRD to assign each complex to an isostructural class or series where possible.

The assignment of isostructural class or series is performed bearing in mind that the water content, type, size and orientation of the guest molecule as well as the temperature at which the data were collected affect peak angular positions in the PXRD trace. Therefore we allow a little more leniency in what we define as a close match between reference and experimental patterns.

α-Cyclodextrin inclusion complexes 1 and 2

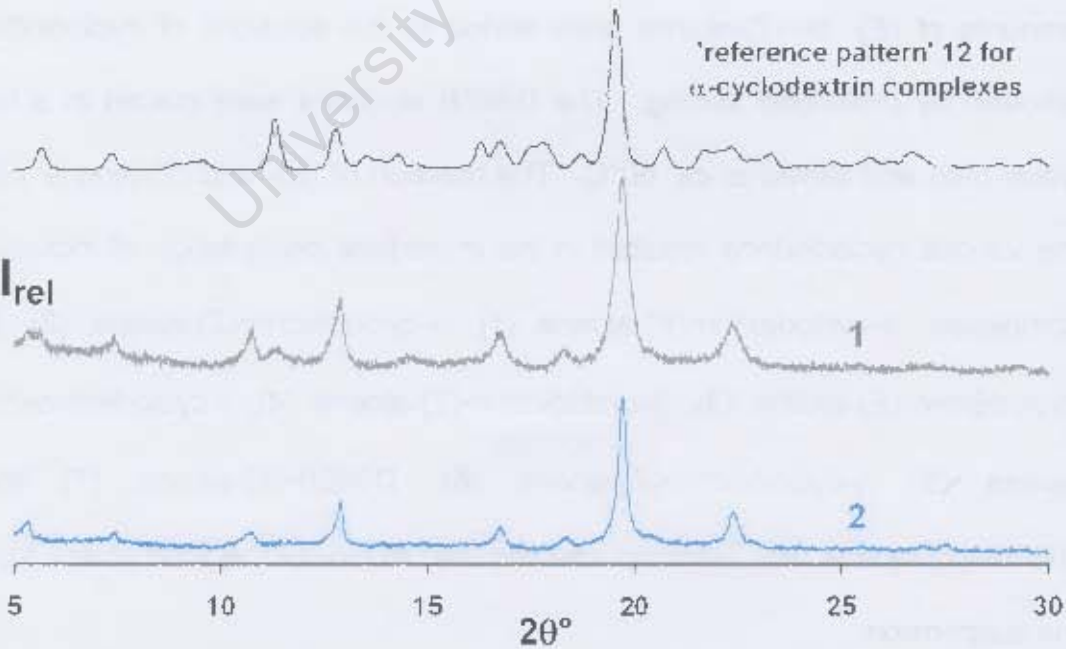

Figure 1. Experimental PXRD traces for complexes **1** and **2** as well as the reference pattern 12 for α-CD complexes.

In comparing traces for the complexes **1** and **2** with the reference patterns for α-CD complexes, we concluded that they matched reference pattern 12

The nature of ajoene (an oil-like substance), coupled with the microcrystalline nature of the product complex, results in an increased possibility of obtaining a mixture of phases. For this reason it was decided not to attempt the determination of complex stoichiometry but rather to use PXRD to assign each complex to an isostructural class or series where possible.

The assignment of isostructural class or series is performed bearing in mind that the water content, type, size and orientation of the guest molecule as well as the temperature at which the data were collected affect peak angular positions in the PXRD trace. Therefore we allow a little more leniency in what we define as a close match between reference and experimental patterns.

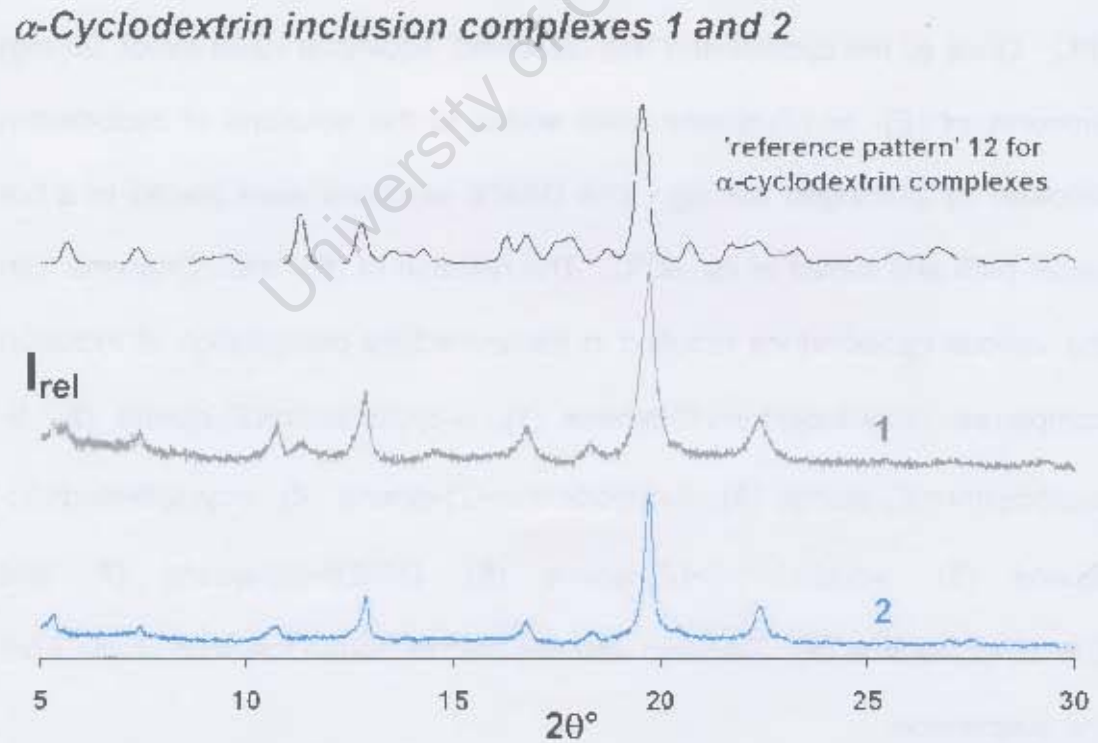

Figure 1. Experimental PXRD traces for complexes **1** and **2** as well as the reference pattern 12 for α-CD complexes.

In comparing traces for the complexes **1** and **2** with the reference patterns for α-CD complexes, we concluded that they matched reference pattern 12

(space group P1, channel packing type (CH)), with a triclinic unit cell. Noticeable from the comparison in Figure 1 is the difference in the peak intensities between experimental and reference patterns. In the known crystal structures of such complexes (e.g. Sicard-Roselli *et al*)[1], the host α-CD molecules are stacked along the crystallographic c-axis to form columns with infinite internal channels. The α-CD molecules are arranged in an alternating head-to-head and tail-to-tail sequence. The approximate unit cell dimensions for complexes **1** and **2**, deduced by comparison with the reference pattern are given in Table 1.

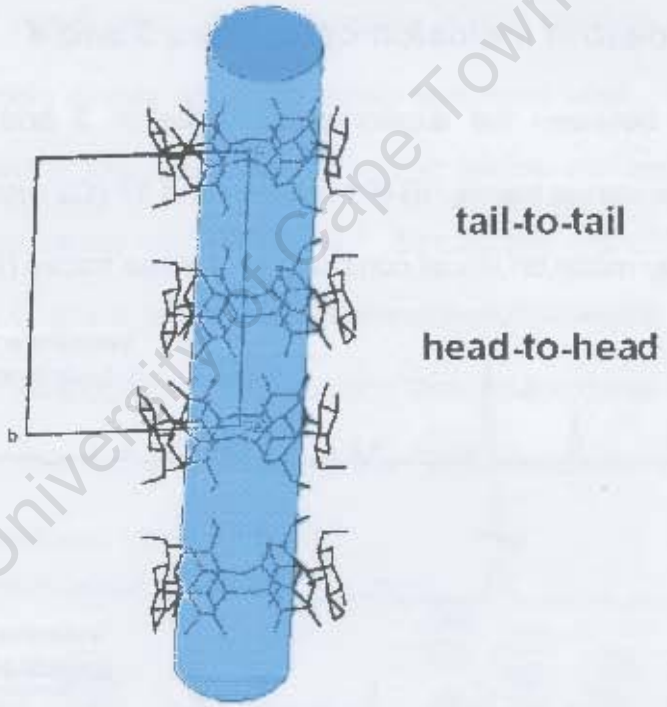

Figure 2. View of the unit cell of the α-CD complex illustrating the head-to-head and tail-to-tail alternating sequence of the host molecules. The blue shaded region shows the infinite channel that accommodates the guest. It also shows the slight misalignment of the head-to-head cyclodextrins.

The choice of channel packing type structure could have been predicted with a degree of certainty for the host α-CD with the guests (*E*)- and (*Z*)-ajoene. It is relatively well established from a survey performed by R. K. McMullan *et al*.[2] that α-CD forms cages when complexed with small molecular guests such

as acetic acid, propionic acid and butyric acid. In the case of long molecular or ionic guests, channels are preferred, a clear and well-defined size-selectivity. Ajoene is a long molecular guest and based on the evidence, has obeyed the size-selectivity rule, lending more support for the choice in reference pattern.

Table 1. Approximate unit cell dimensions for the α-CD complexes.

COMPLEX	Space group	No.	a (Å)	b (Å)	c (Å)	α (°)	β (°)	γ (°)
(1) and (2)	P1	12	13.8	13.9	15.7	93.0	91.8	119.4

β-Cyclodextrin inclusion complexes 3 and 4

A match between the experimental traces of **3** and **4** and isostructural classes/reference traces, 16 (P1 triclinic) and 17 (C2 monoclinic) respectively, were easily made on visual comparison of these traces (Figure 3).

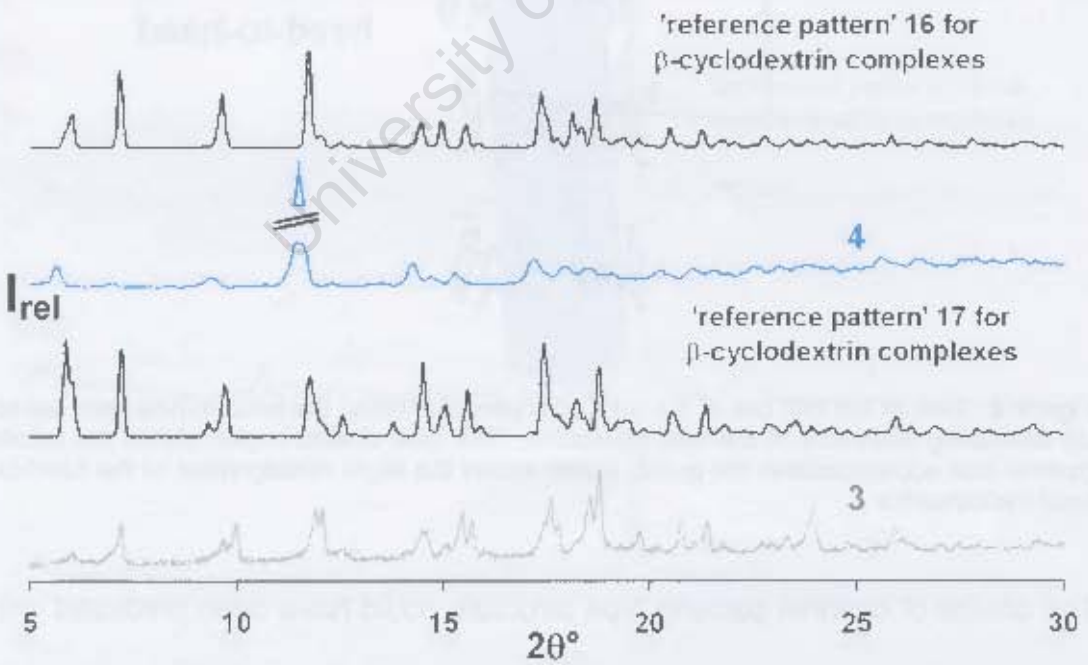

Figure 3. The experimental traces of complexes **3** and **4** compared with reference patterns 16 and 17.

Most encouraging is the agreement of the diffraction peak angles of **3** and **4** with those of the reference traces. It can readily be seen that there are distinct

differences in the peak intensities, which are directly related to differences in the guest and its orientation. On more careful examination of the fine structure of individual experimental traces, it is noticeable that the trace for **3** resembles reference trace 17 more closely than it does 16, while **4** is a better match of 16. This is especially evident from the peaks at 10° and 12° 2θ for all four traces.

Both of the space groups P1 and C2 are characteristic of dimeric β-CD complexes and both are associated with the channel (CH) packing mode (see Figure 4). The net result of a dimeric complex is the creation of double volume cavities wherein guests are more easily accommodated. In special circumstances the metric properties of the triclinic lattice are such that an alternative, monoclinic lattice can be found.[3] Structurally the difference is subtle: the CD-dimer in space group P1 possesses pseudo-twofold symmetry while in C2 it has a crystallographic diad passing through the dimer interface.[3] As a consequence of this subtle relationship the PXRD traces for P1 and C2 are virtually indistinguishable (see Figure 3).[3]

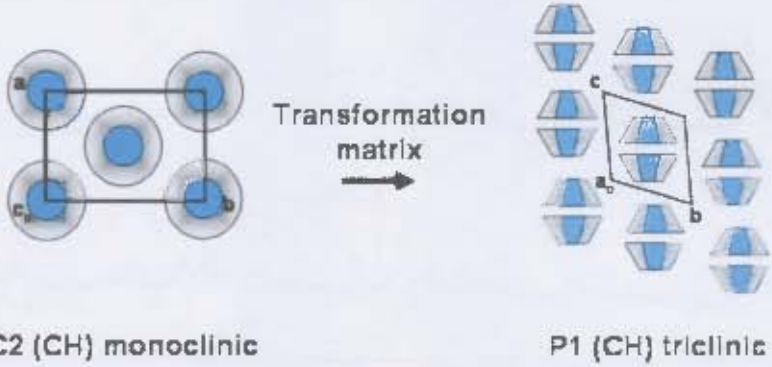

Figure 4. A diagrammatic representation of the channel packing mode for the space groups P1 and C2. The main difference is the choice of the unit cell. The blue shaded areas show the double volume cavity generated within a dimeric β-CD complex.

There has been more than one instance where the wrong space group has been assigned for crystal structure refinement.[4,5] Thus, when unit cell dimensions are available from single crystal X-ray diffraction, if two unit cell parameters are equivalent (i. e. two unit cell lengths or two angles), then according to Herbstein and Marsh, it is best to search for higher symmetry.[5] It is important to note that in the absence of Laue symmetry data, one cannot unequivocally choose between P1 or C2. The main aspect of matching an experimental trace to any reference pattern is that one simultaneously obtains the space group and approximate unit cell dimensions (Table 2) for the new complex.

Table 2. Approximate values for the unit cell dimensions of complexes **3** and **4**.

COMPLEX	Space group	No.	a (Å)	b (Å)	c (Å)	α (°)	β (°)	γ (°)
(3)	C2	17	19.3	24.5	15.9	90	109.1	90
(4)	P1	16	15.6	15.6	15.9	101.6	101.6	103.6

γ-Cyclodextrin inclusion complexes 5 and 6

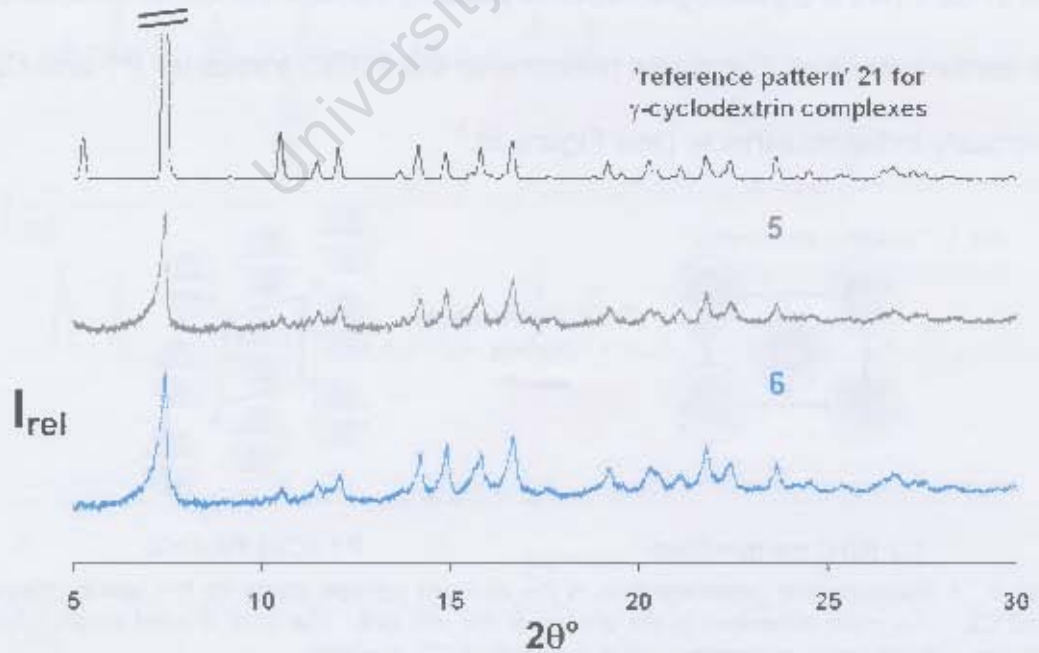

Figure 5. Experimental traces for complexes **5** and **6** with the reference for γ-CD complexes 21.

The experimental PXRD patterns for the γ-CD Complexes **5** and **6** matched

the reference pattern for γ-CD complexes crystallizing in the tetragonal space group $P42_12$ (channel packing mode CH) almost exactly except for the disparity in their peak intensities. It was expected that this match would occur since this space group characterizes all known γ-CD complexes. The relatively small number of peaks in the trace is a reflection of the high symmetry of the space group. One is able to draw certain conclusions from the fact that complexes **5** and **6** matched reference pattern 21: (1) it can be concluded that the guest molecules namely (*E*)- and (*Z*)-ajoene are located in infinite channels formed by the γ-CD molecules in the tetragonal arrangement,[3] (2) it is known from single crystal X-ray analyses that the axis of the host molecule coincides with the tetrad of the space group and thus by implication the guest molecule has at least fourfold disorder.[3] These infinite channels, however, are unique in that they have three cyclodextrin molecules in one asymmetric unit.[6] These are arranged in the head-to-head, head-to-tail and tail-to-tail mode in alternating sequence so that the structure is built up of trimers of γ-CD (Figure 6).[6]

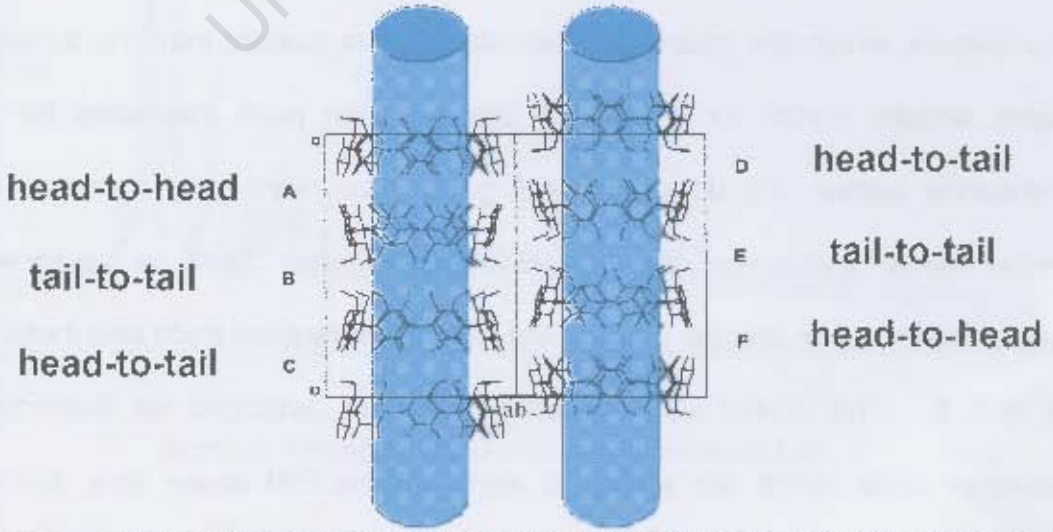

Figure 6. The view along the diagonal *ab* shows the stacking sequence of the trimer in a γ-CD complex with space group $P42_12$. The blue area represents the infinite channels that span the crystal along which the guests are disordered.

The crystal packing is even more complicated since there are two independent stacks in the asymmetric unit. Since the γ-CD molecule is located on a tetrad, only one-quarter is unique. However, there are three independent γ-CD molecules in the unit cell and the asymmetric unit is therefore three quarter molecules of γ-CD.[6] The approximate unit cell dimensions are given in Table 3 below.

Table 3. Approximate unit cell dimensions for the γ-CD complexes.

COMPLEX	Space group	No.	a (Å)	b (Å)	c (Å)	α (°)	β (°)	γ (°)
(5) and (6)	P42,2	21	23.8	23.8	23.2	90.0	90.0	90.0

DIMEB inclusion complexes 7 and 8

A match between the reference pattern 23 ($P2_1$, monoclinic) for DIMEB inclusion complexes was made with the PXRD patterns of the complexes **7** and **8** (Figure 7). There is a considerable mismatch in intensities between the two complexes **7** and **8** with some peak doublets displaying an intensity swap (e.g. the doublet centred at 10° 2θ, Figure 8). Such features must be due to differences in the modes of inclusion of the two ajoene isomers in their complexes, which are otherwise isostructural as is evident from the excellent peak angular match for **7** and **8**. Similarly, the peak intensities for the reference pattern 23 do not reflect good agreement with those of the experimental traces for the complexes, but again there is reasonable agreement in peak angular position between the reference trace and those for **7** and **8**. The crystal packing arrangement is described as monomeric complex units which are arranged along the twofold screw axis, forming infinite chains in a classical herringbone (HB) packing mode (Figure 9).[7] These chains (HB) form sheets parallel to the ab plane which are stacked

seen from Figure 9 that the cavity is isolated by the surrounding cyclodextrin molecules as a result of the inclusion of small guest molecules. The approximate unit cell parameters are presented in Table 4.

Table 4. Approximate unit cell dimensions for the DIMEB complexes.

COMPLEX	Space group	No.	a (Å)	b (Å)	c (Å)	α (°)	β (°)	γ (°)
(7) and (8)	$P2_1$	23	15.1	10.6	23.2	90.0	102.0	90.0

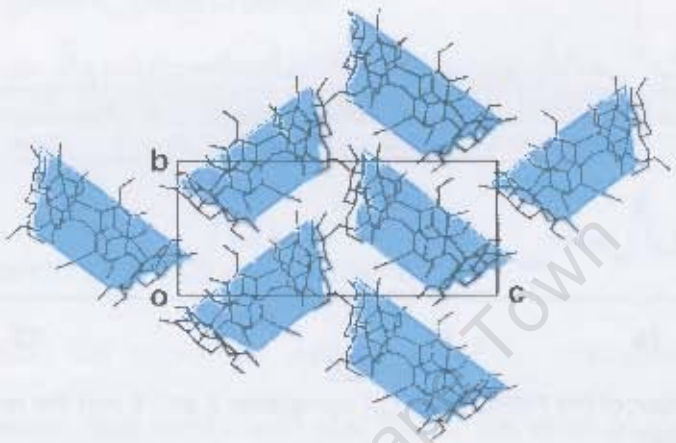

Figure 9. Projection down the *a*-axis showing the (HB) arrangement and the isolated cavities.

CONCLUSION AND DISCUSSION

As the search for newer, faster and more efficient ways of characterizing products (CD complexes) intensifies, driven mainly by the cost of drug development in the pharmaceutical industry, the application of a technique such as PXRD matching based on isostructural series will become more important. This method of characterization provides a considerable amount of information, which may otherwise only be obtained through the crystallization and subsequent complete X-ray structural analysis of the product under investigation. This however is not always possible, as it is often difficult to grow single crystals of CD inclusion complexes of high quality.

In this chapter we have confirmed the formation of eight new cyclodextrin complexes and have classified them into 4 isostructural pairs (**1** & **2**, **3** & **4**, **5** & **6** and **7** & **8**). In two cases we have identified previously unreported isostructural series (α-CD P1 (12) and DIMEB $P2_1$ (23)), confirmed complexation and obtained approximate unit cell dimensions and space groups, while for the other two cases we confirmed complexation, assigned approximate unit cell dimensions and space groups. For **1** and **2**, we concluded that the sizes of the guests (*E*)- and (*Z*)-ajoene respectively, play a role in influencing the type of packing arrangement of the α-CD complexes. As previously mentioned, the size, shape and orientation of the guest molecules greatly influence the intensities of the peaks and fine structure in the diffractogram. For β-CD it is rather interesting that the packing arrangements belong to the dimeric subset of complexes, given the small size and flexibility of the guest molecules. On the other hand γ-CD remained faithful to its preferred packing arrangement for inclusion complexes and confirmed only what was expected. The DIMEB complexes were found to crystallize in the atypical space group $P2_1$ (monoclinic crystal system). Interestingly, the three-dimensional packing arrangement chosen is well suited to small molecules. Evidently this is an instance where the size rule has been obeyed, as with α-CD.

There is little that one can deduce from the diffractogram that would provide information on the role, amount and interaction of interstitial water in the crystal structures. However, we do know that the amount of water present in the crystal structure has a direct effect on the unit cell size, which on the loss

of water from the crystal, is reduced, directly influencing the peak angular positions in the PXRD trace.

CD inclusion complexes are largely unaffected by polymorphism and more specifically there is only one known case that has been published to date.[9] This refers to the crystallization of the inclusion complex β-CD•methylparaben in triclinic and monoclinic modifications at different temperatures. The existence and/or frequency of polymorphism amongst cyclodextrin complexes will determine whether or not isostructurality will be utilised to its full potential as a tool for the identification and characterization of CD inclusion complexes.

Reference

1. Sicard-Roselli, C., Perly, B. and Le Bas, G., *J. Incl. Phenom. Macrocycl. Chem.*, **2001**, 39, 333.
2. McMullan, R.K., Saenger, W., Fayos, J., Mootz, D. *Carbohydr. Res.*, **1973**, 31, 37.
3. Caira, M.R. *Roum. Chim. Rev.*, **2001**, 46, 371.
4. Herbstein, F.H. Marsh, R.E. *Acta. Crystallogr.*, **1998**, B54, 677.
5. Herbstein, F.H. *Acta. Crystallogr.*, **1997**, B53, 968.
6. Saenger, W. *J. Incl. Phenom.*, **1984**, 2, 445.
7. Selkti, M., Navaza, A., Villain, F., Charpin, P. and De Rango, C. *J. Incl. Phenom. Macrocycl. Chem.*, **1997**, 27, 1.
8. Zabel, V., Saenger, W. and Mason, S.A. *J Am. Chem. Soc.*, **1986**, 108, 3664.
9. Caira, M.R., De Vries, E.J.C., Nassimbeni, L.R. *Chem. Commun.*, **2003**, 2058.

PREPARATION, THERMAL ANALYSIS AND STRUCTURAL CHARACTERIZATION OF TRIMEB INCLUSION COMPLEXES OF (E)- AND (Z)-AJOENE

R W James and W L Bragg at UCT 1952

CHAPTER 5

PREPARATION, THERMAL ANALYSIS AND STRUCTURAL CHARACTERIZATION OF TRIMEB INCLUSION COMPLEXES OF (E)- AND (Z)-AJOENE

COMPLEX PREPARATION

TRIMEB solutions were prepared by dissolving the cyclodextrin (0.08 mmol) in cold distilled de-ionised water (0.61 cm^3) at *ca.* 2°C. Once all the cyclodextrin had dissolved, equimolar amounts (0.08 mmol) of (*E*)- and (*Z*)-ajoene were added to the solutions of cyclodextrin with prolonged and vigorous stirring. Precipitates formed immediately on the addition of the respective guest isomers. Each solution was again cooled in an ice bath at *ca.* 2°C until the precipitate dissolved, but the solutions remained turbid. Stirring was continued overnight. The solutions were placed in a hot water bath at *ca.* 60°C for 12 h to induce crystallization. The complexation reactions yielded TRIMEB•(*E*)-ajoene•0.5H_2O (**9**) and TRIMEB•(*Z*)-ajoene (**10**). Several crystals of each complex were removed from the mother liquor, their surfaces dried on filter paper and prepared for analyses.

UV SPECTROPHOTOMETRY

The host-guest ratios (1:1) of complexes **9** and **10** were determined from UV spectrophotometric absorbance measurements recorded at 241 and 235 nm for **9** and **10** respectively. The crystals were dissolved in a water-ethanol solution (40/60 v/v) and the concentrations of the guests were determined by interpolation from the calibration curves for both guests.

FOURIER TRANSFORM INFRARED SPECTROSCOPY (FTIR)

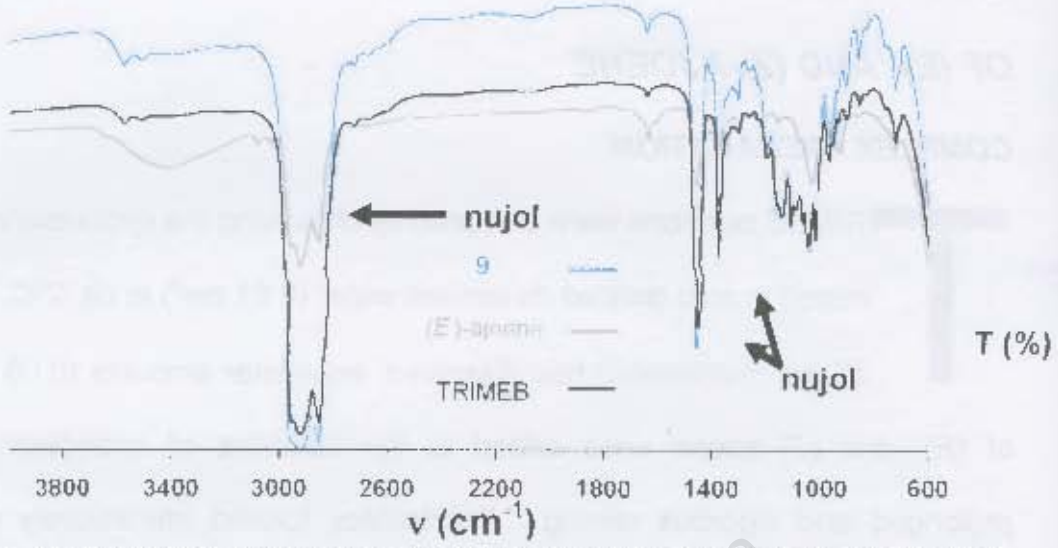

Figure 1. The infrared spectrum of **9** compared with the spectra for (*E*)-ajoene and TRIMEB.

The FTIR spectrum of **9** shows no evidence of the characteristic stretching frequencies of (*E*)-ajoene. These absorptions occur at 1045 cm^{-1} and 1650 cm^{-1} as reported by Block *et al.*[1] and are assigned to the C-S=(O)-C and C=C moieties respectively.

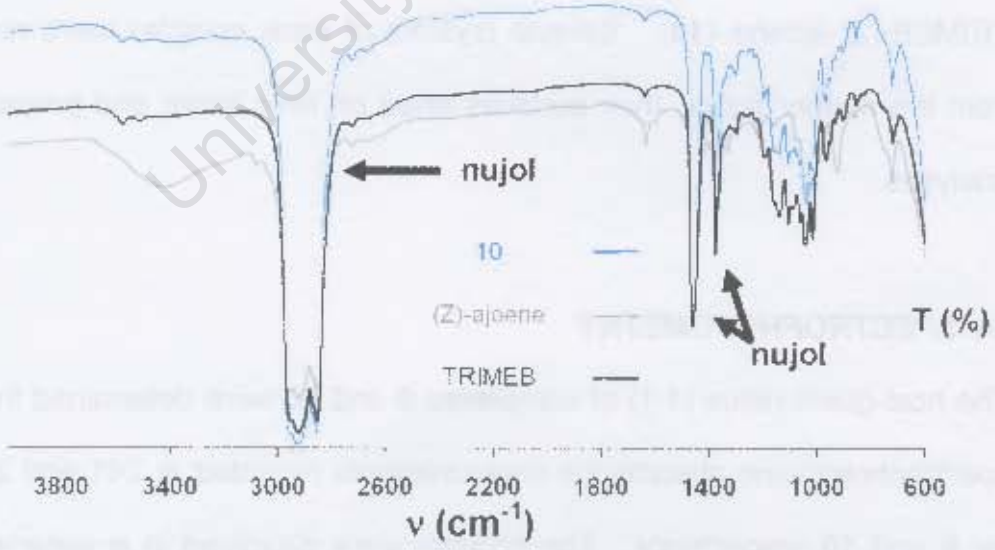

Figure 2. The infrared spectrum of **10** compared with the spectra for (Z)-ajoene and TRIMEB.

It is evident from the spectrum in Figure 1 that both these absorptions coincide with absorptions present in the TRIMEB spectrum. In addition, in

instances where there is little or no overlap between peaks for pure ajoene and pure TRIMEB, the TRIMEB has simply outweighed any contribution made by ajoene to the spectrum of complex **9**. Thus the resultant spectrum for complex **9** is virtually indistinguishable from that of TRIMEB. Similarly, the FTIR spectrum for complex **10** (see Figure 2) is virtually indistinguishable from that of pure TRIMEB. FTIR has thus been unable to provide any evidence of complexation in either case.

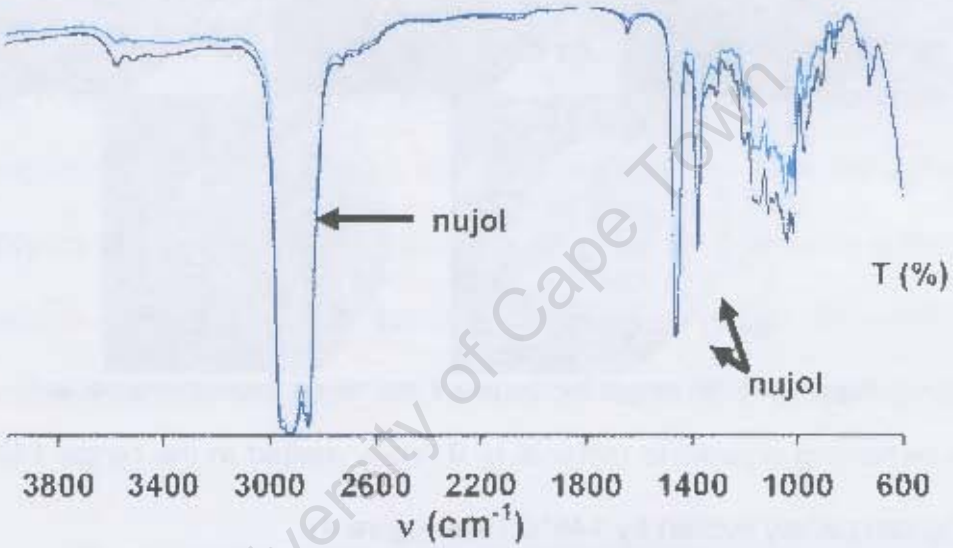

Figure 3. Overlaid infrared spectra of **9** and **10**.

The FTIR spectra for complexes **9** and **10** are indistinguishable from each other as is evident from their overlays in Figure 3.

THERMAL ANALYSIS

HSM

All samples were heated at a scanning rate of 10 K min^{-1}. After the removal from their mother liquor the crystals of both complexes were dried on filter paper, covered with silicone oil and placed between cover slips. This was

done to detect gas evolution (dehydration) through the formation of bubbles upon heating. At the start of the HSM experiment (25°C) the crystals for both complexes **9** and **10** were clear and translucent. At approximately 40°C **9** showed signs of dehydration through bubble formation. This continued for *ca* 20°C with few bubbles remaining at 60°C

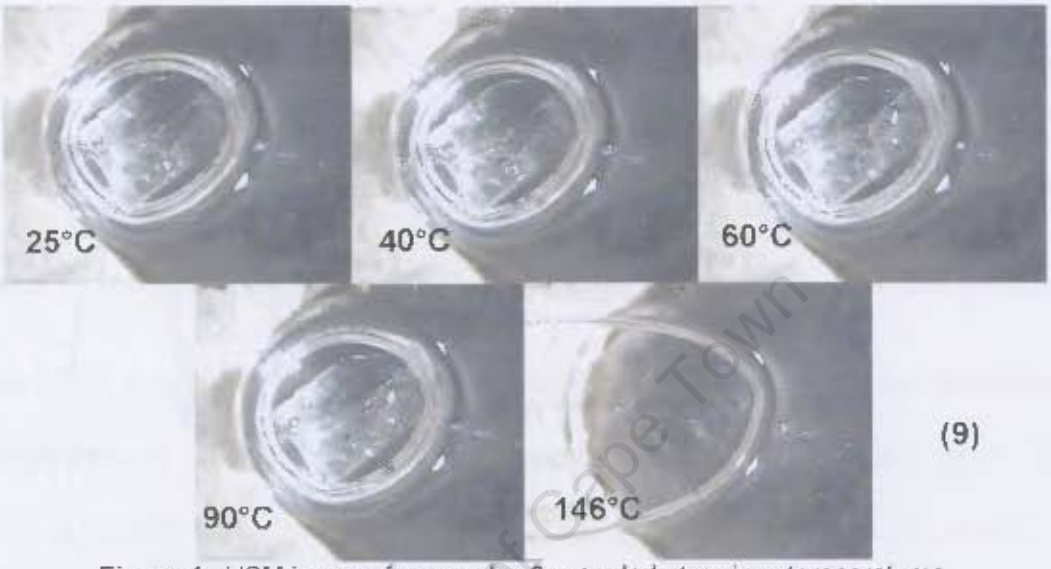

Figure 4. HSM images for complex **9** recorded at various temperatures.

The remaining crystalline material of **9** finally melted in the range 142-146°C being completely molten by 146°C (see Figure 4).

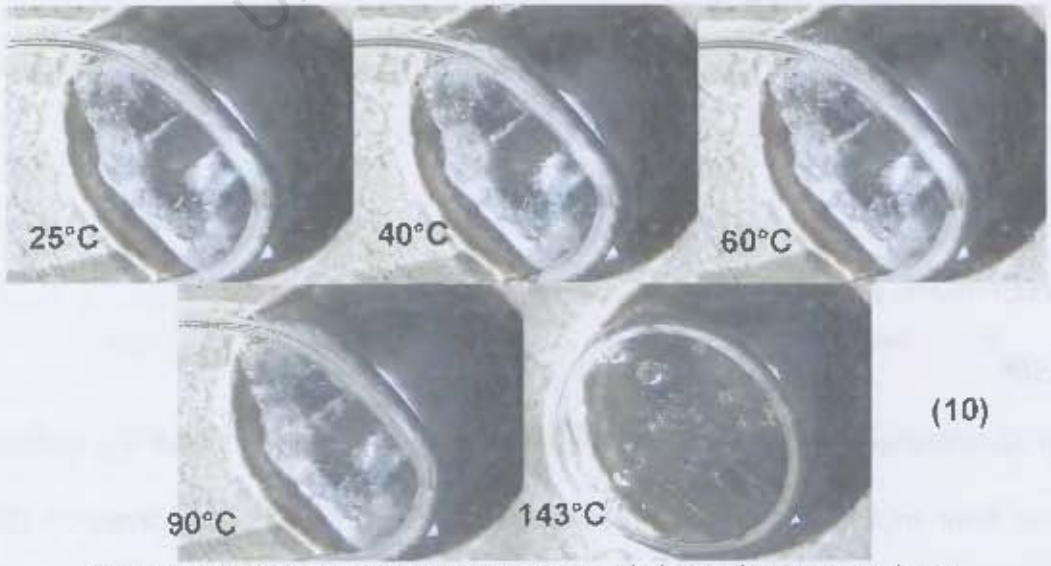

Figure 5. HSM images for complex **10** recorded at various temperatures.

For **10**, the crystal formed micro-fissures from slightly below 40°C continuing to approximately 60°C without the evolution of bubbles (see Figure 5). This, as in the case of **9**, was consistent with TGA data. Sample **10** melted in the range 140-144°C and was completely molten by 144°C.

TGA and DSC

In Figures 6 and 7 the combined DSC and TGA traces are shown for **9** and **10** respectively. The TGA trace for **9** consistently showed a small yet significant mass loss in the temperature range 30-60°C of *ca.* 0.6-0.8 % (for n = 3, where n is the number of measurements taken), equivalent to approximately 0.5 water molecules per complex unit, represented by **A** in the TGA trace (Figure 6). This was interpreted as dehydration of the complex, in keeping with HSM observations above. Thus, the TGA shows two thermal events, dehydration **A** and decomposition **B**, while the DSC shows the fusion **C** and decomposition **D**.

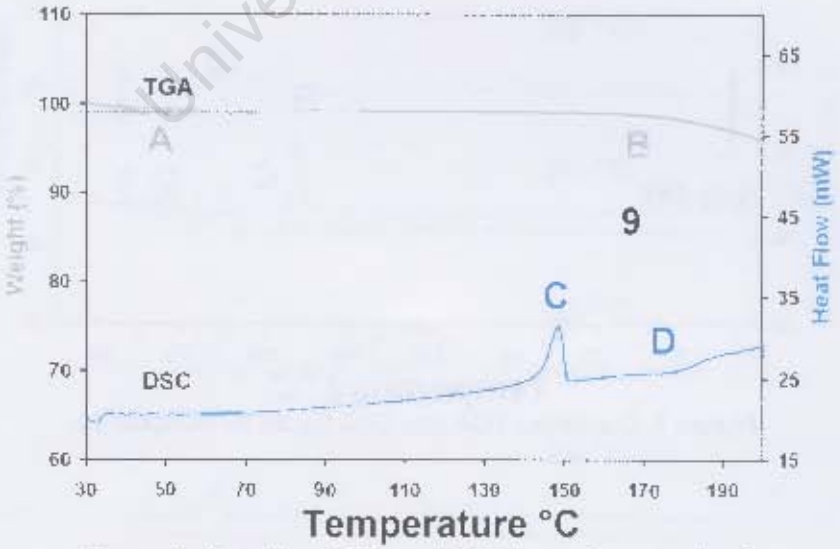

Figure 6. Combined TGA and DSC traces for complex **9**.

The dehydration of **9** is followed by a melt endotherm, **C** in the DSC trace, with a melt onset of 143.8°C. For **10** it was evident from both HSM and DSC that the complex was unsolvated with only a melt endotherm for **10** appearing in the DSC trace represented by **B** and occurring at 140.5°C. The very small, reproducible endotherm, **C** in the DSC trace, following the fusion of **10** has an onset temperature of 144.8°C and is due to contamination by complex **9**, due to the presence of (*E*)-ajoene at a ~5 % level in the sample of (*Z*)-ajoene used for complex **10** preparation (Figure 7). The complex melting points are sufficiently different from that of the pure host (157-159°C) and from one another, to be useful for complex identification. Both complexes **9** and **10** decompose exothermically at onset temperatures of about 160°C, represented by **B** and **D** in the TGA and DSC traces for **9** respectively, while for **10** the corresponding events are labelled **A** and **D**.

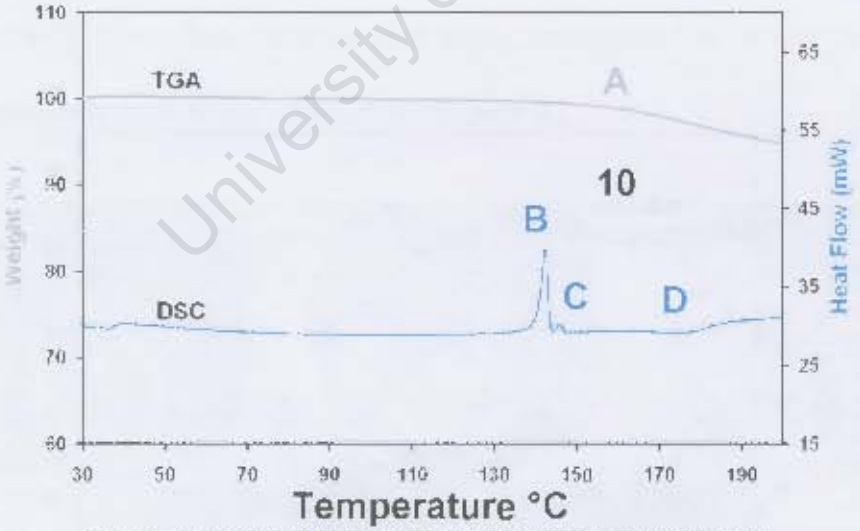

Figure 7. Combined TGA and DSC traces for complex **10**.

Stepped Heated PXRD

Variable temperature PXRD of complexes **9** and **10** was performed at regular intervals (*ca.* 20°C) in the range 25-120°C. Complexes **9** and **10** were

subjected to this form of analysis to determine whether there were any subtle phase changes or any other physical changes due to the heating process. It also provided the opportunity to gather more evidence concerning the thermal stability of these complexes. The PXRD traces for complex **9** (Figure 8) remained unchanged during the heating process and reflected very little change in peak intensity and crystallinity (in the form of peak broadening and intensity reduction) up to and including 100°C. At 120°C there is a considerable reduction in peak intensity accompanied by peak broadening indicating a decrease in the crystallinity. However, there remains enough evidence in the form of remaining peaks to be sure that the sample has not undergone fusion or any other phase change.

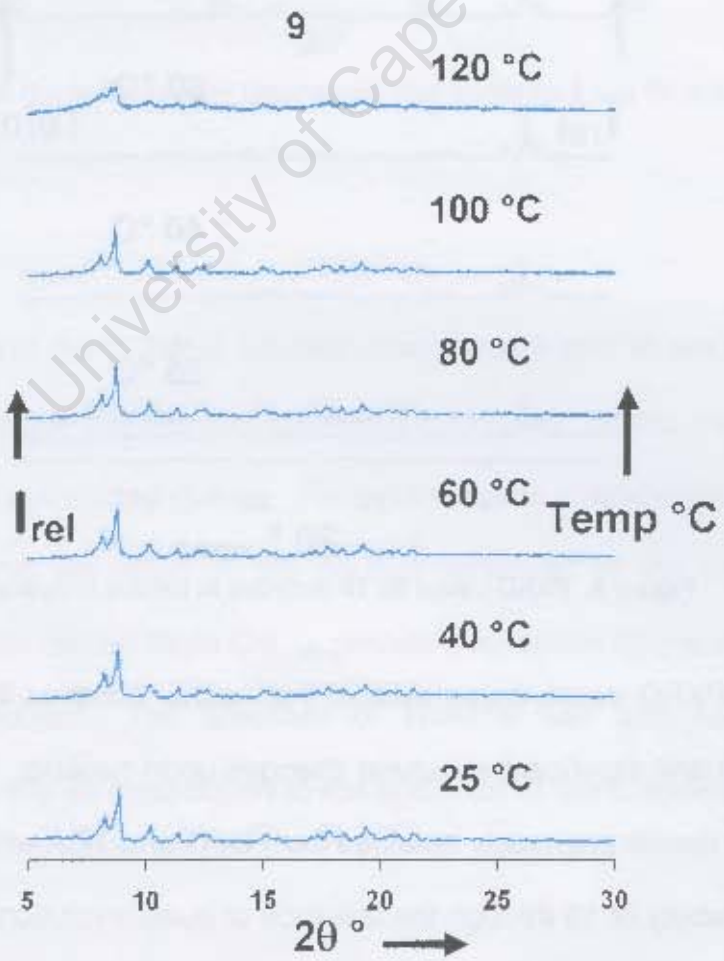

Figure 8. PXRD traces for **9** recorded at various temperatures.

For complex **10**, the PXRD traces in Figure 9 remained unchanged in the range 25-100°C. In the trace recorded at 120°C the only observable change is in the peak intensities. There was no evidence to suggest any major change in the crystallinity of the sample or that any other phase change had occurred.

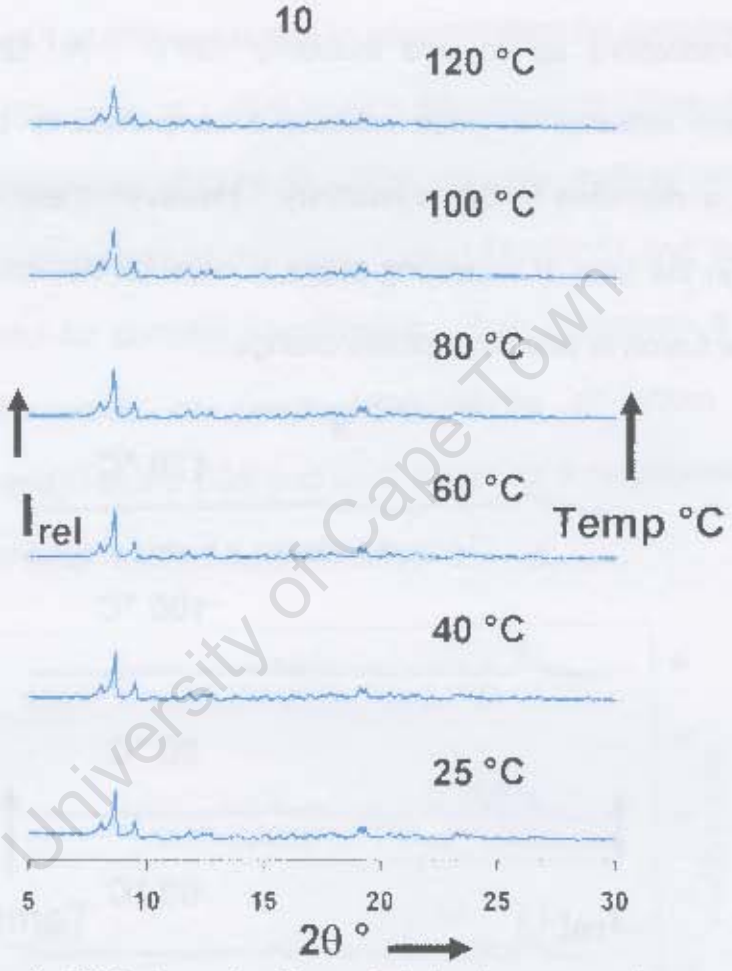

Figure 9. PXRD traces for **10** recorded at various temperatures.

From the PXRD traces it was evident that neither complex **9** nor complex **10** underwent any significant structural changes upon heating. It merely served to confirm results previously obtained from DSC and TGA which indicated the thermal stability of **10** through the absence of guest evolution in the range 25-120°C. However, it confirmed the thermal stability of complex **10** as greater than that of complex **9** through the apparent greater retention of crystallinity at

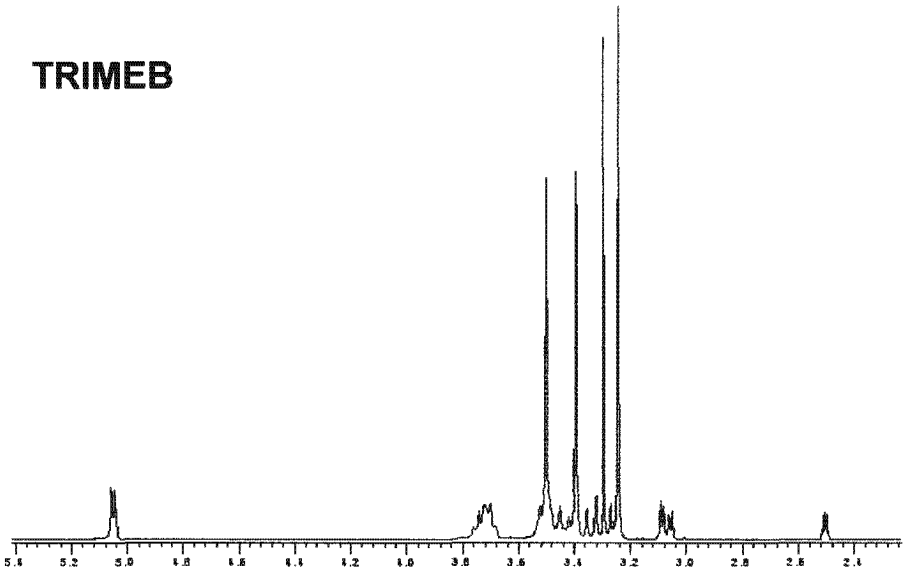

Figure 11. ^{1}H-NMR spectrum for pure TRIMEB in deuterated DMSO.

In the spectrum of uncomplexed (*E*)-ajoene (chapter 3, Figure 1), the doublet generated by the proton H-8 occurs at δ_H 6.35 ppm, while in the spectrum for **9** (Figure 12) the doublet is significantly shifted downfield and occurs at δ_H 6.50 ppm, a shift of $\Delta\delta_H$ = + 0.15 ppm. A shift of this magnitude is indicative of very strong host-guest deshielding interactions which occur upon inclusion.[2]

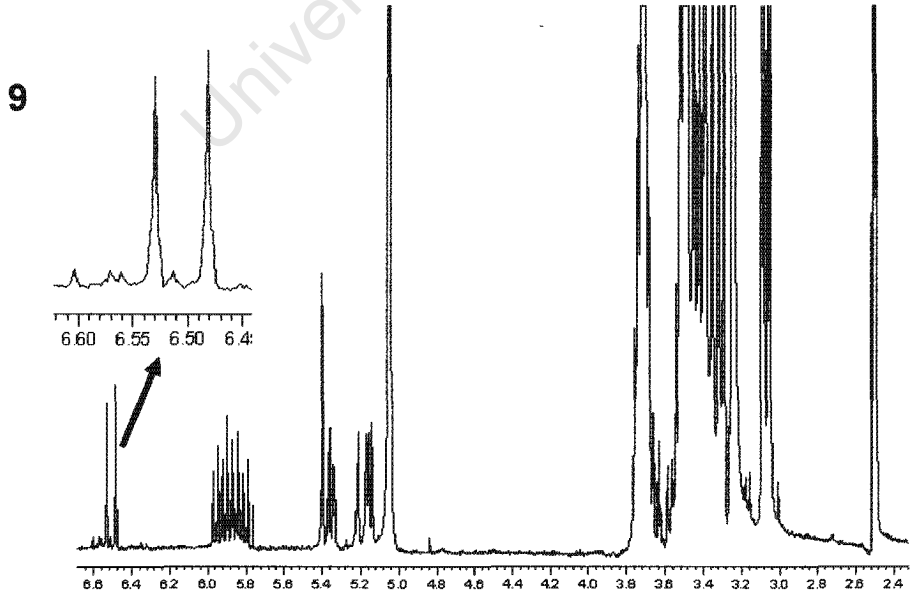

Figure 12. ^{1}H-NMR spectrum for **9**. The insert shows the characteristic doublet for the guest (*E*)-ajoene.

According to A.L. Thakkar *et al.*[3] downfield shifts should be observed for

included guest protons as a result of the hydrophobic interactions between the host and the guest, since the mode of inclusion is usually with the more polar group protruding from the cavity.

In the case of uncomplexed (*Z*)-ajoene (chapter 3, Figure 2), the spectrum shows the doublet generated by the proton H-8 occurring at δ_H 6.58 ppm. In the spectrum for complex **10**, the doublet occurs in two different places, namely at δ_H 6.58 and δ_H 6.50 ppm in a ratio of approximately 1 to 2 with respect to peak height (see insert Figure 13). The magnitude of the shift '$\Delta\delta_H$' is approximately 0.08 ppm (upfield), commensurate with shift values reported in the literature for other examples of cyclodextrin inclusion.[4] The shielding effects of the cavity are a consequence of the host framework being made up entirely of single, less polar and polarizable bonds. The presence of both resonances δ_H 6.58 and δ_H 6.50 ppm in the spectrum of **10** is significant as it may be the result of the dissociation-association equilibrium set up in solution.

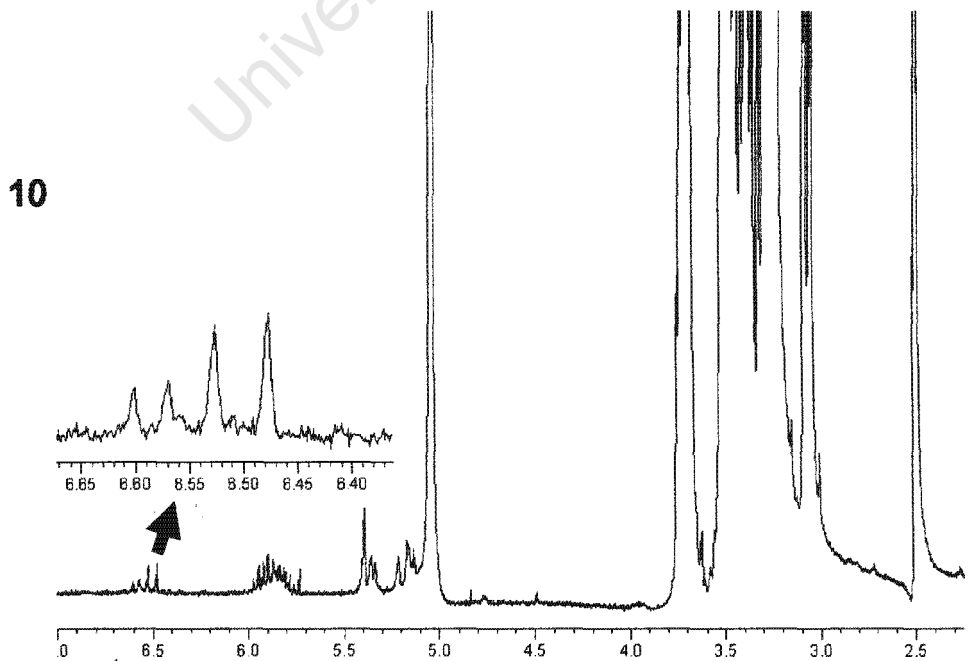

Figure 13. ^{1}H-NMR spectrum for **10**. The insert shows the characteristic doublet for the guest (*Z*)-ajoene.

CRYSTAL STRUCTURE ANALYSIS

Space group determination

Preliminary unit cell parameters and the space groups for complexes **9** and **10** were determined by X-ray photography. With the help of oscillation and Weissenberg methods the Laue symmetry was revealed as *mmm* for **9** corresponding to the orthorhombic system, while for **10** the Laue symmetry was *2/m* corresponding to the monoclinic crystal system. Systematic absences for **9** were hkl : none, h00 : h = 2n + 1, 0k0 : k = 2n + 1, 00l : l = 2n + 1 confirming the space group as $P2_12_12_1$, while those for **10** were hkl : none, h0l : none, 0k0 : k = 2n + 1, indicating the space group $P2_1$ ($P2_1/m$ is excluded as the host is chiral).

Data-collection (COLLECT software)[5] involved a combination of ϕ- and ω-scans of 0.7-1.0° for **9** and 1.0° for **10** with respective crystal to detector distances of 55 and 50 mm. Unit cell refinement and data reduction were performed with the program DENZO-SMN.[6] The structure of complex **9** was solved by Patterson search methods using the rigid host moiety of the complex TRIMEB•(S)-naproxen as trial model.[7,8] The Patterson search methods were applied with the aid of program PATSEE.[7,9] Isomorphous replacement with the same model was used to solve the phase problem for complex **10**. Here all non-hydrogen atoms except for O6, C7, C8 and C9 atoms of each methyl glucose unit were used in the model as the input fragment. Following refinement and optimisation of the host structure, guest atoms generally appeared with low electron densities due to disorder and were tediously located in a series of successive difference electron density

maps. It became evident that each guest molecule was disordered over two positions, each corresponding to a stereoisomer of the respective guest (*E*)- or (*Z*)-ajoene. Least-squares refinements of **9** and **10** were sensitive and several distance restraints were imposed on the individual components of the disordered guest molecules to ensure reasonable geometries. Bond lengths were obtained from F. H. Allen *et al.*[10] (see Appendix 1 for the tabulated values). An overall standard deviation of $\sigma = 0.01$ Å was applied to all bond lengths in order to ensure uniformity. Crystal data and refinement parameters for complexes **9** and **10** are presented in Table 1.

Table 1. Crystal data and data-collection parameters for **9** and **10**.

Complex formula	$C_{63}H_{112}O_{35}$·(*E*)-$C_6H_{14}OS_2$·0.5H_2O (**9**)	$C_{63}H_{112}O_{35}$·(*Z*)-$C_6H_{14}OS_2$ (**10**)
Formula weight	1672.92	1663.91
Temperature	173(2) K	173(2) K
Crystal system	Monoclinic	Orthorhombic
Space group	$P2_1$	$P2_12_12_1$
Unit cell dimensions	a = 11.5531(2) Å	a = 15.1019(2) Å
	b = 27.715(1) Å	b = 21.5196(3) Å
	c = 14.6053(3) Å	c = 27.313(1) Å
	β = 109.386(1)°	-
Volume	4411.4(2) Å^3	8876.4(4) Å^3
Z	2	4
Density (calc.)	1.259 g·cm^{-3}	1.245 g·cm^{-3}
Radiation, wavelength	MoKα, 0.71073 Å	MoKα, 0.71073 Å
Absorption coefficient	0.167 mm^{-1}	0.166 mm^{-1}
F(000)	1798	3576
Crystal size	0.53 x 0.40 x 0.25 mm	0.35 x 0.34 x 0.31 mm
Theta range	1.87 to 23.03°	1.54 to 25.35°
Index ranges	-12 < h < 10, -29 < k < 30, -10 < l < 16	-17 < h < 17, -25 < k < 22, -21 < l < 32
Reflections collected	10160	31007
Observed reflections [I>2σ(I)]	7919	10433
Data/restraints/parameters	8699/21/752	15252/27/950
Goodness-of-fit on F^2	1.051	1.017
Final R indices [I>2σ(I)]	R_1 = 0.0936, wR^2 = 0.2406	R_1 = 0.0906, wR^2 = 0.2321
R indices(all data)	R_1 = 0.1007, wR^2 = 0.2476	R_1 = 0.1344, wR^2 = 0.2657
Largest diff. peak and hole	0.659, -0.638e Å^{-3}	1.172, -1.056 e Å^{-3}

All guest atoms were treated with a common isotropic temperature factor which refined to 0.101(1) Å^2 for **9** and 0.146(1) Å^2 for **10**. The site-occupancy factors of the major stereoisomers in **9** and **10** refined to 0.51 and 0.54 respectively. Except for C7G4 and C999, a disordered methyl group belonging to **9** and the tabulated atoms (see Table 2), host atoms were generally treated anisotropically and refined without restraints.

Table 2. Isotropically refined atom list.

9	C7G5	C9G7	C9G2	C9G4	O6G7	C7G3
10	C9G7	O6G7	*C9G4*	*O6G4*	*C9G2*	-

The oxygen atom of the water molecule in **9** was located and assigned a site-occupancy factor (s.o.f.) of 0.5 on the basis of TGA data (as previously stated) and its close proximity (~2.9 Å) to one of the disordered C atoms of a host methyl group. The latter group was located at two sites with equal electron densities, justifying assignment of 0.5 for the s.o.f.'s of these components, and thus also that of the water O atom. Water H atoms could not be located. Host and guest H atoms were generally added in idealised positions in a riding model with U_{iso} = 1.2 times those of their parent atoms. However, due to the disorder of the included guest some of the H-atoms of the guest could not be placed in idealised positions (as with the riding model) but were placed after their positions were determined using geometric calculations. Full-matrix least-squares refinement against F^2 (SHELX-97) was employed with a weighting scheme $w = [\sigma^2(F_o^2) + (aP)^2 + bP]^{-1}$ and $P = [\max(F_o^2, 0) + 2F_c^2]/3$.[11] Major electron density peaks in **10** were located within 0.10 Å of atom S4A and were attributed to its anisotropic motion. However, guest disorder did not warrant anisotropic refinement.

Overall description of the structures

One TRIMEB molecule, a molecule of each stereoisomer of (*E*)-ajoene (both at 50% occupancy) and half a molecule of water comprise the asymmetric unit of **9**, while the asymmetric unit of **10** consists of one molecule of TRIMEB and half a molecule of each stereoisomer of (*Z*)-ajoene (both at 50% occupancy). Even though the unit cell dimensions and space groups for the two complexes are different, the host conformations for **9** and **10** are similar. The differences in the packing arrangements are due to the contrasting modes of guest inclusion.

Host conformation

The glucose residues will henceforth be referred to as G1, G2, G3, G4, G5, G6 and G7 and the numbering scheme for both complexes follows in Figure 14. Detailed geometrical data for **9** and **10** are listed in Tables 3, 4 and 5.

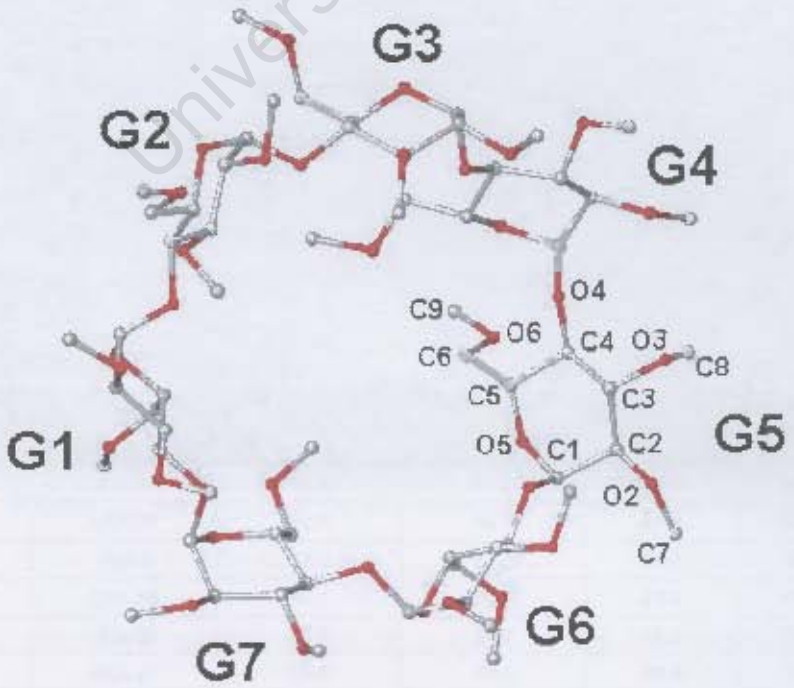

Figure 14. The structure of the macrocyclic host viewed from the secondary face and the numbering scheme of the glucose residues.

Included in these lists are: the glycosidic oxygen angle *O4G(n-1)···O4G(n)···O4G(n+1)*, the radius of the heptagon, the glycosidic *O4G(n)···O4G(n+1)* distance, the tilt angle of each residue and the deviation of each O4 atom from the least-squares plane defined by all seven O4 atoms (all of these as previously defined in chapter 1). All the glucose residues are in the $^4C_1$-chair conformation and both hosts **9** and **10** are elliptically distorted, though not severely, as is evidenced by the values for the radii in Table 4. *O4G(n)···O4G(n+1)* varies within a narrow margin for both complexes, 4.23-4.47 Å for **9** and 4.23-4.49 Å for **10** (Table 3). The *O4G(n-1)···O4G(n)···O4G(n+1)* glycosidic oxygen angle ranges are very similar, namely 118.5-138.0° and 121.0-136.7° for **9** and **10** respectively (Table 3). For both complexes the tilt angle for glucose residue G4 is by far the largest with a value of 54.3(4)° for **9** and a value of 42.8(2)° for **10** (Table 4).

Table 3. Glycosidic oxygen angles and O(4)···O(4') distances

Glycosidic oxygen angle	(9) (°)	(10) (°)	O4···O4' distance	(9) (Å)	(10) (Å)
O4G7···O4G1···O4G2	123.8	127.8	O4G1···O4G2	4.47	4.48
O4G1···O4G2···O4G3	128.5	125.4	O4G2···O4G3	4.33	4.27
O4G2···O4G3···04G4	123.0	124.0	O4G3···04G4	4.36	4.49
O4G3···O4G4···O4G5	138.0	136.7	O4G4···O4G5	4.37	4.23
O4G4···O4G5···O4G6	118.5	121.0	O4G5···O4G6	4.36	4.45
O4G5···O4G6···O4G7	124.9	125.6	O4G6···O4G7	4.44	4.41
O4G6···O4G7···O4G1	134.6	131.5	O4G7···O4G1	4.23	4.26

Table 4. Radii, O(2)···O(3') distances and tilt angles for (**9**) and (**10**).

Residue	Radius (9) (Å)	Radius (10) (Å)	O(2)···O(3') (9) (Å)	O(2)···O(3') (10) (Å)	Tilt angle (9) (°)	Tilt angle (10) (°)
G1	5.06	4.96	3.13	3.06	14.3(3)	13.7(1)
G2	5.07	5.15	3.30	3.35	15.8(4)	15.8(2)
G3	5.07	5.06	3.71	3.52	9.8(4)	11.7(1)
G4	4.67	4.73	3.60	3.36	54.3(4)	42.8(2)
G5	5.20	5.17	3.70	3.75	32.0(2)	36.1(2)
G6	5.07	5.09	3.50	3.46	15.6(5)	13.5(2)
G7	4.75	4.85	3.27	3.26	35.5(3)	34.5(2)

Table 5. Torsion angles and deviations from the O(4) polygon for (**9**) and (**10**).

Residue	O5-C5-C6-O6 (9) (°)	C5-C6-O6-C9 (9) (°)	O5-C5-C6-O6 (10) (°)	C5-C6-O6-C9 (10) (°)	Deviation (9) (Å)	Deviation (10) (Å)
G1	-76.0	-168.8	-74.0	-175.1	-0.420(5)	-0.407(3)
G2	-67.7	-179.1	69.9	-177.4	-0.164(5)	-0.240(3)
G3	-70.6	177.4	-67.3	-179.3	0.404(5)	0.513(3)
G4	-70.5	175.8	87.1	176.6	0.113(5)	0.023(3)
G5	67.2	-175.2	-72.6	178.3	-0.645(5)	-0.556(3)
G6	-76.4	78.3	-81.0	78.1	0.371(5)	0.292(3)
G7	77.3	82.5	69.3	101.5	0.341(5)	0.375(3)
RMS deviation					0.387	0.382

The remarkable similarity found in the host conformations was expected since the TRIMEB skeleton used in the refinements of **9** and **10** was the same (Figure 15). The similarity is reinforced by a careful examination of the tabulated parameters.

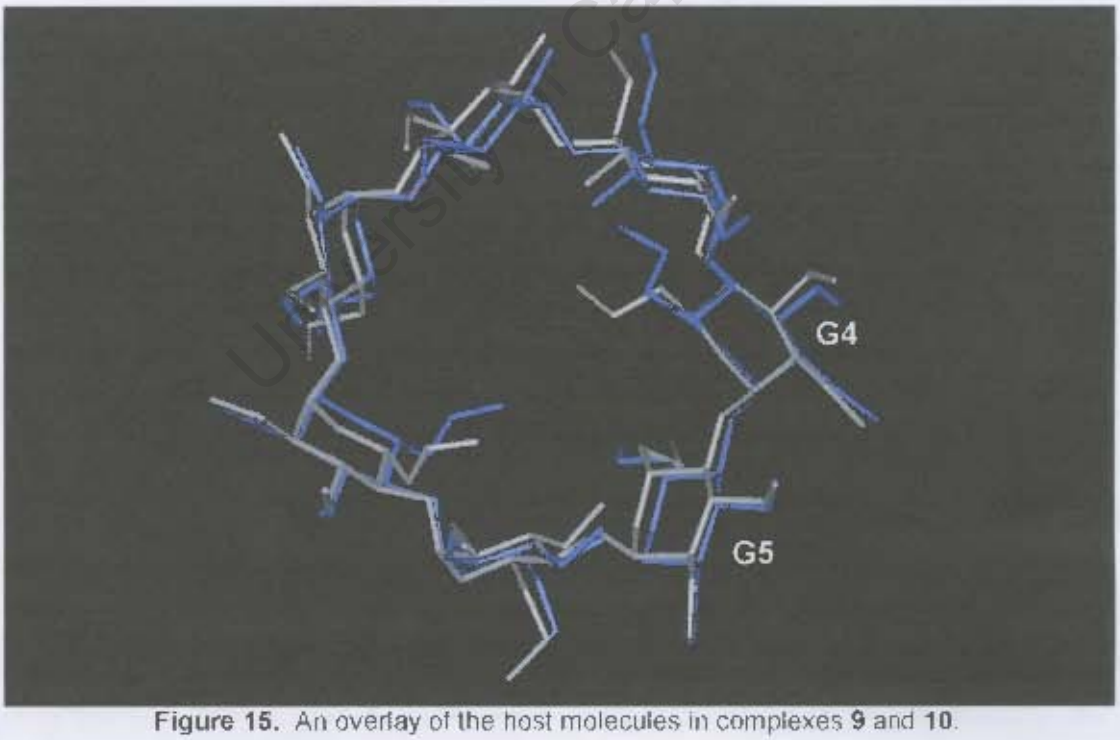

Figure 15. An overlay of the host molecules in complexes **9** and **10**.

A notable difference relates to the tilt angles of the methylglucose residues. The parameters are especially sensitive to small differences at the secondary

face. in this case, the presence of the partial water molecule O1 in **9** (Figure 16).

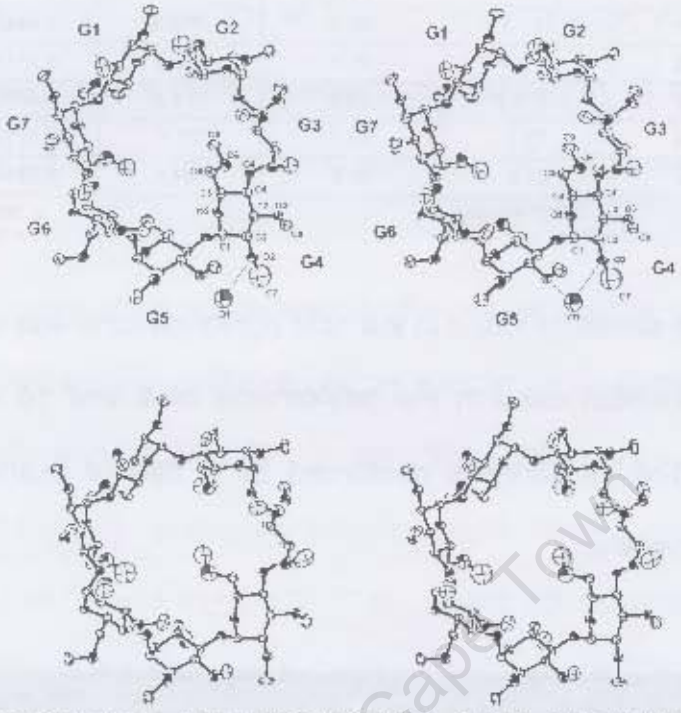

Figure 16. Stereoview of the host conformations in **9** (top) and **10** (bottom). For atoms refined anisotropically, thermal ellipsoids are drawn at the 40% probability level.

Associated with the partial occupancy of the water molecule (O1) there is two fold disorder of the methylglucose residue (C7G4 and C999). The water molecule engages in the hydrogen bond interactions with O3G5 and O2G4 with O1···O distances 2.74(3) and 2.91(3) Å respectively. Also the residues G4 and G5 are significantly twisted towards (+11.5°), and away from (-4.1°), the host primary side respectively, relative to their orientations in complex **10**. All other corresponding residues in **9** and **10** have tilt angles differing by only *ca.* 2° (see Table 4). The host conformations of **9** and **10** are stabilised by several analogous intramolecular C-H···O hydrogen bonds.[8] The host molecule in complex **9** has nine intramolecular C-H···O hydrogen bonds which can be divided into four different types. Five are of the type C6-H···O5, two are C1-H···O3, one is C8-H···O4 and another is of the type C1-H···O6. Eight

of the intramolecular bonds serve to stabilise the host molecule while the remaining one occurs within a glucose residue and is of the type C8-H···O4 (see Table 6). The C···O (donor···acceptor) hydrogen bond lengths are in the range 3.1-3.3 Å, while the C-H···O (donor – hydrogen···acceptor) hydrogen bond angles are in the range 120.2-136.7°. In the case of complex **10**, the host molecule has thirteen C-H···O intramolecular hydrogen bonds split into seven types. These consist of five bonds of the type C5-H···O5, two of the type C7-H···O3, another two in the form of C8-H···O2 and one each of the type C1-H···O3, C1-H···O6, C9-H···O5 and C6-H···O6. Eight of these are involved in the stabilisation of the host molecule, while five occur within glucose units. The C···O hydrogen bond lengths are in the range 3.0-3.4 Å, while the C-H···O hydrogen bond angles are in the range 112.9-159.8° (Table 7).

Table 6. Intramolecular and intermolecular C-H···O hydrogen bonds in the structure of **9**.

Donor-H···Acceptor	D-H (Å)	H···A (Å)	D···A (Å)	D-H···A (°)
C6G6-H6GX···O5G5	0.99	2.37	3.14(1)	134.7
C6G5-H6GA···O5G4	0.99	2.36	3.23(1)	146.6
C1G3-H1G3···O3G4	1.00	2.40	3.08(1)	125.0
C1G6-H1G6···O3G7	0.99	2.49	3.12(1)	120.4
C6G1-H6G4···O5G7	0.99	2.55	3.18(1)	121.2
C6G3-H6G6···O5G2	0.99	2.47	3.26(1)	136.7
C6G2-H6G8···O5G1	0.99	2.53	3.30(1)	135.1
C8G6-H8G7···O4G6	0.98	2.56	3.17(1)	120.2
C1G5-H1G5···O6G6	1.00	2.44	3.19(1)	130.5
Intermolecular C-H···O hydrogen bonds in the structure of 9				
C1G1-H1G1···O6G6[3]	1.00	2.48	3.41(1)	131.9
C8G5-H8GE···O3G2[b]	0.98	2.54	3.43(1)	152.9
C2G1-H2G1···O5G5[c]	1.00	2.50	3.45(1)	171.8
C2G5-H2G5···O6G1[d]	1.00	2.32	3.31(1)	157.8
C2G7-H2G7···O6G3[e]	1.00	2.55	3.47(1)	150.1
C9G1-H9G2···O1[f]	0.98	2.45	3.19(3)	154.5

[3] 2 - x, ½ + y, 2 - z
[b] 2 - x, - ½ + y, 1 - z;
[c] 2 - x, ½ + y, 2 - z;
[d] 2 - x, - ½ + y, 2 + z;
[e] 1 + x, y, 1-z;
[f] 2 - x, ½ + y, 2 - z

Table 7. Intramolecular and intermolecular C-H···O hydrogen bonds in the structure of **10**.

Donor-H···Acceptor	D-H (Å)	H···A (Å)	D···A (Å)	D-H···A (°)
C6G6-H6GX···O5G5	0.99	2.43	3.19(8)	132.9
C7G6-H7GF···O3G6	0.98	2.36	3.02(1)	123.8
C1G3-H1G3···O3G4	0.99	2.42	3.08(7)	123.5
C1G5-H1G5···O6G4	0.99	2.42	3.22(8)	136.7
C8G4-H8GZ···O2G4	0.98	2.55	3.07(1)	112.9
C8G7-H8GI···O2G7	0.98	2.49	3.09(9)	120.0
C9G6-H9GA···O6G6	0.98	2.44	3.03(1)	118.4
C6G1-H6G2···O5G7	0.98	2.56	3.18(7)	121.0
C6G2-H6G3···O5G1	0.99	2.47	3.38(9)	153.3
C6G3-H6G6···O5G2	0.99	2.43	3.19(9)	133.7
C6G5-H6G8···O5G4	0.99	2.46	3.12(9)	123.4
C6G5-H6G8···O6G4	0.99	2.48	3.43(1)	159.8
C7G3-H7G9···O3G3	0.98	2.46	3.08(1)	120.6
Intermolecular C-H···O hydrogen bonds in the structure of 10				
C2G1-H2G1···O6G5[g]	1.00	2.47	3.38(7)	151.0
C2G6-H2G5···O6G1[h]	1.00	2.44	3.37(7)	154.2
C2G7-H2G7···O6G3[i]	1.00	2.47	3.41(8)	156.2
C9G5-H9GY···O3G1[n]	0.98	2.43	3.18(9)	132.4
C9G6-H9GA···O3G4[i]	0.98	2.58	3.19(1)	120.4
C4G3-H4G3···O3G7[i]	0.99	2.57	3.47(8)	149.4
C9G1-H9G2···O3G5[g]	0.98	2.50	3.24(9)	131.6

[g] 3/2 - x, 1 - y, 1/2 + z;
[h] 3/2 - x, 1 - y, - 1/2 + z;
[i] - 1 + x, y, z;
[n] 1 + x, y, z

Other conformational differences noted are the opposite signs of the torsion angles O5-C5-C6-O6 in G4 ((-)-*gauche* in **9**, (+)-*gauche* in **10**), again in G5, but with the reverse sign combination (Table 5). The primary methoxyl groups of residues G2, G4, G5 and G7 are most effective in blocking the primary side of the host in both complexes, as can be seen from the space-filling diagrams below (Figures 17 and 18).

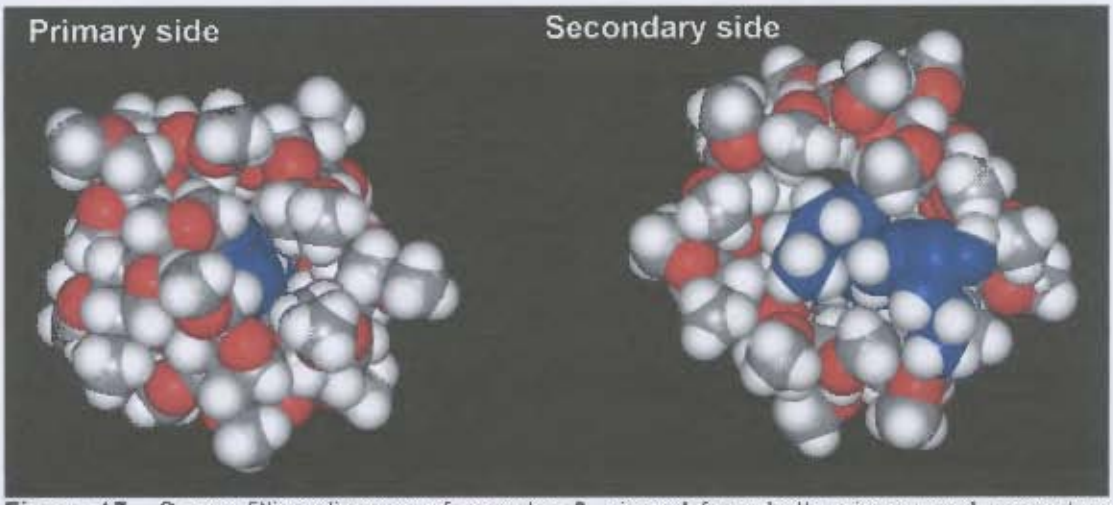

Figure 17. Space filling diagram of complex **9**, viewed from both primary and secondary rims.

The extent of closure of the primary face is similar irrespective of the conformational differences described above. These complexes thus belong to the category of TRIMEB inclusion complexes in which the host cavity is cup-shaped, presenting a large hydrophobic surface to the encaged guest molecule.[8,12]

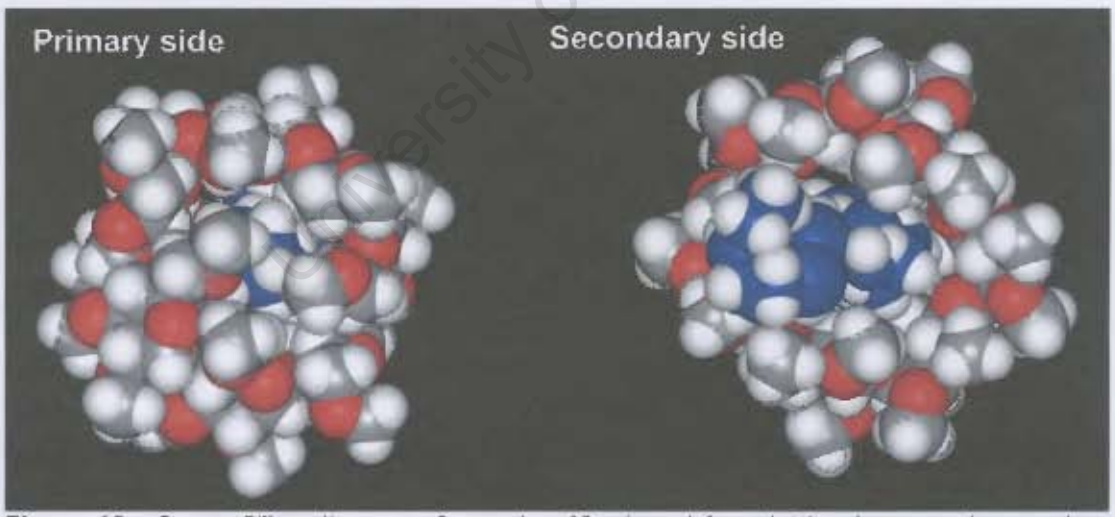

Figure 18. Space filling diagram of complex **10**, viewed from both primary and secondary rims.

Structure and conformation of the guest molecules

For the inclusion complex **9**, between TRIMEB and (*E*)-ajoene, Figure 19 below depicts the peaks assigned and refined as non-hydrogen guest atoms

in the composite electron density image A-B, together with the assigned atom connectivities, while the deconvoluted models are labelled A and B. It is evident that A and B share common terminal atoms C1, C2, C3 and S10, C11, C12, C13 with corresponding atoms being chemically equivalent. However, the indicated connectivities necessitated by the twofold disorder of the sulfinyl group and atom S9 imply that in model A, C7-C8 is formally the central double bond (see Figure 19), while in model B this role is assumed by C8-C8B.

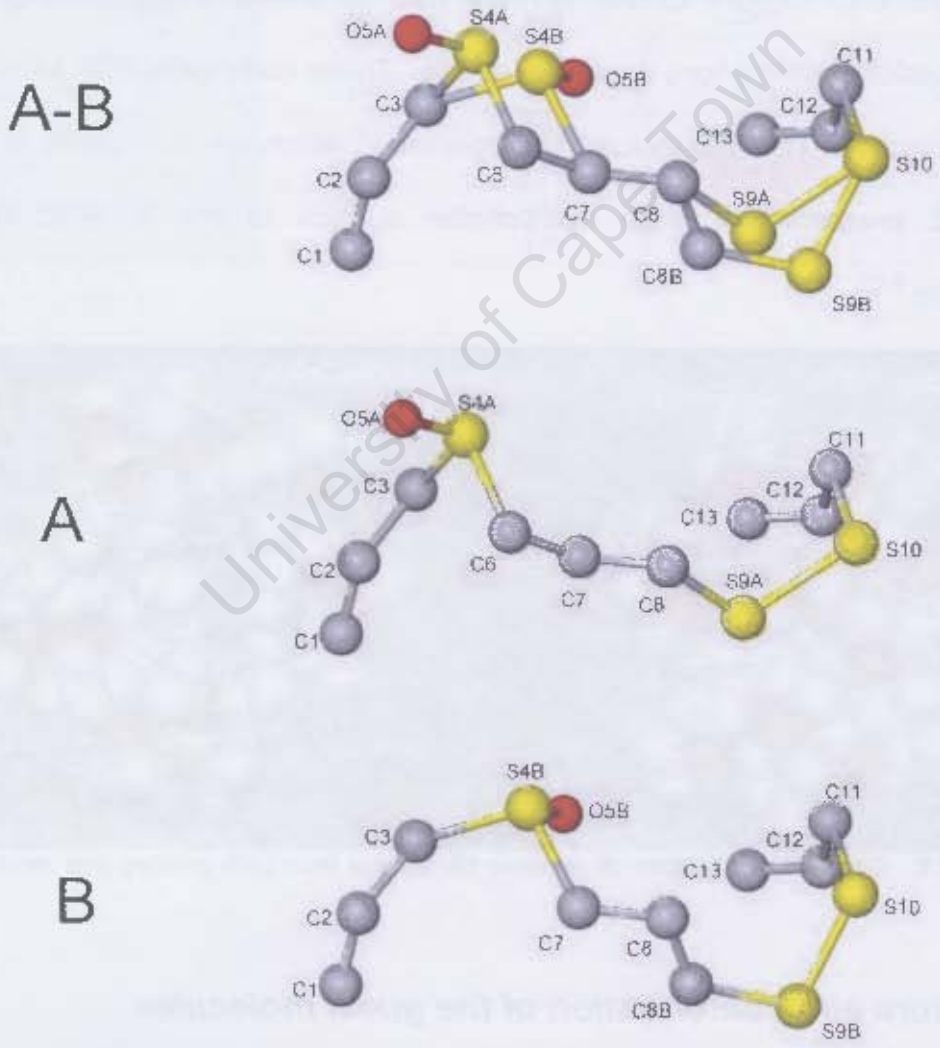

Figure 19. Disordered guest peaks in **9** (A-B) and the individual enantiomers (A = R-enantiomer, B = S-enantiomer) with atom assignments.

The torsion angles (see Table 8) around the respective C-C=C-S bonds are 163(2)° and 172(2)°, approximating the ideal value of 180° for the (*E*)-isomer. It is noted that the stereogenic sulfoxide sulfur atoms S4A and S4B have opposite configurations and hence the process of inclusion of (*E*)-ajoene has 'frozen out' the two stereoisomers, models A and B corresponding to the (R)- and (S)-enantiomers respectively. The refined s.o.f.'s indicate practically equal occupancy of the stereoisomers and therefore the TRIMEB molecule displays no stereo-recognition under the conditions of preparation viz. 1:1 host-guest ratio. The diastereomers TRIMEB•(*E*-ajoene, R-), TRIMEB•(*E*-ajoene, S-) therefore co-exist in the crystal in a 1:1 molar ratio.

Table 8. Torsion angles for (*E*)-ajoene in complex **9**.

Molecule A	Torsion angles (°)	Molecule B	Torsion angles (°)
C1-C2-C3-S4A	-146(2)	C1-C2-C3-S4B	-97 (2)
C2-C3-S4A-O5A	-44(1)	C2-C3-S4B-O5B	120(2)
O5A-S4A-C6-C7	176(2)	O5B-S4B-C7-C8	59(2)
C2-C3-S4A-C6	54(1)	C2-C3-S4B-C7	24(1)
C3-S4A-C6-C7	74(2)	C3-S4B-C7-C8	157(2)
S4A-C6-C7-C8	116(3)	S4B-C7-C8-C8B	-124(3)
C6-C7-C8-S9A	163(2)	C7-C8-C8B-S9B	172(2)
C7-C8-S9A-S10	149(2)	C8-C8B-S9B-S10	22(2)
C8-S9A-S10-C11	-89(1)	C8B-S9B-S10-C11	-72(1)
S9A-S10-C11-C12	-62(1)	S9B-S10-C11-C12	-37(1)
S10-C11-C12-C13	114(1)	S10-C11-C12-C13	114(1)

Figure 20 is the equivalent diagram describing guest disorder in the TRIMEB•(*Z*)-ajoene complex. This disorder is somewhat more complicated as only four atomic sites of the two disordered components A and B coincide, namely C3, C8, S10 and C13 all other atoms being disordered over two sites each. In component A, the central double bond is C7A-C8 while in component B it is C8-C8B.

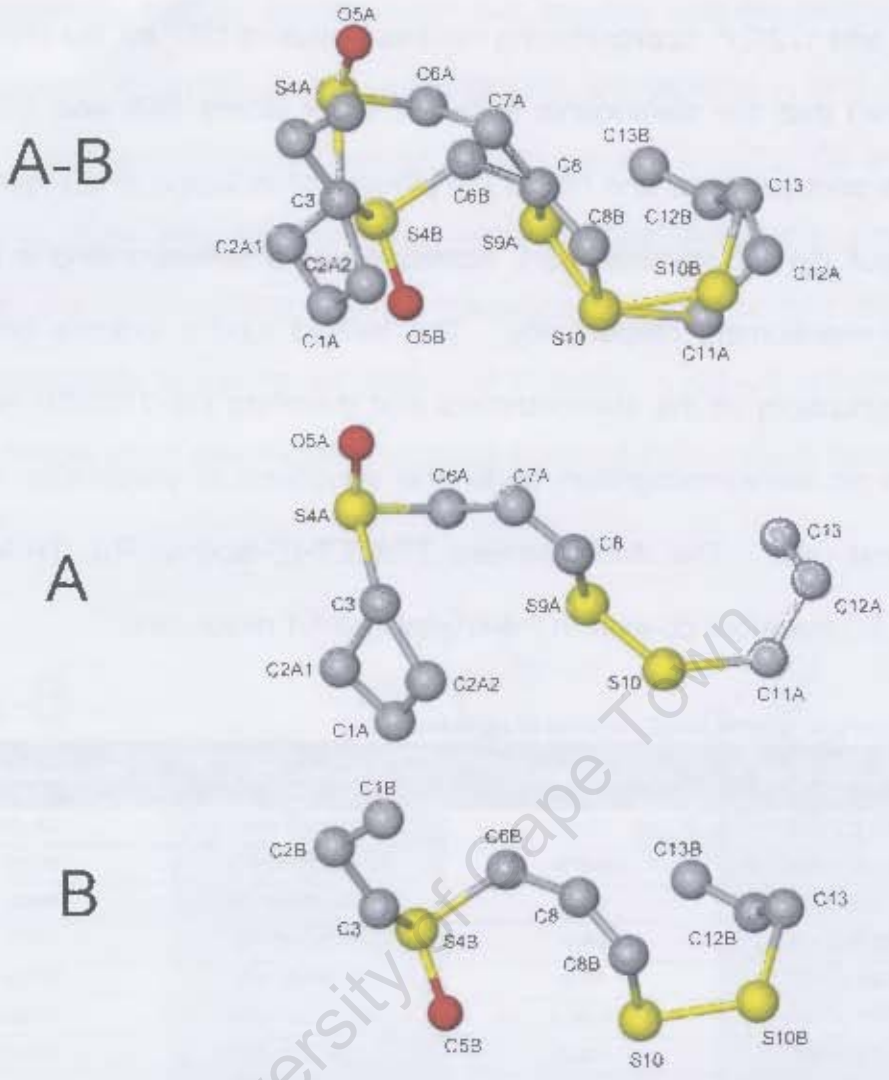

Figure 20. Disordered guest peaks in **10** (A-B) and the individual enantiomers (A = R-enantiomer, B = S-enantiomer) with atom assignments.

The C-C=C-S torsion angles (see Table 9) are 16(3)° and 24(3)°, which approximate the ideal value of 0° for the (*Z*)-configuration of ajoene. Component A is further complicated in that atom C2 is disordered over two sites (C2A1 and C2A2).

Table 9. Torsion angles for (*Z*)-ajoene in complex **10**.

Molecule A	Torsion angles (°)	Molecule B	Torsion angles (°)
C1A-C2A1-C3-S4A	133(2)	C1B-C2B-C3-S4B	-117(2)
C1A-C2A2-C3-S4A	-69(2)	-	-
C2A1-C3-S4A-O5A	153(2)	C2B-C3-S4B-O5B	-170(2)
C2A2-C3-S4A-O5A	-135(2)	-	-
C2A1-C3-S4A-C6A	-95(2)	C2B-C3-S4B-C6B	82(2)
C2A2-C3-S4A-C6A	-23(2)	-	-
C3-S4A-C6A-C7A	-62(2)	C3-S4B-C6B-C8	74(2)
O5A-S4A-C6-C7A	51(2)	O5B-S4B-C6B-C8	-39(2)
S4A-C6A-C7A-C8	133(2)	S4B-C6B-C8-C8B	55(2)
C6A-C7A-C8-S9A	16(3)	C6B-C8-C8B-S10	24(3)
C7A-C8-S9A-S10	-170(2)	C8-C8B-S10-S10B	123(2)
C8-S9A-S10-C11A	-108(1)	C9B-S10-S10B-C13	-80(2)
S9A-S10-C11A-C12A	54(3)	S10-S10B-C13-C12B	-60(3)
S10-C11A-C12A-C13	-71(3)	S10B-C13-C12B-C13B	102(3)

Comparison of the stereochemistries of models A and B shows that again, the S atoms of the respective sulfoxide functions have opposite configurations and hence the process of inclusion of (*Z*)-ajoene in TRIMEB has likewise 'frozen out' its stereoisomers. As for (*E*)-ajoene, the TRIMEB molecule does not discriminate between the enantiomers of (*Z*)-ajoene, the refined s.o.f.'s indicating their presence in virtually equal proportions. The crystal thus contains the two diastereomeric complex units, TRIMEB•(*Z*-ajoene, R-), TRIMEB•(*Z*-ajoene, S-), in equal proportions. Bond lengths and bond angles for each of the stereoisomers of **9** and **10** are listed in Tables 10 and 11 respectively. Generally, the bond lengths of the stereoisomers of (*E*)-ajoene are in good agreement with each other (for chemically equivalent bonds) and with the values set as constraints, while some bond angles are larger than the idealised 120°. Similar remarks apply to (*Z*)-ajoene. This is acceptable given that the guest molecules in complexes **9** and **10** are severely disordered.

Table 10. Final bond lengths and bond angles for (*E*)-ajoene in complex **9**.

Mol A	Bond lengths Å	Mol B	Bond lengths Å	Mol A	Bond Angles (°)	Mol B	Bond Angles (°)
C1-C2	1.27(2)	C1-C2	1.27(2)	C1-C2-C3	133(1)	C1-C2-C3	133(1)
C2-C3	1.50(2)	C2-C3	1.50(2)	C2-C3-S4A	116(1)	C2-C3-S4B	134(1)
C3-S4A	1.71(2)	C3-S4B	1.91(2)	C3-S4A-C6	92(1)	C3-S4B-C7	104(1)
S4A-C6	1.80(3)	S4B-C7	1.84(2)	C3-S4A-O5A	109(1)	C3-S4B-O5B	96(2)
S4A-O5A	1.49(2)	S4B-O5B	1.49(2)	O5A-S4A-C6	96(1)	O5B-S4B-C7	95(1)
C6-C7	1.48(2)	C7-C8	1.39(2)	S4A-C6-C7	105(2)	S4B-C7-C8	121(1)
C7-C8	1.39(2)	C8-C8B	1.30(2)	C6-C7-C8	141(2)	C7-C8-C8B	113(2)
C8-S9A	1.78(1)	C8B-S9B	1.74(3)	C7-C8-S9A	137(1)	C8-C8B-S9B	123(2)
S9A-S10	2.12(1)	S9B-S10	1.97(9)	C8-S9A-S10	105(1)	C8B-S9B-S10	104(1)
S10-C11	1.81(1)	S10-C11	1.81(1)	S9A-S10-C11	97(1)	S9B-S10-C11	114(1)
C11-C12	1.49(2)	C11-C12	1.49(2)	S10-C11-C12	112(1)	S10-C11-C12	112(1)
C12-C13	1.31(2)	C12-C13	1.31(2)	C11-C12-C13	120(1)	C11-C12-C13	120(1)

Table 11. Final bond lengths and bond angles for (*Z*)-ajoene in complex **10**.

Mol A	Bond lengths Å	Mol B	Bond lengths Å	Mol A	Bond Angles (°)	Mol B	Bond Angles (°)
C1A-C2A1	1.29(4)	C1B-C2B	1.29(4)	C1-C2A1-C3	105(1)	C1B-C2B-C3	104(2)
C1A-C2A2	1.29(4)	-	-	C1-C2A2-C3	105(1)	-	-
C2A1-C3	1.50(3)	C2B-C3	1.43(2)	C2A1-C3-S4A	106(1)	C2B-C3-S4B	137(2)
C2A2-C3	1.50(6)	-	-	C2A2-C3-S4A	149(1)	-	-
C3-S4A	1.82(1)	C3-S4B	1.82(2)	C3-S4A-C6A	92(1)	C3-S4B-C6B	99(1)
S4A-C5A	1.81(3)	S4B-C5B	1.81(2)	C3-S4A-O5A	111(1)	C3-S4B-O5B	109(1)
S4A-O5A	1.48(2)	S4B-O5B	1.50(2)	O5A-S4A-C6A	109(1)	O5B-S4B-C6B	105(2)
C6A-C7A	1.51(4)	C6B-C8	1.53(3)	S4A-C6A-C7A	105(2)	S4B-C6B-C8	120(2)
C7A-C8	1.29(3)	C8-C8B	1.30(3)	C6A-C7A-C8	119(1)	C6B-C8-C8B	145(2)
C8-S9A	1.79(2)	C8B-S10	1.76(2)	C7A-C8-S9A	119(2)	C8-C8B-S10	115(2)
S9A-S10	1.83(1)	S10-S10B	1.99(1)	C8-S9A-S10	92(1)	C8B-S10-S10B	92(1)
S10-C11A	1.79(3)	S10B-C13	1.84(2)	S9A-S10-C11A	121(1)	S10-S10B-C13	113(1)
C11A-C12A	1.50(4)	C13-C12B	1.52(3)	S10-C11A-C12A	122(2)	S10B-C13-C12B	109(2)
C12A-C13	1.31(3)	C12B-C13B	1.29(4)	C11A-C12A-C13	102(2)	C13-C12B-C13B	128(3)

Guest inclusion modes

As previously stated, the resolved stereoisomers of (*E*)-ajoene overlap to a large extent (Figure 19), which means that their overall modes of inclusion in TRIMEB are similar. These modes are compared in the stereoviews in Figure 21 which show that in each case, the disulfide moiety is centrally placed and uppermost within the host cavity. The attached allylic and vinylic moieties are also included in the cavity, while the allyl group at the other terminus and its

attached sulfinyl group protrude from the secondary face. The S=O dipole orientations are reversed for the two stereoisomers, and in one case (model A. (R)-enantiomer), there is a weak stabilizing interaction S=O···H-C(host) involving a secondary methyl group (see Table 12).

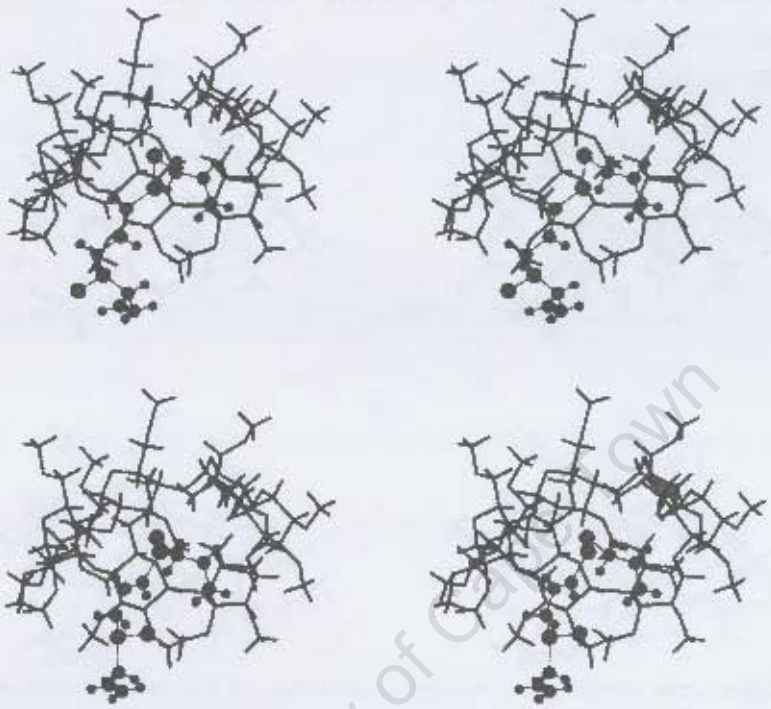

Figure 21. Stereoview showing the modes of inclusion of the enantiomers of (*E*)-ajoene in TRIMEB (R-enantiomer, top; S-enantiomer, bottom).

Table 12. Intramolecular host–guest hydrogen bonds for complex **9**.

Donor-H···Acceptor	D-H (Å)	H···A (Å)	D···A (Å)	D-H···A (°)
C6-H6A1···O2G3	0.99	2.49	3.29(3)	134.5
C6G6-H6G9···O5A[a]	0.98	2.49	3.43(2)	157.2
C7G3-H7G5···S4A	0.98	2.78	3.61(1)	143.1
C7G3-H7G5···O5A	0.98	2.37	3.31(3)	161.5

[a] x, y, 1 + z

The modes of inclusion of the stereoisomers of (*Z*)-ajoene (Figure 22) are distinctly different from those for the (*E*)-isomer, as the disulfide group and its attached allyl group are now located outside the cavity and the sulfinyl group is within the cavity. There is, further, a significant difference between the modes of inclusion of the individual stereoisomers of (*Z*)-ajoene, namely the location of their respective sulfinyl groups. Both are centrally located, but in A

(R-enantiomer) the S=O group is situated at the 'roof' of the cavity, in van der Waals contact with the capping primary methoxyl groups, whereas in B ((S)-enantiomer) it is located near the secondary face. At location A, it engages in a S=O···H-C (host methine) hydrogen bond (Table 13).

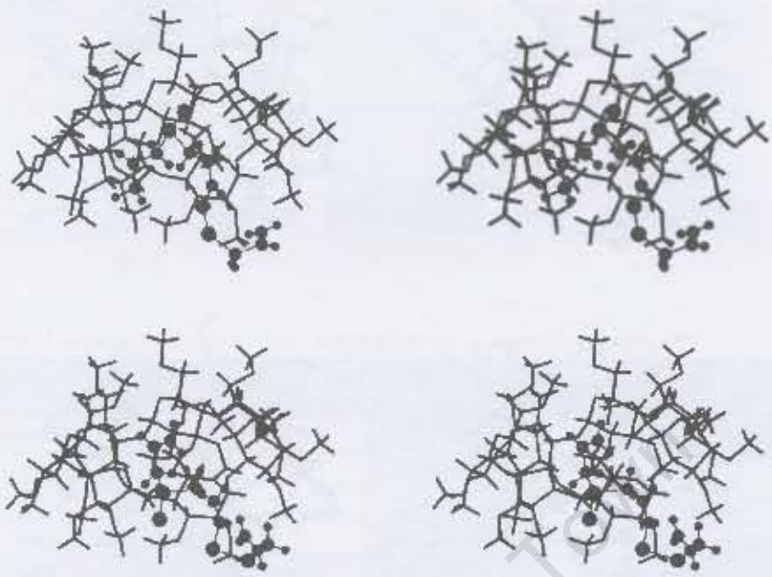

Figure 22. Stereoview showing the modes of inclusion of the enantiomers of (Z)-ajoene in TRIMEB (R-enantiomer, top; S-enantiomer, bottom).

Table 13. Intramolecular host–guest hydrogen bonds for complex **10**.

Donor-H···Acceptor	D-H (Å)	H···A (Å)	D···A (Å)	D-H···A (°)
C5G1-H5G1···O5A	1.00	2.56	3.40(2)	141.3

Crystal packing arrangements and PXRD patterns

Topologically **9** and **10** are very close, apart from the host secondary faces where chemically different moieties protrude. Distinctly different packing arrangements characterise these complexes due to their different modes of inclusion. This was evident from their different PXRD patterns. The orthorhombic crystal system and space group $P2_12_12_1$ for complex **10** were initially deduced by finding a match between the experimental PXRD pattern

and the reference pattern for a known isostructural series of TRIMEB complexes.[13]

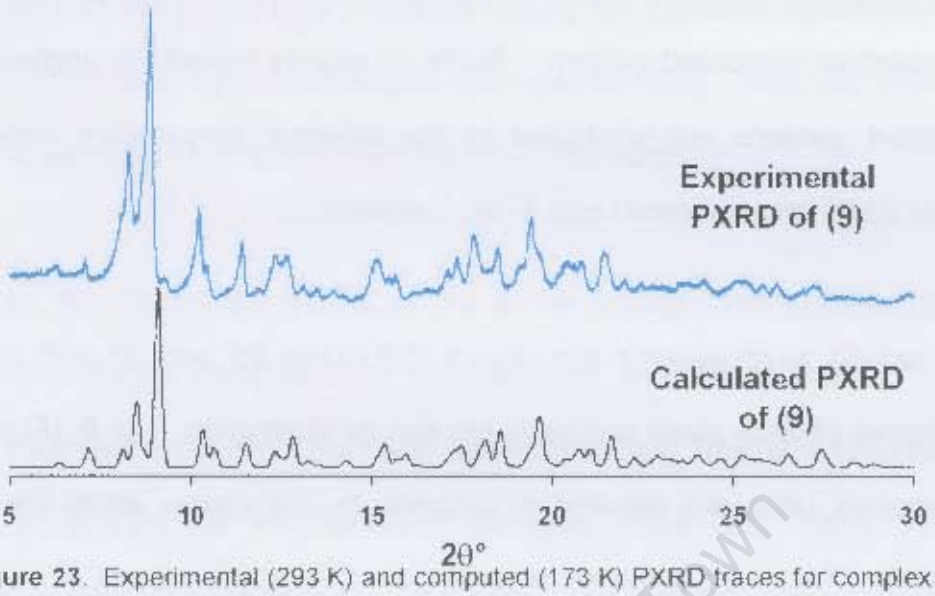

Figure 23. Experimental (293 K) and computed (173 K) PXRD traces for complex **9**.

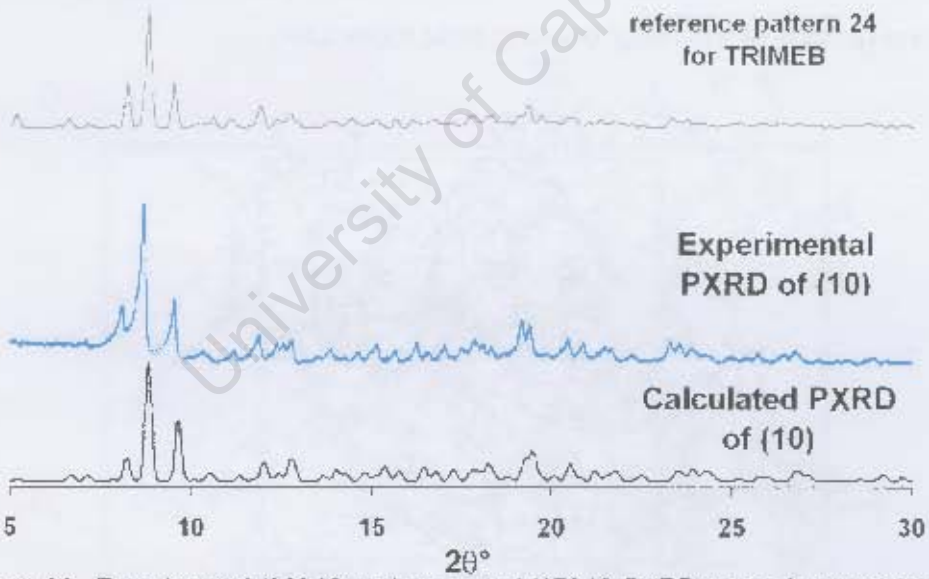

Figure 24. Experimental (293 K) and computed (173 K) PXRD traces for complex **10**.

Although the experimental patterns for **9** and **10** share a superficial resemblance (Figures 23 and 24), detailed investigation showed that the peak positions and relative intensities for **9** are unique.[14] [Recently Caira *et al* reported the first monoclinic crystal structure of a TRIMEB complex, that with the anaesthetic butamben as guest,[15] also crystallizing in $P2_1$, but this has *a* ~

10.89, b ~ 14.86, c ~ 27.58 Å, β = 99.6° and is therefore not isostructural with complex **9**]. Each experimental PXRD pattern is in very close agreement with its respective computed pattern. Shifts to slightly higher 2θ angles in the calculated patterns are attributed to the different temperature conditions, namely 293K (experimental) and 173K (calculated).

The packing arrangements are shown in Figures 25 and 26 with the (R)-enantiomer of each guest arbitrarily chosen for illustration. For **9**, (Figure 25) the complex units are stacked in columns by translation along the *a*-axis (~11.6 Å). The host O4 planes are parallel to the (101) planes (i. e. steeply inclined to the *bc*-plane) and the protruding guest residue is in contact with methoxyl groups of the neighbouring host molecules.

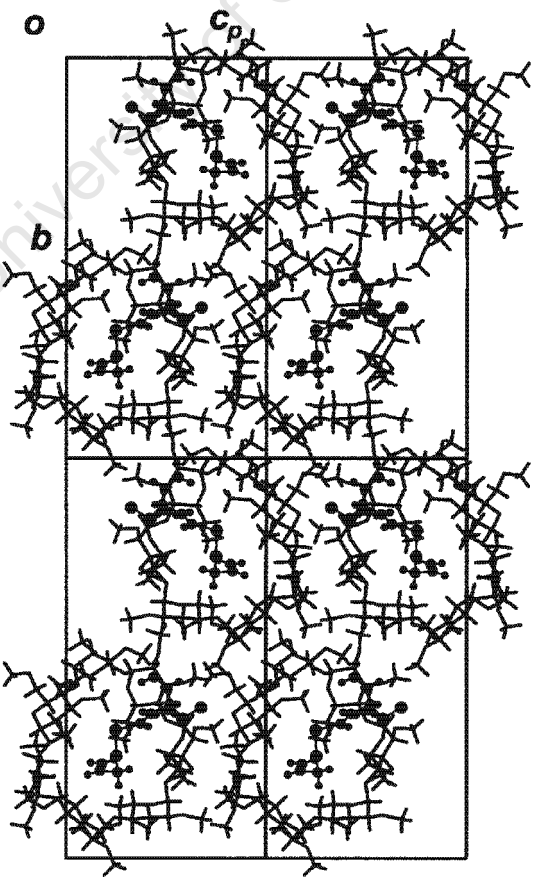

Figure 25. (100) Projection of the crystal packing in **9**.

A single intermolecular hydrogen bond S=O···H-C (methylene)^{g} (g = x, y, 1 + z) for the guest (R)-enantiomer was identified. As the water molecule in **9** is hydrogen bonded to the host shown in Figure 16, it cannot contribute to the crystal stabilization by intermolecular hydrogen bonding. This was confirmed by the absence of short intermolecular O1···O contacts.

Complex **10** (Figure 26) packs in the same arrangement adopted by the TRIMEB inclusion complexes of (S)-naproxen and (S)-ibuprofen.[8,16] The guest fragment protruding from the host secondary face is surrounded by methoxyl groups of neighbouring complex units and there are no intermolecular hydrogen bonds. The complex units are arranged in a head-to-tail manner parallel to the *b*-axis.

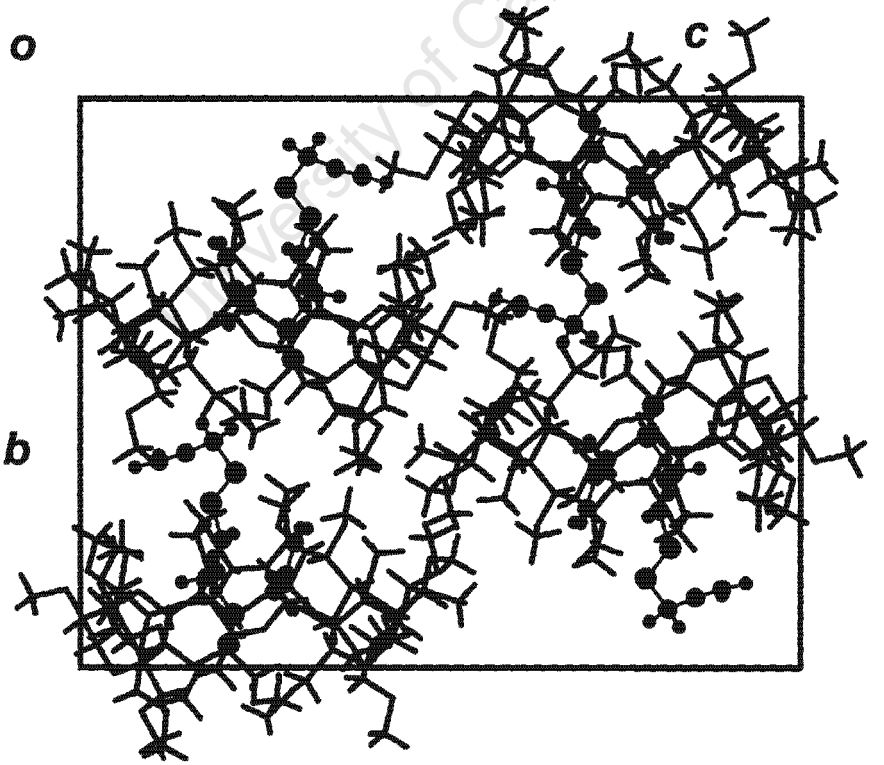

Figure 26. (100) Projection of the crystal packing in **10**.

CONCLUSION AND DISCUSSION

This study has shown conclusively that each of the isomers (*E*)- and (*Z*)-ajoene can be accommodated within the TRIMEB host cavity to form thermally stable inclusion complexes **9** and **10** respectively. X-ray analyses have confirmed the conformational flexibility of the ajoene isomers as well as the expected dominance of the hydrophobic host-guest interactions in these complexes. In each complex, a severely disordered arrangement, comprising both the (R)- and (S)- guest enantiomers, was identified within the host cavity. X-ray refinement of site-occupancies also showed that the TRIMEB molecule shows no stereo-discrimination under the conditions employed for complex preparation. However, it must be stressed that the structure solution process was extremely difficult, as incorrect atom assignments or an overly aggressive attempt at assigning electron density peaks as atoms during the refinement would severely bias the model towards an incorrect one. Thus, the refinement proceeded by means of a 'piecemeal' assignment of guest atoms, eventually resulting in the models presented in this chapter. The type of disorder observed here is significantly more complicated than that for other disordered guests included in cyclodextrins. For example, in the dimeric β-CD complex accommodating both the (R)- and (S)-enantiomers of flurbiprofen,[12] the guest molecules are spatially distinct rendering refinement relatively straightforward. In the dimeric β-CD complex of acetaminophen,[17] each guest molecule is disordered over two positions such that there is a small extent of 'atom-sharing' by the phenyl rings of the separate components. However, here too the complexity of the disorder is at a significantly lower level than that manifested by the isomers of ajoene in complexes **9** and **10**.

An interesting and novel aspect of the study was the finding that in complex **10** significantly different modes of inclusion are adopted by the individual guest stereoisomers. Finally, significant differences in the crystal packing of **9** and **10** are shown to be guest-induced, complex **9** crystallizing in a hitherto unknown arrangement for TRIMEB inclusion complexes.

References

1. Block, E., Ahmad, S., Catalfamo, J.L., Jain, M.K. and Apitz-Castro, R. *J. Am. Chem. Soc.* **1986**, 108, 7045.
2. Fernandes, C.M., Carvalho, R.A., Pereira da Costa, S. and Veiga, F.J.B. *Eur. J. Pharm. Sci.*, **2003**, 18, 285.
3. Thakkar, A.L. and Demarco, P.V. *J. Pharm. Sci.*, **1971**, 60, 652.
4. Schneider, H-J., Hacket, F., Rüdiger, V. and Ikeda, H. *Chem. Rev.*, **1998**, 98, 1755.
5. Hooft, R. *COLLECT*, Nonius B.V., Delft, The Netherlands, **1998**.
6. Otwinowski, Z. and Minor, W. *Methods Enzymol.*, **1997**, 276, 307.
7. Egert, E. and Sheldrick, G.M. *Acta Crystallogr.*, **1985**, A41, 262.
8. Caira, M.R., Griffith, V.J., Nassimbeni, L.R. and van Oudtshoorn, B. *J. Incl. Phenom. Mol. Recognit. Chem.*, **1995**, 20, 277.
9. Egert, E. *Acta Crystallogr.*, **1983**, A39, 936.
10. Allen, F.H., Kennard, O., Watson, D.G., Brammer, L., Orpen, A.G., Taylor, R. *J. Chem. Soc. Perkin Trans. 2.*, **1987**, 12, S1.
11. Sheldrick, G.M. *SHELX-97*. University of Göttingen, Germany, **1997**.
12. Harata, K. *Chem. Rev.*, **1998**, 98, 1803.
13. Caira, M.R. *Roum. Chem. Quart. Rev.*, **2000**, 8, 243.
14. Cambridge Structural Database and Cambridge Structural Database system, version 5.24, November **2003**, Cambridge Crystallographic Data centre, University Chemical Laboratory, Cambridge, England.
15. Caira, M.R., Bourne, S.A., Vilakazi, S.L. and Reddy, L. *Supramol. Chem.*, **2004**, 16, 279.
16. Brown, G.R., Caira, M.R., Nassimbeni, L.R. and van Oudtshoorn, B. *J. Incl. Phenom. Mol. Recognit. Chem.*, **1996**, 26, 281.
17. Caira, M.R. and Dodds, D.R. *J. Incl. Phenom. Macrocycl. Chem.*, **2000**, 38, 75.

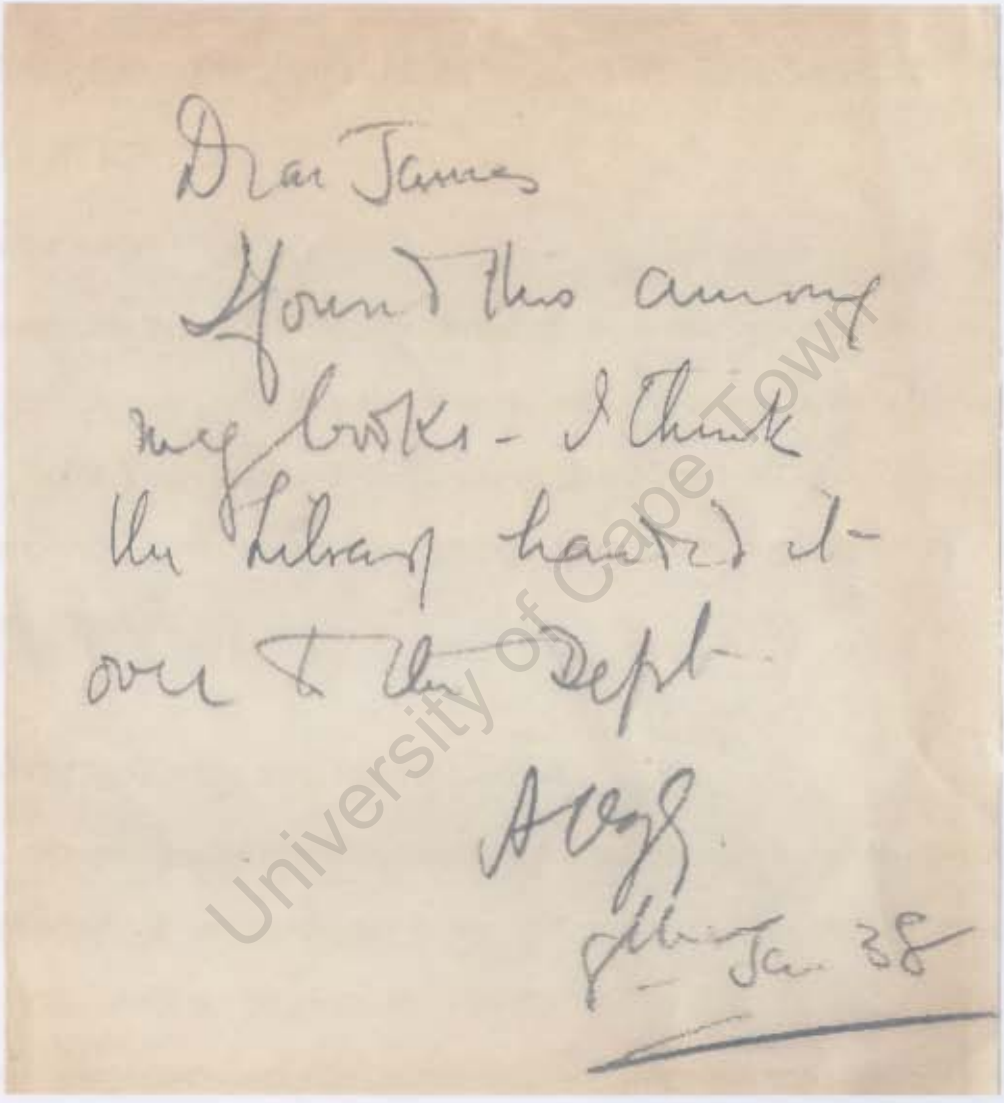
Dear James
Found this among
my books - I think
the Library has it -
over to the Dept -
A Voy
Jan 38

CHAPTER 6

CONCLUSION

At the outset of this study our intentions were to form inclusion complexes between the individual isomers of ajoene and various cyclodextrins.

COMPLEX PREPARATION, CHARACTERISATION AND IDENTIFICATION

Preparation

The reaction between ajoene isomers and the various cyclodextrins (α-, β-, γ-CD, DIMEB and TRIMEB) yielded mainly microcrystalline products, except for the TRIMEB complexes TRIMEB•(*E*)-ajoene•0.5H_2O (**9**) and TRIMEB•(*Z*)-ajoene (**10**), which were obtained as crystals large enough for single crystal X-ray diffraction.

Characterisation and identification

The physicochemical characterisation of the cyclodextrin inclusion complexes proceeded via single crystal X-ray diffraction, powder X-ray diffraction (PXRD), variable temperature PXRD, TGA, DSC, HSM, FTIR, UV spectrophotometry and NMR spectroscopy. Complexes (**9**) and (**10**) were subjected to all the characterisation techniques listed while the other complexes were characterised and identified as inclusion complexes by PXRD. HSM, TGA, DSC and variable temperature PXRD provided evidence of the thermal stability of complexes (**9**) and (**10**). FTIR spectroscopy provided no evidence of complexation and was not useful in the

characterization of these complexes. UV spectrophotometry was used to determine the stoichiometry (1:1) of the TRIMEB complexes. NMR spectroscopy was employed for the purposes of characterising (*E*)- and (*Z*)-ajoene after their synthesis. It also provided tentative evidence of inclusion through the altered resonances/chemical shifts of characteristic protons after complexation with TRIMEB.

SIGNIFICANCE OF THE REPORTED RESULTS

In total, ten cyclodextrin inclusion complexes resulted from the reactions between ajoene ((*E*)- and (*Z*)-isomers) and the various cyclodextrins. Eight of these complexes were identified by the PXRD method and approximate unit cell parameters obtained through the application of the principles of isostructurality. Two new crystal packing arrangements and their corresponding reference patterns were established for complexes of α-CD and DIMEB. The structures of two TRIMEB complexes were determined by single crystal X-ray diffraction, one of them in a space group not previously reported for TRIMEB inclusion complexes. X-ray analysis of complexes **9** and **10** at low temperature revealed that the R- and S- enantiomers of both (*E*)- and (*Z*)-ajoene are 'frozen out' and successful modelling ensued. These results represent the first definitive thermal and structural data for cyclodextrin inclusion complexes of a major pharmacologically active component present in garlic.

Principles of isostructurality

The application of these principles to interpretation of PXRD patterns proved extremely valuable in the absence of large monocrystals suitable for single crystal X-ray diffraction. It has emphasized the importance of comparing complexes with similar guests. However, the procedure adopted provides only a gross description of the three–dimensional structure with no detail regarding atomic and molecular interactions or the role of interstitial water. We obtain from the application of the principles of isostructurality reasonable estimates of the unit cell parameters for new complexes with a reliable description of the host arrangement and void topology.

Apart from our own routine use of reference PXRD patterns to identify new CD inclusion complexes, we have noted from the recent literature that other researchers are beginning to employ this procedure. For example, the reaction products between β-CD and sodium nimesulide,[1] and between β-CD and 2-phenoxyethanol,[2] were recently confirmed as inclusion complexes based on the close similarity of their PXRD patterns to those of known CD inclusion complexes.

Crystal structures

TRIMEB was chosen as an appropriate host because guest molecules are generally ordered within its cavity. However, both complex structures described in this work display severe guest disorder whose resolution presented significant challenges. The disorder resulted from the simultaneous presence of the individual stereoisomers of the guest within the

host cavity. The modes of guest inclusion adopted by these guests in complexes (**9**) and (**10**) gave rise to distinctly different packing arrangements, while the modes of guest inclusion of the R- and S-isomers in complex (**10**) are different from each other.

Medicinal application

Ajoene has a wide range of medicinal activities, as indicated in the introduction to this dissertation. Moreover, (*E*)- and (*Z*)-ajoene have several common medicinal properties while also possessing unique activities individually. One of the aims of this study was the preparation of ajoene – CD inclusion complexes with potential medicinal use. The host carrier molecule TRIMEB is not suited for this purpose, however, owing to its haemolytic properties.[3] The parent CDs have more promise, especially γ-CD since it has a safe toxicity profile and superior solubilising properties to those of the other parent CDs.[4,5,6]

Very recently, ajoene was shown to inhibit proliferation and induce apoptosis of several human leukemia CD 34 negative cells. More significantly, ajoene profoundly enhanced the apoptotic effect of two chemotherapeutic drugs, namely cytarabine and fludarabine, in human CD 34 positive resistant myeloid leukemia cells.[7,8] Thus, ajoene shows excellent promise for further development as a medicinal agent.

ONGOING WORK

Ajoene is currently used as an immuno-booster at RED CROSS CHILDREN'S HOSPITAL in Cape Town, South Africa. It is also used to treat patients with *Candida* infections.

The synthesis of analogues of ajoene is underway in the Department of Chemistry at the University of Cape Town. CD inclusion experiments of these synthetic analogues are also currently underway.

FUTURE WORK

PXRD indexing and structure solution

Complete structural elucidation of the CD – ajoene complexes isolated as microcrystalline powders is a desirable goal. An outline of how this might be achieved in the future follows.

The combination of high resolution PXRD data obtained from a synchrotron source and powder diffraction indexing programs allow for the extraction of very accurate unit cell parameters. This, in conjunction with a set of reference patterns, may be used to confirm the space group of the cyclodextrin inclusion complex. To proceed further, molecular modelling programs could be employed to model the conformation and orientation of the included guest. The final structural model could be optimised by Rietveld refinement.[9]

Selectivity experiments

Currently, the synthesis of ajoene as described in chapter 3 yields a product which is a mixture of (*E*)- and (*Z*)-isomers. The latter are then separated by column chromatography, which is a time–consuming procedure. Cyclodextrin inclusion selectivity experiments performed under competitive conditions between the (*E*)- and (*Z*)-isomers of ajoene may be a useful alternative approach to the separation of these isomers. Efficient separation is desirable if the individual isomers are to be prepared in bulk quantities for medicinal application.

Biological testing

Bioavailability studies would have to be undertaken to determine the effectiveness of ajoene isomers in the form of their CD inclusion complexes. These would include solubility studies, dissolution rate studies and measurements of the rate of intestinal absorption. Permeation studies would also be appropriate for investigating transdermal delivery as a possible route of administration.

In conclusion, the main objectives of the study have been achieved; the potential for CD inclusion of ajoene has been amply demonstrated in this work.

References

1. Braga, S.S., Ribeiro-Claro, P., Pillinger, M., Gonçalves, I.S., Pereira, F., Fernandes, A.C., Romão, C.C., Correia, P.B. and Teixeira-Dias, J.J.C. *Org. Biomol. Chem.*, **2003**, 1, 873.
2. Cunha-Silva, L., and Teixeira-Dias, J.J.C. *New. J. Chem.*, **2004**, 28, 200.
3. Frömming, K.H., Szejtli, J. *Topics in inclusion science - Cyclodextrins in pharmacy*. Kluwer Academic Publishers, Dordrecht, The Netherlands, **1993**, Vol. 5, Chapter 3.
4. Frank, D.W., Gray, J.E., Weaver, R.N. *Am J. Pathol.*, **1976**, 83, 367.
5. Schmid, G. In *New Trends in Cyclodextrins and Derivatives*, Duchêne, D., Ed., Editions de Santê: Paris, **1991**, 27.
6. Irie, T. and Uekama, K. *J. Pharm. Sci.*, **1997**, 86, 147.
7. Hassan, H.T. *Leukemia Res.*, **2004**, 28, 667.
8. Ledezma, E., Apitz-Castro, R., Cardier, J. *Cancer Lett.*, **2004**, 206, 35.
9. Rietveld, H.M., *Acta Crystallogr.*, **1967**, 22, 151.

APPENDIX 1

Restrained bond lengths used during the refinement of complex structures **9** and **10** are presented here in Tables 1 and 2.

Table 1. List of the fixed bond lengths in **9**.

Distance	(9) Mol A	(9) Mol B
1.300	C1-C2	C1-C2
1.300	C12-C13	C12-C13
1.507	C11-C12	C11-C12
1.507	C3-C2	C3-C2
1.806	S4A-C6	C7-S4B
1.806	S4A-C3	S4B-C3
1.498	S4A-O5A	S4B-O5B
1.820	S10-C11	S10-C11
1.755	S9A-C8	S9B-C8B
1.311	-	C8-C8B
[1]1.400	C8-C7	C8-C7
1.507	C7-C6	-
2.029	S10-S9A	S10-S9B

Table 2. List of the fixed bond lengths in **10**.

Distance	(10) Mol A	(10) Mol B
1.507	C11A-12A	C13-C12B
1.507	C3-C2A1/2	-
1.450	-	C3-C2B
1.300	C1A-C2A1	C12B-13B
1.300	C1A-C2A2	C2B-C1B
1.806	S4A-C3	S4B-C3
1.806	S4A-C6A	S4B-C6B
1.507	C6A-C7A	C8-C6B
1.311	C8-C7A	C8-C8B
1.755	S9A-C8	S10-C8B
2.029	S10-S9A	S10-S10B
1.820	S10-C11A	C13-S10B
1.498	S4A-O5A	S4B-O5B
1.300	C13-C12A	-
[2]1.450	-	C3---C2B
[2]2.150	-	C3---C1B

[1] The restrained bond length used here is the average of a double bond 1.311 (MOL A) and a single bond 1.507 (MOL B)

[2] The broken line indicates the application of a non-bonded restraint.

APPENDIX 2

The following supplementary data can be found on the compact disc attached. There are seven files for each structure presented in chapter 5 of this dissertation.

File extension/format	Contents
9.HKL	Reflection data
9.RES	SHELX co-ordinate data
9.CIF	Crystallographic information file
9.FCF	Structure factor tables
9.LIS	Platon output
9.XL	
9.SUP	Tabulated supplementary data

File extension/format	Contents
10.HKL	Reflection data
10.RES	SHELX co-ordinate data
10.CIF	Crystallographic information file
10.FCF	Structure factor tables
10.LIS	Platon output
10.XL	
10.SUP	Tabulated supplementary data

All files are readable using WORDPAD in Windows98 or any later version thereof.